

**Chapter of the Book on “Monitoring “Modern volcanic monitoring” in IAVCEI Book series
Advances in Volcanology and Active Volcanoes of the World (Springer)**

Accepted Version

**Fiber optic sensing for volcano monitoring and imaging volcanic
processes**

Philippe Jousset (GFZ Potsdam, Germany) – ORCID: 0000-0002-5628-0238

Gilda Currenti (INGV Catania, Italy) – ORCID: 0000-0001-8650-5613

Shane Murphy (IFREMER, Plouzané, France) – ORCID: 0000-0003-2795-0463

Eva P. S. Eibl (University of Potsdam, Germany) – ORCID: 0000-0002-0667-0035

Corentin Caudron (Université Libre de Bruxelles, Belgium; WEL Research Institute, avenue Pasteur, 6, 1300 Wavre, Belgium) – ORCID: 0000-0002-3748-0007

Lise Retailleau (IPGP, Paris, France) – ORCID: 0000-0002-0711-4540

Christopher Wollin (GFZ Potsdam, Germany) – ORCID: 0000-0002-3992-787X

Sara Klaasen (ETH Zürich, Switzerland) – ORCID: 0000-0003-4094-7891

Takeshi Nishimura (Tohoku University, Japan) – ORCID: 0000-0002-0979-6602

Andreas Fichtner (ETH Zürich, Switzerland) – ORCID: 0000-0003-3090-963X

Zack Spica (University of Michigan, Ann Arbor, Michigan, USA) – ORCID: 0000-0002-9259-1973

Arnaud Lemarchand (IPGP Paris, France) – ORCID: 0000-0002-4234-3787

Charlotte Krawczyk (GFZ Potsdam and Technische Universität Berlin, Germany) – ORCID: 0000-0002-5505-6293

Abstract

This chapter describes fiber optic sensing methodologies and their applications for understanding volcanic structure and processes. We assess their benefits for volcano monitoring and offer possible solutions to address their challenges. The physical principles at the basis of fiber optic sensing technologies have been known for several decades. These principles are related to various processes involving electro-magnetic interactions of light sent by a laser within glass. Intrinsic physical properties of glass within the optical fiber, when engineered appropriately and interrogated with an adequate light source, enable us to access a number of environmental parameters, such as temperature, strain and rotation over a large frequency range. However, only recently developed instruments have been able to sense these parameters efficiently, either at a point or densely in a distributed way for geophysical and volcanological applications. Rotational sensors allow us to measure the rotational components of the seismic wave field, which have been discarded in the past. Distributed fiber optic sensing provides access to quasi-continuous measurements of temperature, strain and strain rate along km-long fibers with a high spatial resolution (meter) and sampling rate (kHz). We show examples on volcanoes both on land and in submarine environments. We demonstrate that data from optical strainmeters, rotational sensors, distributed fiber optic strain and/or temperature sensing can reveal unknown structural features and processes in volcanoes. These examples testify that fiber optic sensing methodologies owe to be implemented as additional tools for improved volcano monitoring and for volcanic crisis management.

1. Introduction

Approaches and techniques for monitoring active volcanoes have significantly evolved in recent years, mainly due to innovations in instrumentation, to denser spatial observations and to an improved interpretation of data through better integration of geophysical and geochemical observations (Surono et al., 2012). The aim of volcanology is to forecast the behavior of a given volcano and issue timely alerts for effective hazard assessment and risk management (Witze, 2015). To achieve this goal, models of mass and energy transfer are necessary. These models require the knowledge of accurate details of the distribution of physical properties within the volcano, of the full seismic wave field and of key thermodynamic properties and transfer processes within the volcanic system. To achieve such acute description, volcanologists deploy instruments to measure physical and chemical parameters on volcanoes and interpret their spatial distribution and temporal variations in relation with volcanological and geological observations. For example, the use of large-N seismometer networks to densely observe ground motions has enabled volcanologists to gain additional knowledge on volcano seismic structure and processes (Hansen et al., 2016; Yeh et al., 2021). The analysis of the parameter variations over time recorded with multiple instruments, contributes to evaluating the status of the volcanic activity and supports volcano monitoring.

This chapter aims to illustrate how the use of fiber optic sensing methodologies can provide valuable information for achieving various goals in volcanology. This includes understanding structural features and volcanic processes, which can contribute to improved volcano monitoring.

Fiber optic sensors offer several advantages over conventional sensors (Lu et al., 2019; Blanc et al., 2022). On the one hand, sensing can be performed remotely via optical fiber due to the low transmission losses of light within the optical fiber. On the other hand, optical fibers are highly sensitive to external physical processes, allowing for accurate recording of new observables (such as translation, rotation and strain) at a specific position, or at series of distributed locations along a fiber (which can span tens of kilometers), with a dense spatial resolution (e.g., meter, using Distributed Fiber Optic Sensing for temperature and strain). Furthermore, optical fibers are suitable for use in harsh environments due to their immunity to external electromagnetic interference, high temperatures resistance, and ability to withstand corrosive conditions. Additionally, fiber optic cables are lightweight, compact, flexible, easy to deploy, and cost-effective, requiring low maintenance. All these merits explain why fiber optic sensing has been used for many years in a wide range of applications, including civil engineering, mining and energy exploration, and environmental sciences, especially in harsh and challenging-to-access environments (Miah & Potter, 2017). The technologies associated with fiber optic sensing have shown

their potential in replacing conventional electromechanical-based temperature and vibration sensors. This justifies the potential of expansion of their use also in volcanology.

The principles behind fiber optic sensing were discovered several decades ago by Rayleigh (1881), Sagnac, 1913a,b, Brillouin (1914), and Raman (1928). The measurement involves sending light through an optical fiber and analyzing changes in light properties, such as amplitude and/or frequency, after it interacts with the medium it travels through, such as glass fiber. When the environment in which the fiber is located undergoes changes in physical parameters, such as temperature, strain or rotation, the properties of light are modified due to the altered interactions between the light and the glass. The section §2 will provide a detailed explanation of these principles and processes.

However, the implementation of these principles in practice has only been happening in the last few decades for an increasing number of applications, at a reasonable cost. These advances can be attributed to simultaneous substantial technological innovations, particularly in optoelectronics and photonics, which now enable photonic scientists to manipulate light and measure tiny phase shifts at a very high sampling rate. Advancements in fiber optic cable design and manufacturing, as well as improvements in laser (as the source of light) accuracy and stability, have contributed increased accuracy and resolution of fiber optic technologies. Additionally, in computer science, digital information can be processed more quickly using smaller and more efficient electronic chips and new processing algorithms. These advancements enable the recording of new geoscientific information with high temporal and spatial resolutions and improved accuracy. Consequently, optical fiber technologies have become increasingly popular in recent years for geophysics and geoscientific applications (Wassermann et al., 2016; Matias et al., 2017; Bastianini et al., 2019; Lu et al., 2019; Zhan, 2019; Lindsey and Martin, 2021; Chang et al., 2022; Moreno et al., 2022; Noe et al., 2023). Below, we summarize the three main approaches to fiber optic sensing: light transmission sensing, point sensing and distributed sensing.

Light transmission sensing involves analyzing changes in light transmission delay or polarization, occurring within an optical fiber between the point of emission and reception. These changes are linked to perturbations of the refractive index of the fiber glass caused by external vibrations or disturbances, such as seismic waves. This method has been used with trans-oceanic telecom fiber optic cables to detect and/or locate earthquakes over large distances (1000s km), using disturbances in transmission delays (Marra et al., 2018; Bogris et al., 2022) and polarization (Palmieri & Schenato, 2013; Zhan et al., 2021). By using this technique on several successive shorter cable segments, earthquakes on the mid-oceanic ridge can be located (Marra et al., 2022). This opens the possibility of monitoring inaccessible

submarine volcanoes using existing and future telecom networks. Transmission delay or polarization methods may be used in volcanology *sensu stricto* in the near future.

Fiber optic point sensing involves the analysis of changes in light properties in dedicated small size sensor (0.01-0.1 m scale) in order to measure locally an evolving physical parameter affecting the light properties. Several such instruments have been developed to measure seismic ground motion (Feron et al., 2020), rotation (Bernauer et al., 2012, 2018, 2021; Wassermann et al., 2020; Brokesova et al., 2021), tilt (Chawah et al., 2015) and strain (Ferraro & De Natale, 2002; He et al., 2013; Coutant et al., 2015). Fiber optic rotational sensors have been proven successful in controlled huddle tests, in which many similar sensors record at the same time and same location (Izgi et al., 2021). The sensors were deployed for various purposes, including the analysis of tectonic earthquakes in Italy (Simonelli et al., 2018; Yuan et al., 2020), micro-zonation of damages after significant earthquakes (Wassermann et al., 2016; Keil et al., 2021; 2022), exploration seismology (Schmelzbach et al., 2018), and tracking moving sources (Yuan et al., 2021). Rotational sensors can also help to correct for tilt contamination of records from nearby conventional seismometers (Bernauer et al., 2020), to correct measurements on the seafloor (Lindner et al., 2016), or to directly study microseisms generated in the ocean (Hadziioannou et al., 2012; Tanimoto et al., 2015). Rotational sensors have been shown to measure meaningful volcano-seismic signals on volcanoes, such as in Hawaii, USA (Wassermann et al., 2020), on Stromboli, Italy (Wassermann et al., 2022) and at Etna, Italy (Eibl et al. 2022).

Distributed Fiber Optic Sensing (DFOS) involves analyzing changes in light properties after it has interacted with the structure of the fiber glass itself. DFOS typically uses an interrogator device connected to a single optical fiber within a fiber optic cable, which can be deployed on purpose or in existing infrastructure. The interrogator contains a laser that sends light through the fiber. The light interacts with the glass structure of the fiber, typically variations of the glass refractive index, via e.g., scattering processes (see §2 for full details). Part of the scattered light travels back to the interrogator where it is analyzed by a photodetector also inside the interrogator. The properties of the light change in relation to changes in environmental parameters, such as temperature and strain, acting on the fiber glass structure. Thus, the fiber serves not only as a means of transmitting light, but also as a sensor. DFOS is capable of probing kilometers of fiber at once due to the low attenuation during light propagation. As scattering processes occur continuously along the fiber, measurements can be obtained at any chosen spatial interval, making DFOS a distributed sensing method. DFOS enables distributed sensing over distances of 10s-kilometer, with data typically measured every couple of meters. This makes it attractive for a wide range of applications.

DFOS has been developed to measure temperature (Hartog, 1983; Li et al., 2015), dynamic strain (Parker et al., 2014) and static strain (Horiguchi et al., 1989). Local external perturbations along the sensing fiber, such as temperature and strain, can be measured by analyzing the amplitude, the frequency, the polarization or the phase of the light (Lu et al., 2019). DFOS has been widely used in various applications due to its ability to probe the entire length of the fiber for temperature and strain at high spatial resolution. For instance, it has been used to investigate line cuts and quality in telecommunication networks (Barnosky et al., 1976; 1977; Philen et al., 1982) and in ensuring perimeter security (Taylor and Lee, 1993; Szustakowski and Zyczkowski, 2005). DFOS has also been used in petroleum and geothermal industrial applications to log borehole structure with Vertical Seismic Profiling (Daley et al., 2013; Madsen et al., 2013, 2016; Frignet & Hartog, 2014; Hartog et al., 2014; Zwartes & Mateeva, 2015; Willis et al., 2016; Correa et al., 2017; Martuganova et al., 2022; Schölderle et al., 2022), to profile well temperature (Reinsch et al., 2013). DFOS has also been used for monitoring well integrity (Lipus et al., 2018), fluid flow during hydraulic fracturing (Molenaar & Cox, 2013; Richter et al., 2019), and reservoir microseismicity (Verdon et al., 2020). DFOS has been applied in various other applications including structural health monitoring (Tregubov et al., 2016; Barrias et al., 2017) and land subsidence monitoring (Wu et al., 2015).

Applications in non-industrial Earth Sciences are more recent. They often face challenges due to harsh environmental conditions. DFOS has been used to accurately and precisely characterize the Earth's crust over distances ranging from 0.1 to 100 km. These applications cover a range of topics including ice monitoring in a lake (Castongia et al., 2017) and in glaciers (Walter et al., 2020; Klaasen et al., 2021), landslide monitoring (Kogure & Okuda, 2018), teleseismic earthquake detection (Lindsey et al., 2017; Jousset et al., 2018; Yu et al., 2019) and local earthquake detection and location (Jousset et al., 2018; Klaasen et al., 2021; Nishimura et al., 2021). Krawczyk et al. (2019) conducted research on monitoring urban areas. Jousset et al. (2018) and Krawczyk (2021) conducted research on crustal structure and monitoring on-shore, while Lindsey et al. (2019), Jousset (2019), Sladen et al. (2019), Williams et al. (2019) and Janneh et al. (2023) focused on submarine offshore topics, such as microseism or submarine life (Landrø et al., 2022). Global seismology also benefits from the large number of available infrastructures (Jousset et al., 2023; Wuestefeld et al., 2023). The success in using already deployed standard telecom fibers (Jousset et al., 2016; Lindsey et al., 2017; Sladen et al., 2019; Williams et al., 2019) makes DFOS particularly attractive for volcanoes in urban areas and sub-marine environments, such as Campi Flegrei and Vulcano (Currenti et al., 2023), in Italy. However, most volcanoes lack telecom networks, requiring the deployment of optical cables for fit-to-purpose experiments and potential monitoring (Contrafatto et al., 2019; Jousset et al., 2019; Currenti et al., 2021; Klassen et al., 2021; Fichtner et al., 2022; Jousset et al., 2022).

This chapter focuses on technologies and applications that address two quantities relevant in volcanology: temperature and the full seismic wave field (translation, strain and rotation). These quantities are most appropriate for yielding ground property distributions and structural features at volcanoes and for characterizing processes to improve volcano monitoring and hazard assessment. The chapter is structured as follows: Section 2 describes the various optical techniques, highlighting the ability of fiber optic sensing in measuring accurately the full seismic wave field, including translational displacements, rotational and strain components, across a wide frequency range. Section 3 presents the current status and advancements in Point Fiber Optic Sensing and in Distributed Fiber Optic Sensing for volcanology, with examples from Canada, France, Germany, Iceland, Italy and Japan. These examples demonstrate the ability of fiber optic technologies to achieve the following: 1. improve the inference of seismic wave field properties; 2. provide a detailed characterization of subsurface volcanic layers and image faults; 3. detect and locate volcanic earthquakes; 4. quantify volcano deformation and describe its relationship to the tectonic environment; 5. detect small signals related to fluid movement, such as monitoring bubbles in a volcanic lake, and quantify and locate volcanic explosions. In Section 4, we address the limitations and challenges of fiber technologies, and propose potential solutions for real-time operational volcano monitoring. Section 5 concludes by examining the future of fiber optic technologies for research, volcano monitoring, and volcanic crisis management.

2. Fiber optic principles and methods for seismic wave field and temperature measurements

Volcanic phenomena can cause deformation, such as the rotation, tilt and translation of blocks of rocks at different spatial and temporal scales. Therefore, volcanology requires a description and observation of the complete seismic wave field across a wide frequency range (from months to hundreds of Hz). However, until recently (Matoza & Roman, 2022), volcano-seismology was unable to measure the full seismic wave field, in particular its rotational and strain components (Thelen et al., 2022), due to the lack of adequate instruments. This has changed with the development of new fiber-based instrumentation that can measure rotation or strain with small amplitude resolution (nanoradians to microradians or nanostrain to microstrain, respectively) over a broad frequency range (0.0001-100 Hz).

This section provides a brief overview of linear seismology before discussing the physical principles behind fiber optic technologies that describe the ground motion (translation, strain and rotation) and temperature (see also Table 1). To ensure a comprehensive description, we refer to several reviews due to the wide range of tested and existing technologies. In addition to Hartog's (2017) general introduction, the literature comprises general reviews by Kersey (1996), Grattan & Sun (2000), Lu et al. (2019), Pevec &

Donlagic (2019), Fenta et al. (2021) and Moreno et al. (2022). Other literature focus on more specific aspects of fiber optic technologies such as Fabry-Perrot technologies (Nur et al., 2016), distributed temperature sensing (Ukil et al., 2011), Brillouin scattering (Bao et al., 2021), and distributed dynamic strain sensing, also known as distributed acoustic sensing (Masoudi & Newson, 2016; Reinsch et al., 2021; Gorshkov et al., 2022, Liu et al., 2022; Masoudi & Brambilla, 2022; Sun et al., 2022). Ramakrishan et al. (2016) reviewed applications for composite materials. Miah & Potter (2017) studied strain and temperature for geophysical applications, while Schenato (2017) focused on geo-hydrological applications. Di et al. (2018) explored deformation applications, Hartog et al. (2018) monitored marine infrastructures, Zhu et al. (2022) monitored linear infrastructures, and Butt et al. (2022) conducted research on environmental monitoring.

Table 1 - Summary of the main fiber optic techniques and their applications in volcanology.

BOFDA: Brillouin Optical Frequency Domain Analysis
 BOFDR: Brillouin Optical Frequency Domain Analysis
 BOTDR: Brillouin Optical Time Domain Reflectometry
 CP- ϕ -OTDR: Chirped-pulse Phase OTDR
 DAS: Distributed Acoustic Sensing
 DDSS: Distributed Dynamic Strain Sensing
 DVS: Distributed Vibration Sensing

ϕ -OTDR: Phase OTDR
 OTDR: Optical Time Domain Reflectometry
 OFDR: Optical Frequency Domain Reflectometry
 ROTDR: Raman Optical Time Domain Reflectometry
 ROFDR: Raman Optical Frequency Domain Reflectometry
 WS-OTDR: Wavelength Scanning OTDR

		Acronym	Method	Volcano	Time and space samplings	Volcano applications	Bibliography
RAYLEIGH		OTDR	Incoherent distributed Rayleigh power sensing				Rayleigh, 1881 Barnoski, 1977
	STATIC	OFDR	swept wavelength interferometry				Kreger et al., 2016
	DYNAMIC STRAIN SENSING	ϕ -OTDR (DAS DVS)	Coherent distributed Rayleigh power sensing	Reykjanes Etna Aso Meagler Grimsvötn Laacher See Stromboli	Seismic, high frequency applications. Challenge for low frequencies, except in engineered fiber Typical freq: 0.1-500 Hz Typical sensitivity: few nanostrain Gauge length 5-30 m (for seismic usually 10 m)	Jousset et al., 2018 Currenti et al., 2021 Nishimura et al., 2021 Klaasen et al., 2021 Jousset et al., 2022 Fichtner et al., 2022 Currenti et al., 2023 Diaz-Meza et al., 2023 Bagioli et al., 2024 This chapter	Parker et al., 2014 Hartog et al. 2017 Posey et al., 2000 Peng et al., 2014 Tu et al., 2015 He et al., 2018 Chen et al., 2019
		WS-OTDR					
	CP- ϕ -OTDR	Rayleigh and Raman scattering		1 mK/4 nanostrain		Pastor-Grael et al., 2016 Xiong et al., 2018	
BRILLOUIN	DEFORMATION/TEMPERATURE	BOTDR	Brillouin OTDR	Etna	Long term deformation. Low sensitivity at high frequency. Typical frequencies: minutes Typical sensitivity: microstrain Gauge length 1-3 m	Gutscher et al., 2019 Murphy et al., 2022 Gutscher et al., 2023	Brillouin, 1914
		BOTDA					Horigushi et al., 1989
		BOCDA	Correlation-base technique				Hasagawa & Hotate, 1999
		BOFDA					Nöther et al., 2008 Wosniok et al., 2009 Bernini et al., 2012
RAMAN	TEMPERATURE	ROTDR/ROFDR	Raman OTDR/OFDR	Erebus Campi Fleigrei	10 minutes	Curtis & Kyle, 2011 Carlino et al., 2016 Somma et al., 2019	Raman, 1928 Grattan and Sun, 2000 Tyler et al., 2009 Briggs et al., 2011

S A G N A C	ROTATION		Rotational sensor	Hawaii Etna, Stromboli	High frequency	Wassermann et al., 2020 Eibl et al., 2022 Wassermann et al., 2022	Sagnac, 1913a,1913b
----------------------------	----------	--	-------------------	------------------------------	----------------	---------------------------------------------------------------------------------------	---------------------

2.1 Analysis of strain

The description of ground motion includes translation, rotation and strain components (Aki & Richard, 2002). This can be understood by analyzing the transformation of a body subjected to an external force (Müller, 2007; Schmelzbach et al., 2018). Let us consider a Cartesian referential system with x , y and z as the coordinate axes, and two close positions $P(x, y, z)$ and $Q(x + \Delta x, y + \Delta y, z + \Delta z)$ within the body on which a force is applied. The initial distance between points P and Q is denoted $PQ(\Delta x, \Delta y, \Delta z)$. Following the application of the force, point P moves to P' by the displacement vector $\mathbf{u}(u_x, u_y, u_z)$ and point Q moves to Q' by a displacement $\mathbf{u} + \Delta \mathbf{u}$.

In the linear theory of continuum mechanics, the transformation $PQ \rightarrow P'Q'$ is assumed to be linear. The components of the vector $\Delta \mathbf{u}$ can thus be written as

$$\begin{aligned}\Delta u_x &= \frac{\partial u_x}{\partial x} \Delta x + \frac{\partial u_x}{\partial y} \Delta y + \frac{\partial u_x}{\partial z} \Delta z + O(u_x^2), \\ \Delta u_y &= \frac{\partial u_y}{\partial x} \Delta x + \frac{\partial u_y}{\partial y} \Delta y + \frac{\partial u_y}{\partial z} \Delta z + O(u_y^2), \\ \Delta u_z &= \frac{\partial u_z}{\partial x} \Delta x + \frac{\partial u_z}{\partial y} \Delta y + \frac{\partial u_z}{\partial z} \Delta z + O(u_z^2),\end{aligned}$$

where we neglect, as indicated by the sign $O(\cdot)$, the second (and higher) order terms of the transformation. ∂ denotes the partial derivative operator. The transformation can be expressed in a matrix form $\left(\frac{\partial u_i}{\partial x_j}\right)$, where we use the Einstein summation convention on indices i and j , which can represent x , y or z . This matrix describes the gradient of the displacement at all points of a continuous medium. By decomposing

$$\frac{\partial u_i}{\partial x_j} = \frac{1}{2} \left(\frac{\partial u_i}{\partial x_j} + \frac{\partial u_j}{\partial x_i} \right) + \frac{1}{2} \left(\frac{\partial u_i}{\partial x_j} - \frac{\partial u_j}{\partial x_i} \right),$$

we find the first term to be strain (symmetric matrix) and the second term rotation (antisymmetric matrix), by definition. Therefore, one can generally express the transformation $PQ \rightarrow P'Q'$ as a combination of

- a translation \mathbf{u} (u_x, u_y, u_z);
- a strain $\boldsymbol{\varepsilon}$, which can be seen as the change of length of lines, and is defined by the tensor

$$\boldsymbol{\varepsilon} = \begin{pmatrix} \varepsilon_x & \gamma_{xy} & \gamma_{xz} \\ \gamma_{yx} & \varepsilon_y & \gamma_{yz} \\ \gamma_{zx} & \gamma_{zy} & \varepsilon_z \end{pmatrix},$$

in which the components are expressed by

$$\begin{aligned} \varepsilon_x &= \frac{\partial u_x}{\partial x}, \varepsilon_y = \frac{\partial u_y}{\partial y}, \varepsilon_z = \frac{\partial u_z}{\partial z}, \\ \gamma_{xy} &= \gamma_{yx} = \frac{1}{2} \left(\frac{\partial u_x}{\partial y} + \frac{\partial u_y}{\partial x} \right), \\ \gamma_{xz} &= \gamma_{zx} = \frac{1}{2} \left(\frac{\partial u_x}{\partial z} + \frac{\partial u_z}{\partial x} \right), \\ \gamma_{yz} &= \gamma_{zy} = \frac{1}{2} \left(\frac{\partial u_y}{\partial z} + \frac{\partial u_z}{\partial y} \right); \end{aligned}$$

- and a rotation of the whole region (including P and Q), defined by a tensor

$$\boldsymbol{\Omega} = \begin{pmatrix} 0 & \omega_{xy} & \omega_{xz} \\ \omega_{yx} & 0 & \omega_{yz} \\ \omega_{zx} & \omega_{zy} & 0 \end{pmatrix},$$

in which the components are expressed by

$$\begin{aligned} \omega_{xy} &= -\omega_{yx} = \frac{1}{2} \left(\frac{\partial u_x}{\partial y} - \frac{\partial u_y}{\partial x} \right), \\ \omega_{xz} &= -\omega_{zx} = \frac{1}{2} \left(\frac{\partial u_x}{\partial z} - \frac{\partial u_z}{\partial x} \right), \\ \omega_{yz} &= -\omega_{zy} = \frac{1}{2} \left(\frac{\partial u_y}{\partial z} - \frac{\partial u_z}{\partial y} \right). \end{aligned}$$

Rotation is sometimes expressed as a pseudo-vector $\boldsymbol{\Omega}_v = \begin{bmatrix} \Omega_x \\ \Omega_y \\ \Omega_z \end{bmatrix} = \begin{bmatrix} -\omega_{yz} \\ \omega_{xz} \\ -\omega_{xy} \end{bmatrix} = \begin{bmatrix} \omega_{zy} \\ \omega_{xz} \\ \omega_{yx} \end{bmatrix}$.

The three elements (translation, strain and rotation) are at the basis of the description of ground motion by the equation of motion (Aki & Richards, 2002; Müller, 2007; Schmelzbach et al., 2018), from which ground deformation and seismology originate from.

Global Navigation Satellite System (GNSS) measures ground displacement, and has been successful on many volcanoes (e.g., Palano et al., 2023). Its relative resolution is limited to several millimeters over distances of kilometers Applications of GNSS focus on large ground motions (larger than few millimeters) occurring over long term (days to months). Seismometers measure ground velocity or acceleration in the micrometer/second range, and form the basis of monitoring networks at many volcanoes. Broadband seismometers measure the three components of the seismic wave field over a typical range of 0.01-100

Hz. However, they are also sensitive to changes in the tilt of the instrument, as noted by Rodgers (1968). Tiltmeters can record long-term ground tilt (e.g., Gambino & Cammarata, 2017). In conventional seismology and volcano-seismology, the rotational components have been disregarded because they were thought to be sufficiently small (Bouchon & Aki, 1982). Until recently, portable instruments capable of detecting rotational components were not available, making direct measurement of rotation difficult. Strainmeters are designed to measure the strain field (Gladwin & Hart, 1985; Agnew, 1986). However, they often only measure certain components of the strain tensor, such as single axial components (Zumberge et al., 1988; DeWolf et al., 2015; Hatfield et al., 2022), volumetric strain (Linde and Sacks, 1995; Bonnacorso et al., 2016; Canitano et al., 2021) or 3-components of the strain tensor (Maccioni et al., 2019). The volumetric strain ($\epsilon_x + \epsilon_y + \epsilon_z$) can be accurately measured by dilatometers in boreholes (Sacks et al., 1971). These instruments provide a better understanding of volcano deformation processes at low amplitude and low frequencies (Linde and Sacks, 1995; Currenti & Bonnacorso, 2019). Studies have investigated higher frequencies of strain (> 0.1 Hz, e.g., seismic frequencies) and co-seismic strain changes associated with seismic events have been investigated in mines (McGarr et al., 1982; Ogasawara et al., 2005). Although some strain measurements exist on certain volcanoes, there are very few publications reporting volcanic strain at high frequencies (e.g., Di Lieto et al., 2020).

The description and interpretation of volcano-seismic wave fields have mainly been conducted using truncated observations of the ground motion. These observations only consider the translational components, neglecting both rotation and high-frequency strain. Volcanic processes generate a large variety of seismic signals, including volcano-tectonic events (VT, 3–40 Hz), long period events (LP, 0.2–5 Hz), very-long period signals (VLP, 0.05–0.2 Hz), tremor (~0.1–10 Hz), and volcano-explosive signals (VEQ, explosion quakes, ~1–10 Hz). Therefore, it is necessary to further explore the volcanological signatures of rotation and strain.

The development of fiber optic instruments provides new opportunities to access to the full wave field over a wide range of frequencies, enabling a more complete description of volcanic events and a better understanding of their nature. Figure 1 shows several portable instruments that use fiber optic technologies, allowing for the measurement of components of the full seismic wave field. The following section describes methods for sensing the translational, strain and rotational components of the seismic wave field at a point, followed by methods for distributed sensing of strain and temperature.

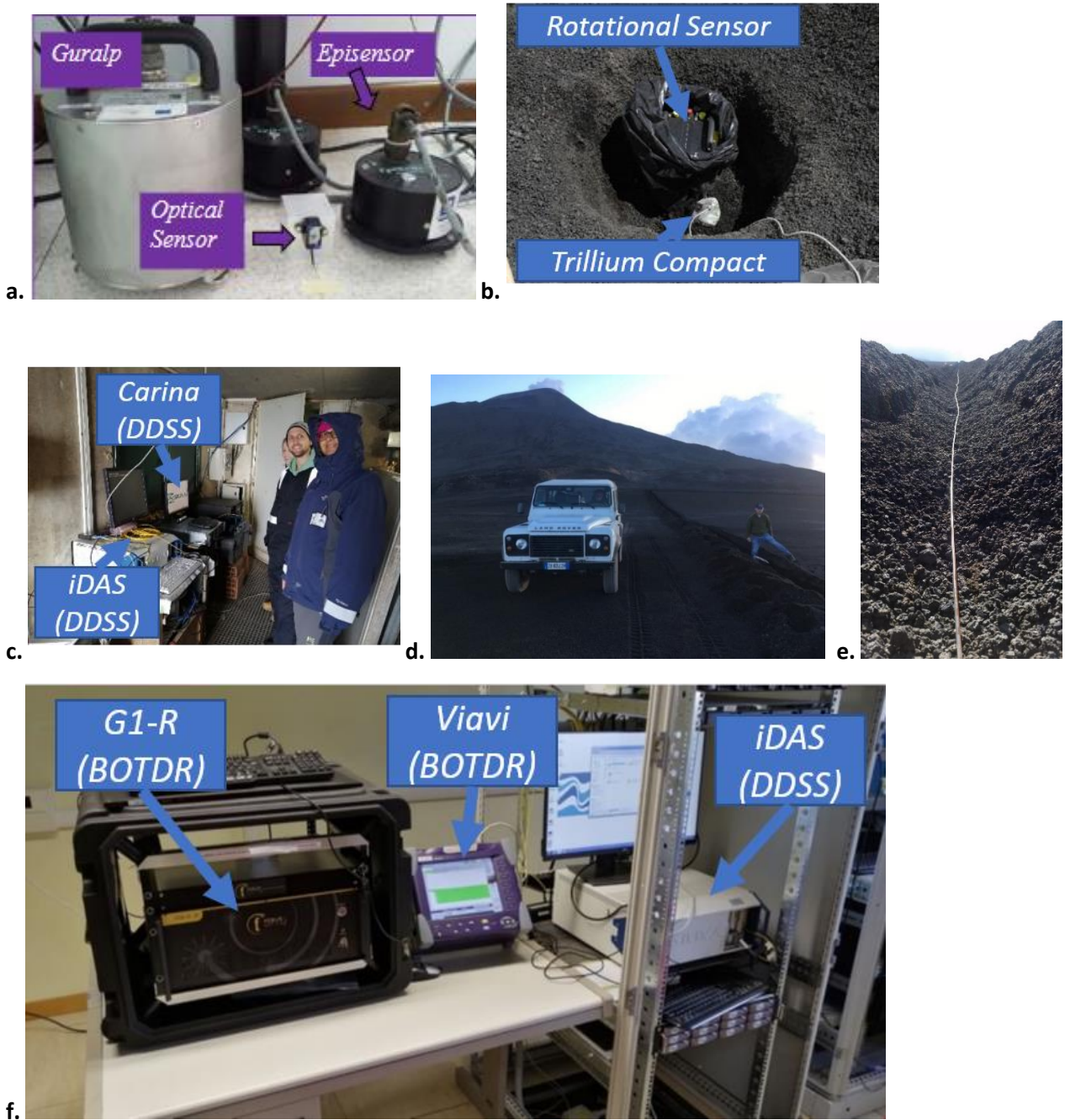


Figure 1. Pictures of several sensors using fiber optic sensing. BOTDR stands for Brillouin Optical Time Domain Reflectometry and DDSS stands for Distributed Dynamic Strain Sensing. These techniques are explained in detail in section 2.3. **a.** various seismic sensors: the optical sensor contains a micro-opto-mechanical cavity on a fiber tip (Pisco et al., 2018). Note the smaller size of the optical sensor as compared to other conventional sensors (picture from Pisco et al., 2018, supplementary information). **b.** rotational sensor and broadband seismometer deployed at Etna volcano (Eibl et al., 2022) (picture: E. Eibl, U. Potsdam). **c.** iDAS and Carina interrogators deployed at Pizzi Deneri observatory at Etna volcano in July 2019 (Picture: P. Jousset, GFZ). **d.** deployment of a fiber in a trench of about 30 cm depth at Etna volcano in July 2019 (picture: M. Weber, GFZ). **e.** standard telecom cable (~0.5 cm diameter) deployed in

the trench (picture: P. Jousset, GFZ). **f.** various Distributed Fiber Optic Sensing interrogators in the framework of the Focus Project (Gutscher et al., 2019; 2023): a BOTDR interrogator G1-R (Febus); a BOTDR (T-BERD) interrogator (Viavi); an iDAS interrogator (Silixa). Each of these interrogators is connected to a different fiber within a submarine cable of about 30 km length, belonging to the infrastructure from the European Multidisciplinary Seafloor and water column Observatory and from the Istituto Nazionale di Fisica Nucleare - Laboratori Nazionali del Sud (Italy – Sicily).

2.2. Fiber optic point sensing

2.2.a. Seismometer and strainmeter point sensing: the Fabry-Perot interferometer.

The Fabry-Perot interferometer is an optical cavity composed of two parallel light reflectors. It was designed by Perot and Fabry (1899) and has since then been utilized in numerous fiber optic point sensing devices to measure strain variation (Nur et al., 2016). The cavity can be between 0.1 and 1 mm in length and allows light to enter only when it resonates with the cavity. The resonance of the cavity enables the measurement of the light wavelength, or alternatively, when the cavity deforms, the resonance frequency changes for a fixed light wavelength. Instruments that use this principle include seismometers (Pechstedt & Jackson, 1995; Pisco et al., 2018; Feron et al., 2020), tiltmeters (Chawah et al., 2015) and strainmeters (Ferraro & De Natale, 2002; Coutant et al., 2015; Bernard et al., 2022).

For instance, Feron et al. (2020) developed an optical seismometer that utilizes Fabry-Perot interferometry. The EW, NS and vertical components rely on the distance between the end of a glass fiber that emits infrared laser light and a reflecting mirror on the mobile mass of a passive geophone (Seat et al., 2012). The space between the mirror and the glass fiber is the optical cavity, i.e., the Fabry-Perot interferometer. Coutant et al. (2015) developed a strainmeter that utilizes a series of Fabry-Perot cavities (~ 1 cm long) and a high-performing spectrometer to measure strain with great sensitivity over a large frequency band. The system has the advantage of being able to be interrogated at a long distance from the sensor via standard fiber optic cable. The sensor can be set up in a harsh environment, such as an active fumarole field, while the electronics can be located in a safer location. This ensures a longer life for the monitoring system.

2.2.b. Rotational sensors (Sagnac effect)

To measure the rotational component of the wave field, the so-called “Sagnac effect” is used (Sagnac, 1913a, 1913b), although its full understanding is still under discussion (Bhadra et al., 2022; Gautier et al., 2022). The technique involves an interferometer which analyses the light sent around a closed loop of a fiber optic cable (beams) mounted on a rotating platform. As the platform rotates, the interference fringes are displaced from their initial positions (when the platform is not rotating). Sagnac (1913a, 1913b) determined that the phase shift $\Delta \Phi_S$ of the interference fringes as being proportional to the rotation rate vector $\vec{\Omega}_v$ of the platform:

$$\Delta \Phi_S \approx \frac{8\pi A}{\lambda c} \vec{n} \cdot \vec{\Omega}_v,$$

where A is the area of the loop oriented by \vec{n} , λ is the light wavelength and c is the speed of light in vacuum. The phase difference is determined by multiplying the difference in travel times by the optical frequency c/λ , as stated by Lefèvre (2014).

Ground rotations were initially measured in laboratory conditions using records of artificial explosion signals (Nigbor, 1994) or large earthquakes (Igel et al., 2005). The development of portable rotational sensors has provided opportunities to gain a better understand of the composition of the seismic wave field from volcanic earthquakes. Rotational sensors measure the rotation directly, and hence also tilt of the ground. They are not sensitive to translational ground motion, as noted by Bernauer et al. (2012) and Kislov & Gravirov (2021). The seismic wave field consists of different phases, including body waves (P- and S-waves) and surface waves (Love and Rayleigh waves) (Aki and Richards, 2002). In a homogeneous medium, P-waves do not cause rotation. S-waves can be divided into polarized S-waves, and we refer to these as SH and SV waves, respectively. A three-component seismometer can detect all these phases. Volcano-tectonic earthquakes (VT) are generally triggered by the rupture of faults, which can be approximated by a double-couple source mechanism. As with tectonic earthquakes outside volcanic areas, P-waves are followed by S-waves and by surface waves, such as Rayleigh and Love waves. However, long-period events (LP) or long-lasting tremors have been explained by various source mechanisms. For example, resonance of fluid-filled fractures (Chouet, 1996) or of the volcanic conduit (Neuberg, 2000; Jousset et al., 2003; 2004), slow deformation processes (Bean et al., 2014), or fluid flow (Julian, 1994; Hellweg, 2000; Rust et al., 2008). The translational components from seismometer records may present challenges in distinguishing various seismic phases for LP events due to emergent and overlapping signals. For instance, it may be challenging to distinguish between P-waves polarized parallel to the propagation direction from S-waves polarized perpendicular to the propagation direction and the different surface wave types. However, a rotational sensor can be used to directly identify the wave field

composition of LP events or tremor. For a rotation sensor located at the free surface of a semi-infinite homogeneous medium, the vertical component is sensitive only to SH and Love waves, whereas its horizontal components are sensitive to SV waves or Rayleigh waves (Sollberger et al., 2018). As a first approximation, if the rotational sensor displays a signal in its vertical component only, then this signal represents a wave field which is dominated by SH waves, neglecting topography and subsurface structures.

The six-component (6-C) ground motion, consisting of three translational and three rotational motion components (see Figure 2), enables the derivation of ground properties from dispersion curves. Additionally, it provides information, including back azimuth (direction measured from north to direction of the incoming waves), phase velocities, and wave types, on transient signals such as earthquakes or tremor. One way to study transient signals is to estimate the back azimuth by using the similarity of the horizontal components of the rotational sensor (Wassermann et al. 2020; Yuan et al. 2020). Another approach involves using the similarity of the vertical rotation rate and the transverse acceleration to derive the back azimuth and phase velocity of the arriving waves (Hadziioannou et al., 2012, Wassermann et al., 2016). In theory, back azimuth estimation can be performed without any frequency constraint. However, at higher frequencies, the wave field may be affected by scattering of the seismic waves in the ground, which can result in less reliable back azimuth estimation compared to those obtained at lower frequencies. Additionally, the 6-C setup enables correction of the seismometer data for tilt contamination (Bernauer et al., 2020).

In 2018, Wassermann et al. (2020) deployed various sensors, including a rotational sensor, seismometers, accelerometers and tiltmeters, during the eruption at Kilauea volcano in Hawaii. They recorded three Mw 5 earthquakes and identified clear coseismic-rotation steps (offset in the value of the rotation measurement) in 3D (Wassermann et al., 2020). Wassermann et al. (2022) deployed three rotational sensors on Stromboli volcano, Italy. This allowed for the description of the wave field, which was composed of SV- and SH- type waves. The location of seismic events was determined using waveform similarity and a new class of volcanic events caused by jetting was detected. Eibl et al. (2022) conducted a study on translational and rotational sensor records at Etna volcano, Italy. The study aimed to evaluate the performance of a rotational sensor in comparison to a co-located seismometer and the INGV network concerning the detection and location of tremor and LP and VT events together with wave field characterization (see §3.2 of this chapter).

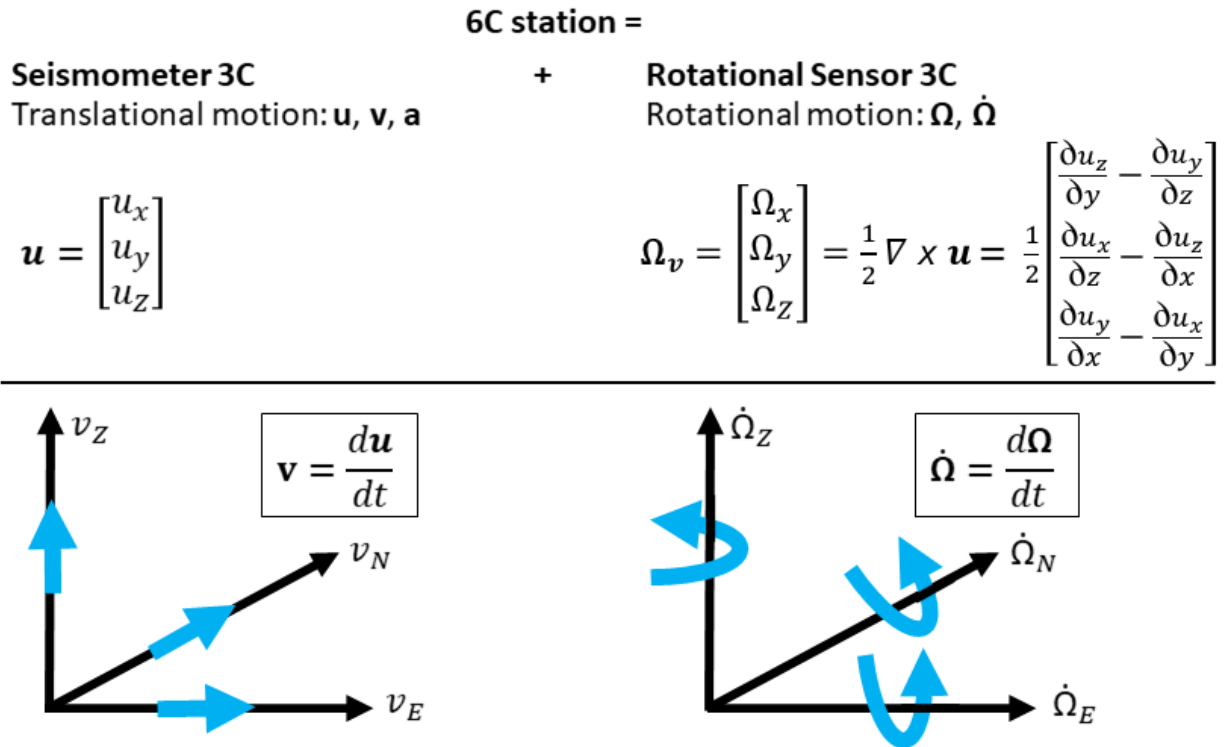


Figure 2. Definition of a 6C station composed of a co-located seismometer and rotational sensor. For notation see equations in §2.1. $\mathbf{u}, \mathbf{v}, \mathbf{a}$ stands for displacement, velocity and acceleration, respectively; Ω and $\dot{\Omega}$ are rotation and rotation rate, respectively; \times is the curl operator.

2.3 Distributed Fiber Optic Sensing (DFOS)

2.3.a. Fundamental concepts

Distributed Fiber Optic Sensing (DFOS) enables simultaneous strain (or strain rate) measurement at thousands of points using an unmodified optical fiber as the sensing element (Parker et al., 2014). The term “Distributed Fiber Optic Sensing” encompasses many techniques (Nickès & Ravet, 2010; Masoudi et al., 2013; Masoudi & Newson, 2016, 2017), all resulting in distributed measurements along the fiber (Table 1). The fundamental principle of DFOS involves an optical fiber connected to an interrogator. The interrogator comprises a laser that shoots light within the fiber and a system that analyses the modified properties of the light after its interaction with the glass (e.g., through scattering). The laser emits infrared light pulses, typically lasting a few nanoseconds, which propagate in the forward direction (interrogator towards fiber). The light scatters in all directions along the fiber and part of the scattered light then propagates backward towards the interrogator. A photo detector, also located in the interrogator detects the backscattered light, where it is also analyzed. Environmental parameters such as temperature, strain, pressure, and force can influence the properties of the backscattered light. The fiber

serves as both the carrier of the light and as the sensing elements. Interrogation methods can be conducted in either the time domain, using incoherent or coherent light pulses, or in the frequency domain, such as with swept wavelength interferometry.

The quantities typically measured for each emitted pulse include

- the time of flight, which is the travel time between the laser emitting the light pulse and its return to the photo detector;
- the amplitude of the backscattered light;
- the frequency or the phase of the backscattered light.

Various sensing techniques are being developed that use different

- scattering processes of the light within the optical fiber, such as Rayleigh, Brillouin and Raman (see below);
- type of light sent (coherent or incoherent light, pulses or frequency sweep);
- fiber structure, which determines how the light propagates in the fiber. The core diameter defines whether the fiber is so called “single mode” or “multi-mode”. Fibers can be “standard” (e.g., telecom fiber) or “engineered” to enhance light interactions with the glass for increased sensitivity.

To perform the measurement for time domain approaches, pulses are sent successively at a frequency of several kHz. When a pulse of light is sent, at any time, it spans a certain section of the fiber, over which the measurement is performed. Fast processing and analysis of the light amplitude and phase is conducted computationally after analog-to-digital conversion. The details of the complex processing on the light properties (phase and amplitude, stacking and filtering processing) depend on the interrogator. The outcome is a set of measurements distributed along the fiber, which provides information on various environmental parameters, such as axial strain and temperature probed over the gauge length. The acquired data, which can be extensive depending on the sampling rate (spatial and temporal) and the length of the probed fiber, is saved on a hard drive also located in or near the interrogator.

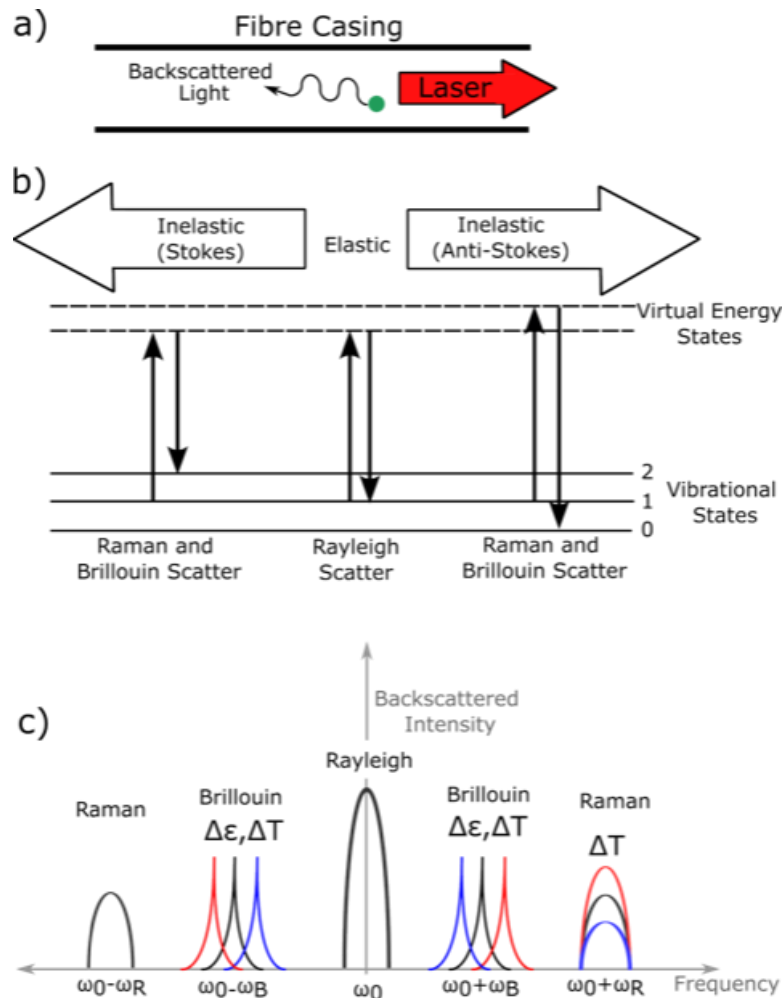


Figure 3. Distributed Fiber Optic Sensing (DFOS) techniques are based on sending coherent pulses at one end of the fiber and analyzing the backscattered light, after it has interacted with the fiber glass structure. a) An example of light backscattered by an inhomogeneity in the fiber optic cable. b) A schematic of the evolution of the energy state of the molecule/atom causing the backscattered light depicted in subplot a). Rayleigh scattering is an elastic process where the scattered energy equals the incidence energy of the laser. Brillouin and Raman scattering are inelastic processes that alter the vibration state of the atom or molecule in the fiber in two different ways. When the backscattered light has a lower frequency than the incident light, the medium has absorbed some of the light energy. This is referred to as the Stokes process. Conversely, when higher frequency light is emitted relative to the incident light, the medium has released some energy. This is referred to as the anti-Stokes process (Hartog, 2017). c) A summary of the expected location of the Rayleigh, Brillouin, and Raman spectra relative to the frequency ω_0 of the incident light (Muanenda et al, 2019). The Brillouin peaks shift from the original frequency toward higher frequencies with increasing temperature and strain (red line) and towards lower frequencies with decreasing strain/temperature (blue line). Only the anti-Stokes Raman spectra displays a variation in peak intensity with changing temperature, i.e., increasing (red line) or decreasing (blue line) temperature.

2.3.b Scattering of light with the fiber glass structure

When light is transmitted through an optical fiber in the forward direction, it interacts with the glass through scattering processes. The scattered light then propagates in the opposite direction (backward) until it reaches the photo detector. The wavelength of the incident source affects light scattering, which is also influenced by various parameters such as the size, shape, concentration and refractive index of the scattering particles. Irregular surfaces, even at the molecular level, can cause light to scatter in random directions. In optical glass fiber, the scattering of light is caused by compositional fluctuations, such as molecular level irregularities, in the glass structure, as noted by Archibald & Bennett (1978). Fluctuations in the fiber structure are caused by variations in glass density and compositional inhomogeneities. These are naturally acquired and frozen in the structure of the fiber during its fabrication process as the temperature decreases from the glass softening temperature (a few hundred degrees) to room temperature (Lu et al., 2019). Fig. 3 shows the frequency spectrum of the scattered light which typically involves three main scattering processes: Rayleigh, Brillouin and Raman scatterings.

Rayleigh scattering is an elastic process that does not alter the frequency of light.

Brillouin and Raman scattering are inelastic processes that cause shifts in the frequency of light (Bao and Chen, 2012; Lu et al., 2019). According to quantum mechanics, microscopic vibrations in solid media are quantized, meaning that vibration energy is exchanged in the form of so-called “phonons”. Phonons are collective excitations in a periodic, elastic arrangement of atoms or molecules which are condensed specifically in solids and some liquids. In simple terms, a phonon is a discrete unit of vibrational mechanical energy. It is calculated by multiplying the phonon frequency by the Planck's constant. Various vibration modes exist, each with different frequencies and thus phonon energies:

- Acoustic phonons are linked to long-wavelength vibrations, where neighboring particles oscillate almost in phase. They have relatively low frequencies, for example, in the gigahertz region;
- Optical phonons are linked to vibrations where neighboring particles oscillate almost in anti-phase. The frequencies of optical phonons are in the terahertz region, resulting in significantly higher phonon energies than those of acoustic phonons.

Phonons participate in both Brillouin scattering, which involves acoustic phonons, and Raman scattering, which involves optical phonons. In Raman scattering, an incident photon is converted into a photon with slightly lower energy, and a phonon carries away the difference in photon energies.

When a pulse of light is transmitted through the fiber, all scattering processes occur simultaneously. Each process is addressed using different instruments, resulting in numerous techniques and acronyms.

Optical Time Domain Reflectometry (OTDR), Rayleigh Scattering

In 1881, Lord Rayleigh demonstrated (Rayleigh, 1881) that light propagating in a medium is scattered by small particles within the medium, up to about a tenth of the wavelength of the light. The color blue to the sky is due to Rayleigh scattering off the molecules of the atmosphere. Rayleigh scattering in optical fibers is typically caused by refractive index fluctuations within the glass along the fiber. Rayleigh scattering results in a spectral broadening of the incident light without any frequency shift, which is an elastic scattering process. In a fiber glass, this principle is used to measure the time of flight, which is the time interval between emitting the light from the laser and observing the backscattered light at the photo detector. The distance d along the fiber can be calculated using the formula

$$d = \frac{c}{2n} t,$$

where t is the backscattered detection time, c is the speed of light in vacuum, n the average refractive index along the fiber; the factor 2 comes from the forward and backward travel of the light. The technique to measure the time of flight of the light between the interrogator and the scattering point is called Optical Time Domain Reflectometry (OTDR). As Rayleigh scattering occurs along a fiber, it is defined as a distributed fiber optic sensing method (Barnoski et al., 1977). The dynamic range in OTDR depends on the sensitivity of the equipment, including the pulse duration, pulse power, and photodiode sensitivity. A high pulse power with a wide pulse duration can increase the signal-to-noise ratio (SNR), allowing for long-distance measurements (typically tens of kilometers). However, this increase in sensitivity comes at the cost of spatial resolution, as the pulse is wider. If the power of the pulse is too high, non-linear effects may occur in the fiber, rendering the measurement irrelevant (Lu et al., 2019). Additionally, Rayleigh scattering is the primary cause of light intensity attenuation as it propagates through the glass (Personick, 1983). Telecommunication companies have been using OTDR for years to find faults, such as optical loss and reflections in their networks (Philen et al, 1982). The conventional OTDR used in testing telecommunication network quality employs pulses of 10 ns which correspond to 1-m resolution, while maintaining a high dynamic range. One of the great advantages of OTDR is that it only requires access to one end of the fiber to make measurements along the entire cable.

Distributed Dynamic Strain Sensing (DDSS), Rayleigh Scattering

Most Distributed Dynamic Strain Sensing techniques use Rayleigh (elastic) scattering (Masoudi et al., 2013) to measure the strain or strain rate of the fiber over the gauge length, which is caused by the strain in the ground transmitted to the fiber. This sensing technique is commonly referred to as “Distributed Acoustic Sensing”, although this term is inappropriate. Acoustic waves are linked to variation in pressure, which are characteristic of seismic P-waves, also known as “compression waves”. Rayleigh scattering can detect the ground strain tensor projected along the fiber direction, which is generated by any source of

dynamic strain, including pressure, shear, and vibration. Therefore, DDSS can record all seismic waves, including P-, S-, and surface waves rather than just pressure or P- waves (which are sometimes incorrectly referred to as “acoustic waves” by the oil and gas industry).

Techniques for retrieving distributed information from Rayleigh scattering use various measurement methods, which differ in the type of light, light pulse length, light pulse frequency content etc. For instance, Lu et al. (2019) describe several methods including OTDR (see above), phase-sensitive OTDR (φ -OTDR), which utilizes phase changes of the scattered light, polarization-sensitive OTDR (P-OTDR), which uses changes in the light polarization, and heterodyne OTDR (H-OTDR), which employs a complex pulse (Mussot et al., 2018; Naveau et al., 2021), Optical Frequency Domain Reflectometry (OFDR), where the analysis of the light is performed in the frequency domain and not in the time domain, etc.

The phase-sensitive OTDR (φ -OTDR) is a highly efficient technique for observing high-frequency strain associated with seismic and volcanic events, such as earthquakes and explosions. OTDR utilizes successive light pulses with a low coherency between them. In contrast, φ -OTDR is used to measure light phase changes. It is based on successive fully coherent pulses of light with a very narrow linewidth and a stable frequency laser. The coherence length of the laser light is much longer than the fiber length. The φ -OTDR implementation of Taylor and Lee (1993) measures the intensity resulting from the interference of light backscattered at different scattering points along the fiber as explained by Zhang et al. (2019). Using an interferometer (e.g., Mach-Zehnder interferometer, Zetie et al., 2000; Yang et al., 2003; Cai et al., 2015) the Rayleigh backscattered light’s phase φ_R is continuously analyzed in time, at all locations (time of flight) along the fiber (Masoudi et al., 2013, Parker et al., 2014; Masoudi et al., 2016; 2017). When a fiber section of length L is elongated or contracted by ΔL (due to external strain), a change in the relative positions of scatters induces a small phase change $\Delta\varphi_R$ in the backscattered light between two successive pulses. The phase change is expressed as

$$\Delta\varphi_R = \frac{4\pi n\zeta}{\lambda} \Delta L,$$

where λ is the wavelength of the light pulse, ζ is a material dependent constant around 0.78 for fiber glass (SEAFOM, 2018), n is the group refractive index (usually 1.468). This equation enables the accurate retrieval of the fiber elongation/contraction using an interferometer. The measured signal is the dynamic strain rate, as the interrogator analyses changes in strain over time (Lu et al., 2019). Temperature also affects the refractive index resulting on an apparent phase change. Therefore, the resulting signal contains both strain and temperature effects that cannot be distinguished. When the strain signal has a frequency content much higher than that of temperature changes, such as in high frequencies

applications in seismology, optical dispersion is neglected and the refractive index is assumed to be constant over time (Lindsey et al., 2020).

As light propagates through the fiber over long distances, its amplitude decreases due to attenuation, which in turn reduces the signal-to-noise ratio. The attenuation of light depends on the refractive index profiles along the fiber and the material itself. Furthermore, it is necessary to ensure that the backscattered light is completely returned before shooting the next pulse to avoid interferences between successive pulses. Hence, for longer cables, the number of pulses per second need to be reduced, decreasing the bandwidth. The strain rate resolution and sensitivity are therefore reduced with increasing fiber length. Increasing of the pulse duration or the gauge length has a significant impact on overall sensitivity and range of interrogation, but at the expense of the spatial resolution. Artificial discontinuities in the refractive index distribution can be introduced in so called “engineered fibers” to increase the signal-to-noise ratio (Shatalin et al., 2021). The benefits of using engineered fibers over standard telecom fibers were illustrated at Etna volcano (Diaz-Meza et al., 2023).

Distributed Dynamic Strain Sensing (DDSS) is well-suited for monitoring strain changes associated with the seismic wave field. It provides more accurate results on single-mode fibers, although experiments have been successfully carried out with multi-mode fibers (Chen et al., 2018; Jousset et al., 2022). The method was first used in the oil and gas industry and has been adopted by the Earth Sciences community for hazard assessment, including detection and characterization of landslides (Huntley et al., 2014; Lienhart, 2015; Picarelli et al., 2015; Michlmayr et al., 2017; Schenato, 2017; Kogure & Okuda, 2018), teleseismic earthquakes (Dou et al., 2017; Lindsey et al., 2017; Jousset et al., 2018; Wuestefeld et al., 2023), volcano-tectonic earthquakes (Jousset et al., 2018; Nishimura et al., 2021), volcanic long-period events (Currenti et al., 2021), volcanic very long period signals (Currenti et al., 2023), volcanic tremor (Fichtner et al., 2022; Jousset et al., 2022) and volcanic explosive activity (Currenti et al., 2021; Jousset et al., 2022).

Distributed Strain and Temperature Sensing (DSS), Brillouin Scattering

Leon Brillouin (Brillouin, 1914) predicted light scattering from propagating acoustic phonons (see definition earlier). Acoustic waves that are thermally excited create periodic density waves, resulting in changes in the refractive index of the fiber glass. This process causes a frequency shift of the scattered light, which depends on the velocity of the sound wave. Measurable parameters in a Brillouin scattering spectrum comprise the Brillouin frequency ν_B , the Brillouin spectrum linewidth, and the Brillouin intensity (Lu et al., 2019). The measurement involves stacking records from successive pulses over integration time ranges of several seconds to minutes. Brillouin-based distributed sensors can address

both static strain and temperature over long distances, typically exceeding 10 km (Horiguchi et al., 1995; Soto & Thévenaz, 2013).

BOTDR (Brillouin Optical Time Domain Reflectometry) is a technique that involves the analysis of Brillouin scatter through the use of OTDR. It is based on the detection of spontaneous Brillouin scattering light and was developed by Kurashima et al. (1990; 1993). BOTDR is *de facto* the most established technique for use in Earth Sciences. This method requires access to only one end of a fiber, as conventional OTDR. The location of the strain/temperature change along the cable can be determined simultaneously using Rayleigh scattering (with OTDR). BOTDR involves the interaction of the light with fiber properties that are sensitive to strain and temperature. The Brillouin frequency shift increases in proportion to the temperature or strain induced in the fiber. The change in strain $\Delta\varepsilon$ and/or temperature ΔT that the fiber experiences relative to the initial recording can be expressed as:

$$\Delta\nu_B = \Delta\varepsilon C_\varepsilon + \Delta T C_T,$$

where $\Delta\nu_B$ represents the change in Brillouin frequency observed at two different recording times. The strain coefficient C_ε and the temperature coefficient C_T range from 0.04 – 0.05 MHz/ $\mu\varepsilon$ and 1.08 – 1.26 MHz/ $^\circ\text{C}$ respectively (Bao and Chen, 2012; Galindez-Jamioy & López-Higuera, 2012), depending on the fiber type (Lu et al., 2019). The change in frequency is caused by a linear change on the cable to the external strain tensor projected along the fiber (Horiguchi et al., 1989) and/or in temperature (Kurashima et al., 1990). One significant advantage of BOTDR is that measurements using the same fiber can be performed independently at two different times (weeks or months), yet the difference between the two measurements remains valid. Although several improvements have been attempted (Chow et al., 2018), BOTDR remains less sensitive than DDSS (Bao and Chen, 2012). The spatial resolution depends on the pulse width (Thévenaz, 2010). Typically, BOTDR sensing range spans 1 to 100 km, with a spatial resolution from 0.2 to 100 m, a temperature accuracy from 0.37 to 5 $^\circ\text{C}$ and a strain accuracy from 7.4 to 100 $\mu\varepsilon$. Some recent instrument providers claim a strain accuracy of 1 $\mu\varepsilon$.

BOTDR has various applications, including structural health monitoring (Ohno et al., 2001), studies on gravitational instabilities (Sun et al., 2016), submarine faults (Gutscher et al., 2019) and sinkhole detection and monitoring (Linker and Klar, 2017). Zhang et al. (2018) have successfully converted strain to displacement in the case of a field shear test where the orientation and width of the shear zone relative to the cable, as well as the cable coupling, were known *a priori*. Like DDSS, distributed strain sensing (DSS) is highly dependent on cable coupling with the surrounding media. Geotechnical pull-out tests have demonstrated that there are three degrees of cable coupling, dependent on the amount of shearing: elastic (fully coupled), elastoplastic (partially coupled) and purely plastic (decoupled) (Zhang et al., 2016). Different strain-displacement relationships have been developed based on the degree of cable

coupling (Zhang et al., 2018). Initial laboratory tests indicate that block and tube anchors on fiber cables increase cable-sediment coupling (Wu et al., 2020). However, further experimental studies are required in order to better understand their effect on both coupling and observed strain distribution.

BOTDR is based on spontaneous Brillouin scattering which involves analyzing backscattered light. An alternative approach is to use stimulated Brillouin scattering whereby two light sources propagating in opposite directions cause a stimulated Brillouin scattering along the cable (Bao & Chen, 2012; Bao et al., 2021; Lu et al., 2019). The interaction of the two wave types travelling in opposite directions creates acoustic waves through electrostriction. This phenomenon is utilized in a number of distributed techniques using various types of light signals at either end of the fiber, leading to enhanced Brillouin scatter (Hartog, 2017). For instance, Brillouin Optical Time Domain Analysis (BOTDA) involves shooting a pulse and continuous wave into the fiber at both ends. Brillouin optical frequency-domain analysis (BOFDR) operates similarly, but with the pulsed signal substituted with a frequency modulated continuous wave (Horigushi et al., 1989). The advantage of these techniques is that they provide rapid temperature and strain sensing at high resolution along the cable (Hartog, 2002; Culshaw, 2004, Ravet, 2011; Bernini et al., 2012). However, the disadvantage is that access to both ends of the fiber is required and should the cable be cut, measurements are no longer possible. Brillouin optical coherence domain analysis (BOCDA) involves shooting frequency modulated light waves at either end of the fiber and using the correlation of the two signals within the fiber to observe Brillouin scatter at a precise location along the cable (Hasegawa & Hotate, 1999; Song & Hotate, 2007). This technique can provide millimeter-scale resolution rapidly at specific locations. However, scanning the entire cable can take longer compared to other distributed techniques, such as BOTDA and BOFDR. Like for BOTDA and BOFDR, access to both ends of the cable is required.

Experiments in Geosciences have primarily focused on landslide environments (Sun et al., 2016; 2022), where fibers are deployed specifically to cross high strain deformation zones. This indicates the potential for studying deformation over large spatial scales in volcanic settings. A BOTDR experiment is currently underway in the eastern region of Etna volcano beneath the Ionian Sea. The aim is to detect strain associated with fault movement and its link to Etna's volcanic activity (Gutscher et al., 2019; see also §3 of this chapter).

Distributed Temperature Sensing (DTS), Raman Scattering

Chandrasekhara Venkata Raman first reported Raman (inelastic) scattering in 1928 (Raman, 1928). This scattering process occurs when photons interact with the natural high frequency vibrations of bonds

between atoms or molecules in the fiber glass. The scattered photons are emitted in a different frequency spectrum than that of the initial light. Distributed Raman measurement systems can use either time-domain or frequency domain techniques to extract distributed information. Distributed Temperature Sensing (DTS) is a type of distributed sensing based on Raman scattering that address temperature sensing through the measurement of the light property variations, and without sensitivity to strain (Watson et al., 1981). Temperature changes affect the Raman spectrum in three ways: Raman frequency shift, intensity and peak width (Lu et al., 2019). Only the anti-Stokes Raman spectra exhibit a variation in peak intensity relative to temperature changes (Fig. 3). Therefore, comparing the ratio of the anti-Stokes and Stokes intensities provides a measure of the temperature (Ukil et al., 2011). The resolution and distance measured depend on the laser power used. However, if the power used is too high, accurate measurements cannot be obtained, due to interference between the laser light source and the Raman scattered light. Long distance measurements above a certain power of laser light are hindered by this issue. For example, a 10 km fiber can be measured with a maximum power threshold of about 3W (Lu et al., 2019). Achieving better temperature resolution necessitates a longer measurement time, typically ranging from minutes to hours. The most commonly used technique is Raman OTDR. Commercially available DTS systems usually provide spatial resolutions of 1-meter or less, utilizing a laser with a light pulse width of 10 ns or less. DTS has a better resolution when light is transmitted in multimode fibers. For example, Liu et al. (2018) designed a dedicated fiber and resolve 1°C temperature with a spatial resolution of 1.13 m at a distance of 25 km, and average measurement of 90 s.

DTS finds most of its applications in ground water temperature projects, such as coal, oil and gas, and geothermic studies. There are few examples of DTS applications in volcanology, such as at Mount Erebus, Antarctica (Curtis & Kyle, 2011), at Campi Flegrei (Southern Italy) with submarine temperature profiling (Carlino et al., 2016) and borehole temperature monitoring (Somma et al., 2019).

2.3.c. Gauge length, instrumental response and limitations

Gauge length and spatial sampling

DFOS provides a quasi-continuous spatial profile of strain measurements along the optical fiber, spanning several tens of kilometers. The sensing section of the fiber is defined by the length of the pulse launched in the fiber, which although short in duration (a few nanoseconds), has a certain spatial length. The length of the sensing section can be adjusted by varying the duration of the pulse. The gauge length refers to the section of the fiber from which backscattered light is effectively sampled and analyzed in terms of intensity, frequency or/and phase. The integrated value of temperature and/ strain is typically allocated to the midpoint of the gauge length along the fiber (Dean et al., 2016). As time passes, the

pulse propagates and another section of the fiber is probed and allocated to the middle point of that section. For any given gauge length, the spatial sampling refers to the distance between the midpoints, where the measurement over a gauge length is recorded. Therefore, each measurement covers a gauge length and is not a single point measurement. The analysis of the successive spatial sections may overlap, depending on the gauge length and the required spatial sampling for the records. Independent records are separated by a distance equivalent to at least one gauge length. The sensitivity of each measurement decreases as the gauge length becomes shorter. The user can choose the spatial sampling (SS) and the gauge length (GL) depending on the objective of the study. Typical values for DDSS of a ~20 km long fiber could be GL=10 m, SS=4m resulting on 5000 records of dynamic strain per time sample. According to Jousset et al. (2018), a gauge length of 10 meters is the optimal value for dynamic strain sensing in seismology studies (0.1 – 100 Hz).

Instrumental response, frequency range

Until 2017, the use of fiber optic sensing in geophysics was primarily focused on seismic frequencies commonly used in the oil and gas industry (>1-100 Hz). The objective was to obtain more precise measurements in boreholes, which could replace strings of geophone observations (Daley et al., 2015). The goal of these studies was to accurately define the geometrical structure of the reservoir by obtaining precise seismic phase contrasts. Recorded amplitudes are poorly constrained at low frequencies (< 0.5 Hz), even in boreholes (Becker et al., 2017). DDSS instruments with cables deployed at the shallow surface of the Earth have also measured low frequencies, which expands their potential applications beyond boreholes. Examples reporting low frequencies associated to surface waves (20 s) from remote large earthquakes include the Indonesia Mw 7.4 earthquake recorded in Iceland (Jousset et al., 2018) as well as several other earthquakes, such as Alaska's Mw 7.9 (Lindsey et al., 2020), and the Turkey earthquake on 14.02.2023 (Jousset et al., 2023). At lower frequencies (below 30 seconds), the temperature effect increases, and may obscure low frequencies of geophysical interest.

2.3.d. Validation of fiber optic rotational and distributed dynamic strain sensing

Recent technological advances have made it possible to sense rotation and dynamic strain with high spatial and temporal resolution over a broad frequency range, using rotational sensors and Distributed Dynamic Strain Sensing. This allows for probing the full wave field. However, the application of both rotation and DDSS in seismology and volcanology is an emerging field. Therefore, many open questions arise regarding the DDSS response and the coupling between the fiber and the ground, which are strongly dependent on the fiber installation conditions.

Understanding records in detail can be challenging, especially when dealing with BOTDR, DDSS and DTS measurements. These measurements do not correspond to a single point, unlike conventional point sensors, but rather represent an integrated response over a certain distance (the gauge length). Therefore, direct comparison with point source measurements is not simple. Preliminary experiments were conducted to validate DDSS measurements by comparing them with indirect strain estimates from co-located or nearby conventional sensors, such as geophones and broadband seismometers (Daley et al., 2015; Bona et al., 2017; Jousset et al., 2018; Wang et al., 2018; Yu et al., 2019; Lindsey et al., 2020). Estimates of strain and rotational fields can be obtained indirectly by using conventional sensors that are adequately deployed to reproduce displacement gradients (Oliveira & Bolt, 1989; Bodin et al., 1997; Jousset & Rohmer, 2012; Van Renterghem et al., 2018). These estimates can then be compared with observations from the new sensors. Estimates of strain and rotational components have been relevant in numerous seismic (Basu et al., 2013; Langston, 2018) and geodetic studies, including strainmeter response and calibration (Currenti et al., 2017; Donner et al., 2017), performance of rotational seismometers (Suryanto et al., 2006), computation of strain rate maps (Shen et al., 2015), estimates of the stress field induced by the passage of seismic waves (Spudich et al., 1995), determination of seismic phase velocity (Gomberg & Agnew, 1996; Spudich and Fletcher, 2008) and estimates of wave attributes (Langston and Liang, 2008). In general, the methods can be grouped in two main families, relying on single or multiple station methods.

On the one hand, the single station method utilizes the property that strain rate can be derived from the ground velocity records knowing the ground phase velocity (Mikumo & Aki, 1964; Jousset et al., 2018; Lindsey et al., 2020). However, determining the ground phase velocity is not straightforward and requires approximations on both the wave field and the subsurface velocity structure. This method is only relevant to seismology. It has been widely used to estimate dynamic gradient displacements, the strain tensor (Gomberg & Agnew, 1996; Langston and Liang, 2008) and rotational components from the translational components of a 3C seismometer. This assumes that seismic energy is carried by plane waves with known horizontal velocity in a laterally homogeneous medium.

On the other hand, multiple station procedures involve using of displacements or velocity recordings from dense arrays of at least three closely located sensors (Basu et al., 2013, 2017; Currenti et al., 2017). In this case, spatial interpolation approaches (Sandwell, 1987; Paolucci and Smerzini, 2008; Sandwell and Wessel, 2016) or the seismo-geodetic method (Spudich et al., 1995; Shen et al., 2015; Basu et al., 2013; Langston, 2018; Yuan et al., 2020) are used to process the measurements. Various interpolation schemes have been developed to derive maps of the displacement field from which gradient components can be analytically or numerically computed. In addition to geostatistical approaches, which are generally used

for optimal interpolation of a discrete scalar field, several interpolation schemes have been formulated using the solutions of suitable elasticity problems (Paolucci & Smerzini, 2008; Shen et al., 2015; Currenti et al., 2021). Sandwell and Wessel (2016) provide a thorough review of these latter methods. The seismo-geodetic method is based on the Taylor expansions of the displacement field of first (Spudich et al., 1995) or higher order derivatives (Basu et al., 2013; Langston, 2018). Both interpolation and seismo-geodetic methods have been used for seismic dynamic and geodetic quasi-static strain estimates. The single station procedure provides strain estimates at the exact position of the sensor, while the other two methods use sensor array measurements to derive maps of strain and rotational components at irregular grid points.

In 2019, a DDSS interrogator, a dense seismic array consisting of 26 Trillium Compact – 120 s broadband seismometers and a rotational sensor were jointly deployed at Etna summit. This deployment provides a unique opportunity to observe and accurately quantify the strain and rotational ground motions generated by volcanic activity (Currenti et al., 2021; Eibl et al., 2022). The direct DDSS and rotational measurements associated with an LP event on 27 August 2021 correspond well with the indirect strain and rotation estimates derived by the dense seismic array (see Fig. 4). A similar agreement is also observed using the single station method at co-located sensors (Currenti et al., 2021; Eibl et al., 2022). Overall, there is a good agreement between the array-derived strain and DDSS measurements along the fiber optic cable. Short wavelength discrepancies correspond with fault zones, indicating the potential of DDSS for mapping local perturbations of the strain field and thus site effects due to small-scale heterogeneities in volcanic settings (Pätzelt, 2023). These findings validate both the proposed methods and the accuracy of DDSS (Currenti et al., 2021), which was further confirmed by Bagioli et al. (2023) at Stromboli volcano.

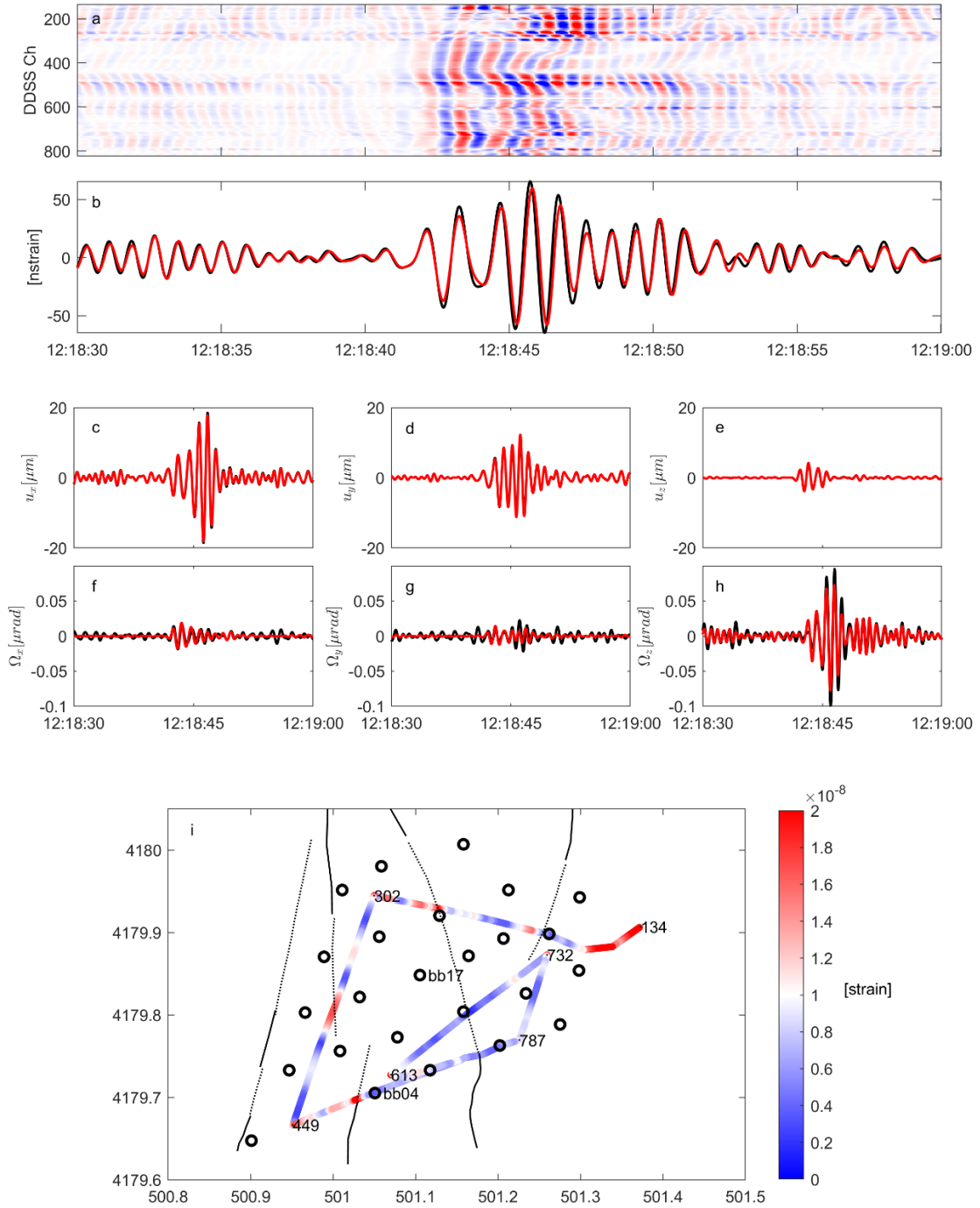


Figure 4. Comparison between rotation and strain derived from a broadband seismic array (26 Trillium Compact 120 s sensors) and records from a rotational sensor and distributed dynamic strain sensing during a Long-Period event at Etna volcano (27 August 2019). **a.** DDSS strain is obtained by integrating the DDSS strain rate records over time. Data is filtered in the frequency range 0.6 to 1.4 Hz. **b.** Strain estimated from the seismic array using the biharmonic interpolation method (Sandwell; 1987) and projected along the fiber direction (red line) and measured DDSS strain at channel 501 (black line) close to bb04. **c-e.** Displacements u_x , u_y , u_z obtained by integration of the velocity components at the broadband sensor bb17 (black line) and array derived displacements (red line). **f-h.** Rotations Ω_x , Ω_y , Ω_z

computed by integrating the rotation rates measured by blueSeis-3A sensor at bb17 (black) and array derived rotations (red line). In **c-h**, data at bb17 station are omitted from the interpolation computation. **i**. Root Mean Square residuals between DDSS strain measurements (from panel **a.**) and strain derived from the seismic array along the fiber for the LP event. Black lines and open circles indicate faults and seismometers deployed in the test area, respectively. In **i**, geographic coordinates (in km) are in the UTM33S system. The rotational sensor is located at the same location as bb17.

3. Fiber optic sensing for volcano research

3.1 Motivation

Volcanology aims to understand the structure and processes involved in the distribution and transfer of mass and energy within a volcano. This is achieved through the interpretation of volcanic signals associated with earthquakes, deformation and fluid flows. This section illustrates the benefits of using fiber optic technologies and their ability to probe the full seismic wave field, addressing fundamental questions in volcanology relevant to monitoring:

1. Volcano-seismology: event detection and location.

Volcanic events generate seismic waves and infrasound acoustic signals, which can be used to determine their source location. Accurately estimating the location of volcanic activity is crucial for effective volcano monitoring. Volcano-seismology seeks to comprehend volcanic processes by identifying the source mechanism of the various volcanic events using signals generated within a volcano (Chouet & Matoza, 2013; Jousset et al., 2022). VT earthquakes suggest a highly stressed zone at shallow depths, associated with the ascent of magmatic bodies that may reach the ground surface. The detection and location of earthquake hypocenters depend on well-designed networks of individual seismic sensors (Toledo et al., 2020). We provide examples on land and in submarine environments using DFOS and/or rotational instrumentation, with the aim of locating the source of seismic VT and LP events.

2. Structural features imaging.

Accurately determining earthquake hypocenters is limited by poor knowledge of the seismic velocity distribution within the volcano structure (Koulakov & Shapiro, 2021). Studies have shown hypocenter determination is ineffective without a proper velocity model. Numerous projects in seismology, volcanology and geothermal studies are utilizing an increasingly number of sensors, e.g., the USarray (Burdick et al., 2009), and the iMush network at Mount St Helens

(Hansen et al., 2016) and in geothermal studies, e.g., the IMAGE network (Blanck et al., 2020). Fiber optic methods have also begun to contribute to seismic tomography (Biondi et al., 2023). We focus here on several examples illustrating how DFOS can determine structural features, including the location of faults and subsurface ground structure.

3. Volcano dynamics.

Proper interpretation of the signatures of volcanic phenomena, such as long-term deformation, is crucial for effective monitoring. Understanding the processes that trigger these phenomena, such as gas flux in the volcanic conduit is also essential. Fiber optic technologies have been shown in several studies to improve our knowledge on volcanic processes. Here, we provide examples of two end-members in degassing processes: volcanic explosions and passive degassing. We also demonstrate how fiber optic sensing can help in understanding long-term deformation processes.

3.2 Volcano seismology: volcanic events detection and location with fiber optic methods

Active volcanoes encompass a great variety of processes, and thus generate a great variety of signals including VT earthquakes and LP events. Locating their hypocenters is fundamental for volcano monitoring, as they may indicate where stress accumulates due to magma and volcanic fluid transfer. For instance, volcano-tectonic earthquakes are typically located by measuring the arrival times of seismic P- and S-waves generated by rock rupture. To accurately locate earthquakes and determine their occurrence time, a minimum of four seismic stations is required. However, the optimal distribution of the stations for perfect earthquake location is unfortunately earthquake location dependent. An “ideal” network should then be capable of locating earthquakes at various depths and within the span of the network (Toledo et al., 2020). This is one reason why volcano-seismologists often deploy large-N networks, which cover the entire volcano. The use of DFOS offers the advantage of natural densification of observation points with a single cable, resulting in dense information of travel times. A significant step in seismology has been achieved by the use of so-called “dark fibers”, which are unused fiber optic telecommunication infrastructures (Lindsey et al., 2017; Jousset et al., 2018). However, despite the dense distribution of records obtaining the “ideal” network for accurate earthquake locations with fiber optic cable may not be possible, depending on the cable layout. When there is no pre-existing fiber optic infrastructure, such as at most volcanoes, installation of the fiber is necessary. This can be performed at wish, e.g., for monitoring purposes, yet within the limits of the physical constraints of the volcanic site (Currenti et al., 2021; Klaasen et al., 2021; Fichtner et al., 2022; Jousset et al., 2022). There have been few reported examples of using fiber optic cables to detect and locate earthquakes in the literature

(Jousset et al., 2016, 2018; Reinsch et al., 2016; Lindsey et al., 2017). Jousset et al. (2018) demonstrated that DDSS can be used on dark fiber to detect and locate a volcano-tectonic (VT) earthquake in Reykjanes, even in a not-ideal cable configuration. For other types of volcanic events, such as tremor, long-period events, pyroclastic flows, and explosions, the arrival times of the seismic waves may not be accurately determined. Therefore, other methods of event location have been developed, such as relative amplitude location methods (Jolly et al., 2002; Battaglia et al., 2003). The amplitude method presents challenges when used with fiber optic cable due to the increased sensitivity of strain signals to local variations caused by subsurface heterogeneities, and the spatial amplitude variations generated by coupling variability of the cable (Nishimura et al., 2021). However, the spatially dense data enables the use of coherency methods, which compares the similarity of densely recorded signals (e.g., Schwarz, 2019; Jousset et al., 2022). In the following, we illustrate several examples of detecting and locating volcanic long-period (LP) events using DDSS. Additionally, an example is provided on how to analyze the volcano-seismic wave field using a rotational sensor.

Seismic LP swarm analysis (Mayotte, Indian Ocean)

In May 2018, a seismic swarm began in Mayotte (Indian Ocean) accompanied by ground subsidence (Cesca et al., 2020, Lemoine et al., 2020). A year later, a new volcanic edifice, over 800 m height above the sea floor, was discovered 50 km east of the island (Feuillet et al., 2021). As of the summer of 2022, the seismic activity was still ongoing with earthquakes felt daily by the population (REVOSIMA, 2021). The volcanic activity has generated various types of earthquakes, including VT, LP and VLP events. LP events occur in swarms lasting a few tens of minutes and have a frequency band between 0.5 and 6 Hz (Retailleau et al., 2022). The monitoring network consists of land seismic stations. However, strong anthropogenic noise hinders detailed analysis of the sequence of LP events. In October 2020, DDSS recordings were conducted on an existing telecommunication fiber optic cable that extends from Mayotte island towards the east at the ocean bottom (Fig. 5). The DDSS records allow for the identification of individual LP events within the swarm, except for the on-land part of the cable (0-5 km). Beyond 5 km, the cable is situated in the lagoon and then subsequently enters the ocean, where successive LP events can be more accurately identified.

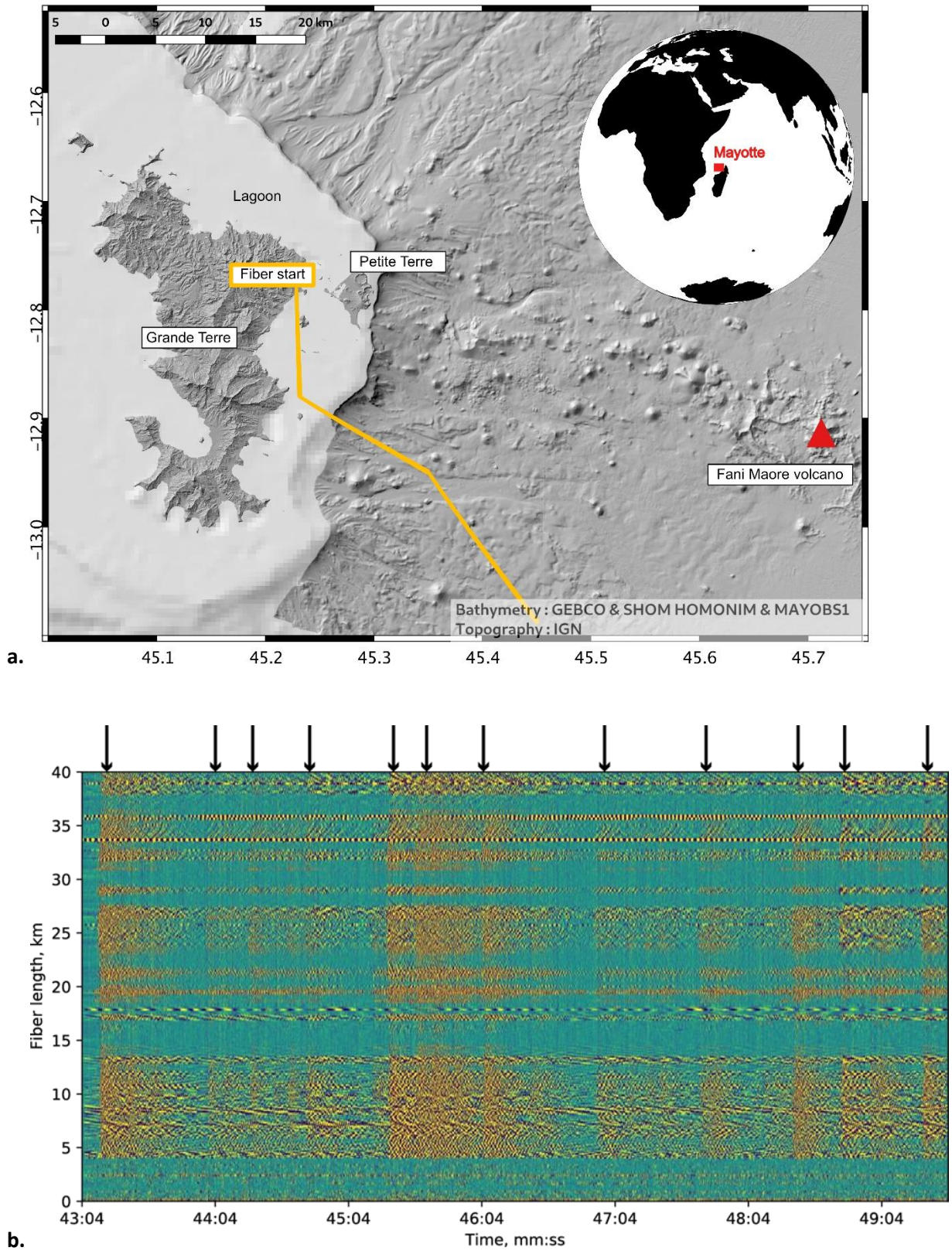


Figure 5. a. Map of Mayotte and the fiber optic cable in orange. This telecommunication cable interlinked Comoros main island to Mayotte. The volcano is represented by the red triangles. **b.** LP swarm recorded on the 11th October 2020 at 23:43 UTC. Vertical arrows identify the occurrence times of single LP events during the swarm.

Locating volcanic low-frequency earthquakes (Mt. Azuma, Japan).

Volcanic long-period (LP) earthquakes and tremor have been associated with various source mechanisms, such as volcanic fluid movement (Chouet, 1996). These events are difficult to locate due to the ambiguous emergence of P- and S-wave onsets. However, seismic arrays consisting of several to tens of seismometers deployed within a small area can record correlated seismic waveforms. By measuring the arrival time differences of coherent waveforms at the array sensors, it is possible to locate LPs and tremors. Deploying seismic arrays with a large aperture and recording seismic signals at all stations simultaneously is a challenging task. Nishimura et al. (2021) demonstrated the usefulness of DDSS records at Mt. Azuma, Japan, for locating LP events and tremor. Azuma volcano comprises andesitic edifices, including Issaikyo, Azuma-Kofuji, Higashi-Azuma, and Takayama. Volcanic activity during the Holocene period occurred around Jododaira (Fig. 6a). The fiber optic cable at Mt. Azuma extends along a winding road on the southern flank from the active craters. However, its spatial distribution is not optimal for accurate hypocenter determination (Fig. 6). To locate the hypocenters as accurately as possible, Nishimura et al. (2021) used arrival time differences and amplitudes of LPs. Each LP has a different spatial resolution. The differences in arrival time, measured for pairs of channels along the fiber cable, are related to the propagation direction of seismic waves. However, the resolution deteriorates for locations far from the cable. The amplitudes of LPs are corrected by the coda waves of regional earthquakes to evaluate the site amplification factors at each measurement point. The spatial resolution worsens in the east-west direction because the cable mainly runs in the north-south direction. To improve the spatial resolution as much as possible, the source locations are determined by minimizing residuals between observed and theoretical data for both arrival time differences and amplitudes using a grid search. The estimated locations of LPs are distributed very close to an active crater, and match well with the hypocenters determined using onset times of P- and S-waves recorded at permanent stations of Japan Meteorological Agency. This study provides evidence that the DDSS system is effective in identifying and locating volcanic LPs and tremor. The fiber optic cable is permanently deployed allowing for continuous recording of seismic signals, even during eruptions and thunderstorms, at the station at the foot of the volcano.

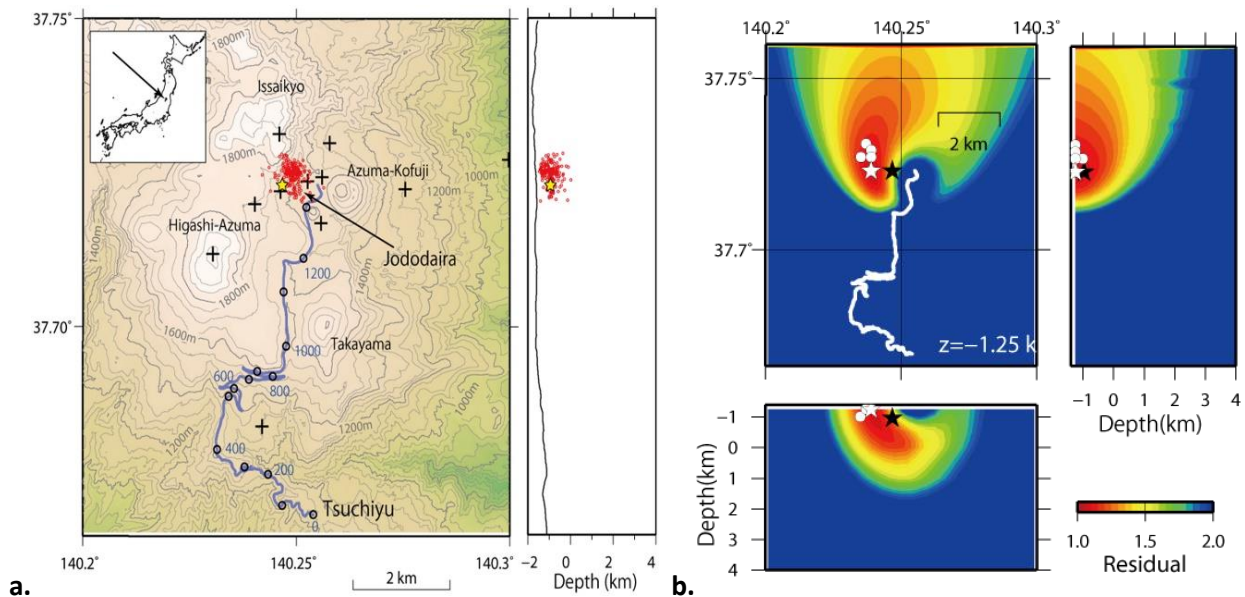


Figure 6. (adapted from Nishimura et al., 2021). **a.** Locations of the fiber optic cable; the DDSS system is located in Tsuchiyu station, at the south end of the fiber optic cable. The fiber optic cable is indicated by the purple line, and the open black circles denote the locations of the measurement points every 200 channels. “Plus” symbols indicate permanent stations maintained by Tohoku University and the Japan Meteorological Agency. Hypocenters of volcanic earthquakes determined by routine analyses of permanent station data for the period from January 1 to July 4, 2019 are indicated by red circles. In particular, the hypocenter of a volcanic earthquake on July 4 is indicated by the yellow star. This figure was created by Generic Mapping Tools (GMT) v4.5.5 **b.** Source locations of six long-period events (LPs). The white star represents the July 4, 2019 LP source location estimated from the DDSS data combining both travel time and amplitude location methods. White circles indicate locations of five other LP source. The black star indicates the hypocenter (LP event on July 4) obtained by routine hypocenter determination using P- and S-wave arrival times. White lines indicate the location obtained from the fiber optic cable. Color contours represent the residuals between the observed and theoretical values of the arrival time differences and amplitudes for the LP on July 4, 2019.

DFOS on ice-covered volcanoes (Mt Meager, Canada and Mt Grímsvötn, Iceland)

Ice-covered volcanoes hide themselves from direct observation, thereby limiting the level of preparedness and possibilities for early warning. Their hazardous features are often related to the rapid melting of ice in the event of an eruption, and they include phreatomagmatic explosions, lahars and subglacial floods. This highlights the need for spatially dense monitoring at ice-covered volcanoes, even though the lack of pre-existing fiber-optic networks complicates the data acquisition in the often remote and extreme environments. New fibers have to be deployed and coupled with ice and snow, which potentially moves, melts, or accumulates rapidly, which may limit the longevity of the cables. This section

provides a brief summary of fiber optic sensing experiments on two ice-covered volcanoes, Mt. Meager, Canada (Klaasen et al., 2021) and Grímsvötn, Iceland (Fichtner et al., 2022; Klaasen et al., 2022). The focus here is on logistical challenges and the detection of previously undetected volcano-seismicity.

Mt. Meager is an active volcano in the Garibaldi Volcanic Belt in British Columbia, Canada. Much of its scientific relevance derives from the potential for both geothermal energy exploitation and large landslides, which are expected to become more frequent in response to the rapid melting of its glacier. A major challenge for fiber optic sensing on Mt. Meager was the construction of an autonomous and reliable electrical power source. It consisted of a 5.5 kW generator that charged a 550 Ah battery pack. Nearly 450 l of fuel in a separate tank enabled the experiment to run for 4 weeks. A cable of 3 km length was deployed on the ridge of Mt. Meager and the upper part of its glacier, above 2000 m altitude. Trenching on the volcanic deposits along the ridge was done by hand. On the glacier, a chain saw was used to produce a trench of around 30 cm depth. All of the equipment was transported by helicopter.

The installation in autumn 2019 was followed within a few days by the first snowfall of the winter, which visibly improved cable coupling and signal-to-noise ratio. This enabled the unexpected detection of around 3000 seismic events at frequencies between 5 - 45 Hz, thereby demonstrating that Mt. Meager is considerably more active than previously thought. Beamforming locates most of these events within five major clusters possibly beneath the main peak and in the nearby Lillooet Valley, suggesting a geothermal origin. At lower frequencies, between 0.01 - 1 Hz, the fiber optic data reveal the presence of volcanic tremor periods that tend to last for several hours and have not been observed before. Both the high- and low-frequency seismicity may become a valuable component in the monitoring of future geothermal energy projects.

While the last eruptive period of Mt. Meager dates back nearly 2500 years, Grímsvötn produces major eruptions on a decadal time scale and is one of the most productive volcanic systems on Earth. Covered entirely by Europe's largest glacier, Vatnajökull, its caldera with 10 km diameter hosts a subglacial lake that regularly produces outburst floods and inundations of the coastal plains. During springtime, the research huts located on the highest point of the caldera can be reached with skidoos, meaning that the transportation of equipment does not require expensive helicopter flights. The installation of a 12.5-km-long fiber optic cable around and inside the caldera was achieved within 3 days thanks to the construction of a custom-built trenching sled, equipped with a ca. 50 cm deep plough that placed the cable directly into the ice. Electricity and an internet connection were available in one of the huts, thereby permitting continuous recording for 3 weeks, as well as online trouble-shooting and optimization of the interrogator setup.

The excellent shielding from wind and temperature variations enabled the recording of a wide range of seismic signals, sometimes with amplitudes below 10 nanostrain/s. During the experiment, nearly 2000 local events could be detected using an image processing algorithm adapted to distributed fiber optic sensing (Thrustarson et al., 2021). Most of these events occurred within few clusters between 1 and 3 km depth beneath the western part of the caldera. Possibly owing to their low magnitudes, roughly between -2 and 0.5, the majority of these local earthquakes have not been detected by the regional seismometer network, which attests to the importance of fiber optic sensing in high-resolution volcano monitoring.

A more exotic observation at Grímsvötn is the nearly monochromatic oscillation of its caldera at 0.22 Hz, which corresponds to the fundamental-mode resonance frequency of the ice sheet that floats atop the subglacial lake (Fig. 7). The time dependence of the oscillation amplitude does not correlate with the amplitude of the ocean wave-generated ambient field, suggesting that the resonance is driven by a local process. In the absence of other plausible explanations, the ice sheet apparently acts as a natural amplifier of nearly continuous volcanic tremor that would otherwise not be observable (Fichtner et al., 2022).

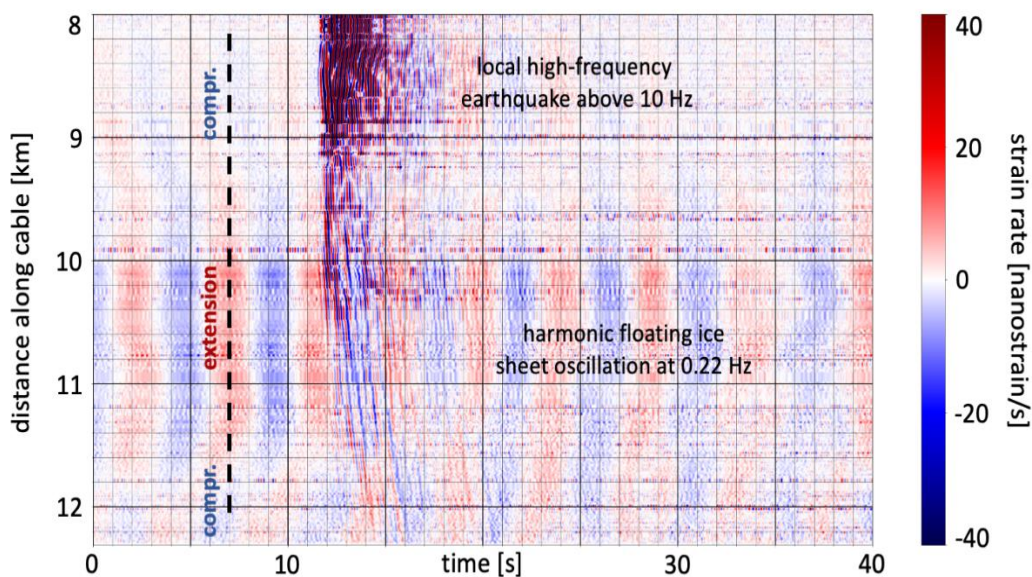


Figure 7. (Adapted from Fichtner et al., 2022). DDSS record section of 40 s length from within the caldera of Grímsvötn. The signal from a high-frequency local earthquake is superimposed onto the nearly monochromatic oscillations of the ice sheet that is floating atop the subglacial lake. The dashed black line marks at this chosen time where one can observe extension in one and compression (“compr.”) in another part of the caldera.

Earthquake detection and location with a rotational sensor (Etna volcano, Italy)

Eibl et al. (2022) conducted a performance test on the blueSeis-3A rotational sensor, which was co-located with a broadband seismometer. The blueSeis-3A sensor has a height of 30 cm, a diameter of 30 cm and weighs approximately 20 kg (Fig. 1). It consists of three fiber loops arranged in three orthogonal axes that measure the rotation rate in nanoradian/second (Bernauer et al., 2018). The sensor has a flat instrument response from 0.001 to 50 Hz and the ground motion is typically digitized and recorded at 200 Hz. To protect the instrument from wind noise, it should be buried. Currently, the instrument has a power consumption of 21 W. Although the portable rotational sensor blueSeis-3A is less sensitive than a conventional seismometer, it can still measure weak volcano-seismic signals if the distance between the source and the sensor is less than a few kilometers. The use of a rotational sensor (3C, rotational components) in combination with a seismometer (3C translational components) defines a “6C station”. This type of combined station is best suited for computing back-azimuth and locating seismic events.

Eibl et al., 2022 deployed a 6C station at approximately 2 km from the five active craters of Etna volcano (See Fig. 4, station bb17) to test its ability to detect and locate volcano-tectonic (VT) events, long-period (LP) events and tremor. The validation was performed by comparing the locations of volcanic earthquake locations recorded by the 6C station with the locations from the permanent monitoring network of the Istituto Nazionale di Geofisica e Vulcanologia - Osservatorio Etneo (INGV-OE). During a one-month of acquisition period in August and September 2019, Eibl et al., 2022 compared the number of detections obtained by each instrument separately with the number of events detected by the permanent seismic network. The number of VT events detected using either only the rotational sensor or only the seismometer is similar. However, in both cases, this number is slightly less than the number of events detected by the INGV-OE network. The seismometer detected a comparable number of LP events compared to the INGV-OE network on most of the days, and three times more LP events than the rotational sensor. The rotational sensor revealed the SH-type wave nature of the LP events, as they were only detected on the vertical component of the rotational sensor (Fig. 8). Similarly, during weak strombolian activity, the tremor wave field is dominated by SH-type waves. However, during sustained strombolian activity, the wave-field changes to a mixed-type. The back azimuth of the derived tremor is consistent with the INGV-OE estimates, and the derived phase velocities derived by (Eibl et al., 2022) are consistent with the velocities derived using DDSS records (Jousset et al., 2022).

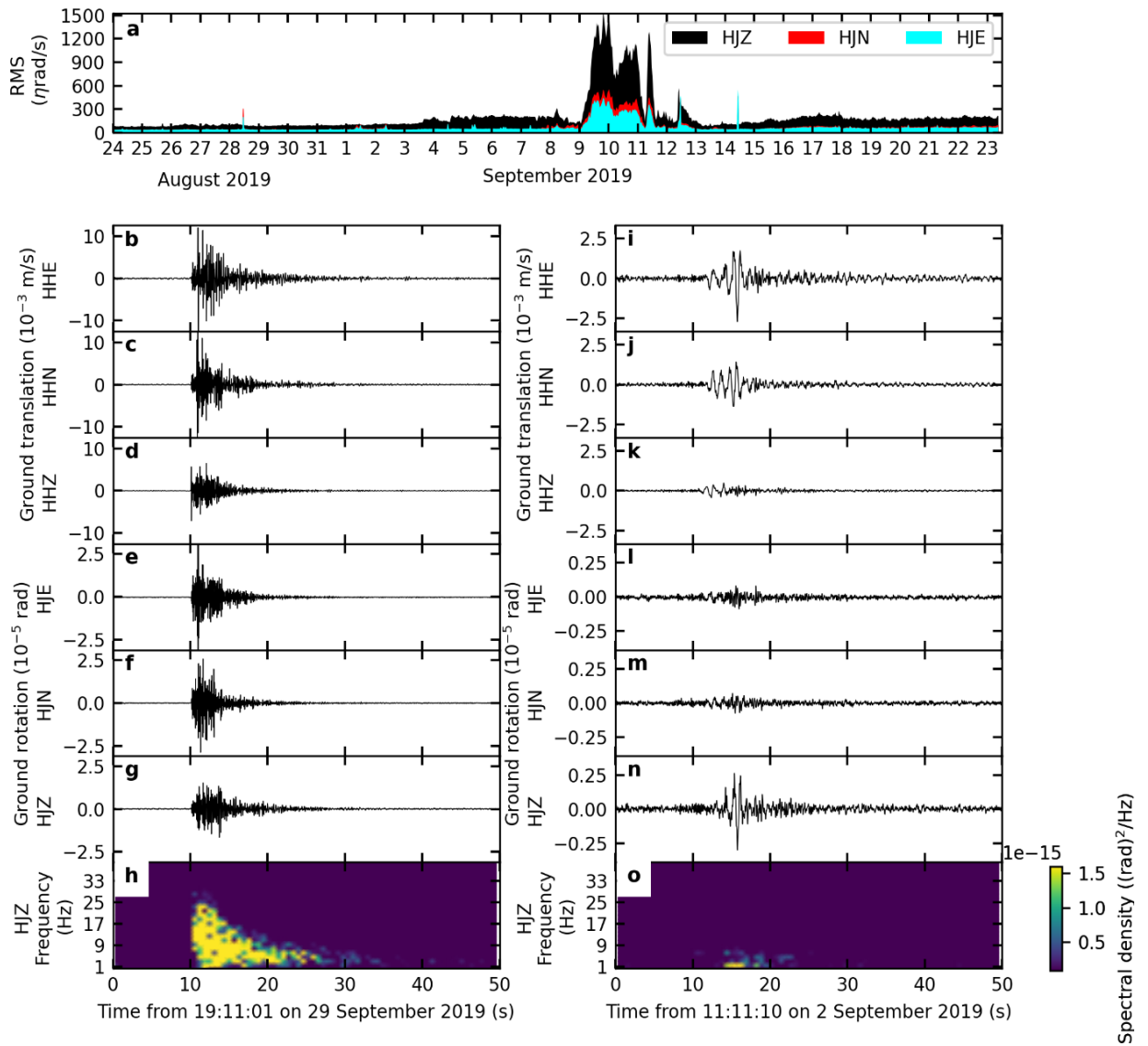


Figure 8. (Adapted from Eibl et al., 2022). VT, LP and tremor events were recorded with conventional seismometer and rotational sensor at Etna volcano, Italy (Eibl et al., 2022). The transition from a SH-wave dominated to a mixed wave field occurred in the period 9 to 13 September 2019. **a.** Amplitude of the rotational sensor signal for one month of record. **b. to h.** Records for a volcano-tectonic (VT) event recorded on 29.09.2019. **b. to d.:** conventional seismometer and **e. to g.:** rotational sensor. **h.** spectrogram (HJZ component). **i. to o.** Records for a long-period (LP) event recorded on 2 September 2019. **i. to k.:** conventional seismometer and **l. to n.:** rotational sensor. **o.** spectrogram (HJZ component).

3.3 Structural features of volcanic media

Understanding the structure of a volcano is crucial for comprehending its internal dynamic processes. For instance, the locations of volcanic hypocenters (Koulakov and Shapiro, 2021) or source mechanism (Bean et al., 2008) may be entirely inaccurate, if an unsuitable velocity or structural model is employed.

DFOS has been demonstrated to be a valuable tool for near-surface characterization (Ajo-Franklin et al., 2019) particularly in urban areas where performing conventional active seismic surveys is challenging.

The dense network of dark fibers in cities enables the investigation of shallow subsurface properties using techniques such as ambient and anthropogenic noise, such as cars (Jousset et al., 2018). In this section, we show that DFOS can be valuable for conducting thorough structural analyses of volcanic materials.

Fault detection (Reykjanes, Iceland).

A clear example of the impact of DFOS on discovering structural features associated with faults in volcanic environments was demonstrated in the South-West of Iceland (Jousset et al., 2018). The objective was to show that fiber cables already deployed for telecommunications could be interrogated with Distributed Dynamic Strain Sensing in a useful manner for volcano-seismology. The goal was achieved by recording of a local earthquake (M 1.1) that occurred beneath the cable. The cable used in this study was buried 80–90 cm below the ground surface crossing the Svartsengi geothermal field from the southern tip of Reykjanes to Grindavík. Fig. 9 shows the response of a local fault zone that is partially visible at the surface, with a clear indication of the diverging plate tectonic processes. When seismic waves propagate, their energy tends to remain in areas where the seismic impedance is lower (Jousset et al., 2003). The dense spatial sampling (one time series every 4 m) allows for clear observations of trapped waves inside the fault zone. Scattering of waves can be observed, opening up possibilities for studying the physical properties of materials inside fault zones (Atterholt et al., 2022; Yang et al., 2022).

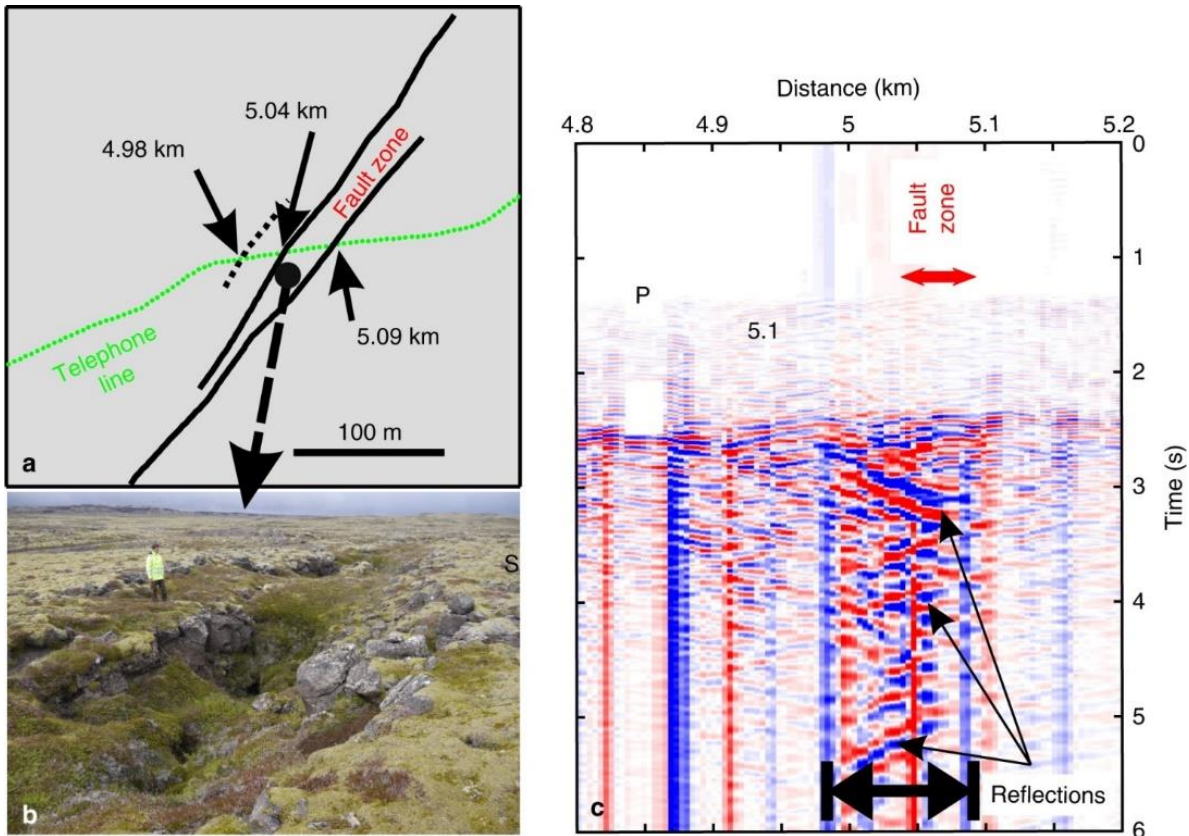


Figure 9. (adapted from Jousset et al., 2018). Structure of a fault damage zone within an active geological rift. **a.** The road and the cable (distance ~ 5 km) cross several faults, e.g. a clearly visible fault zone with more loose material in the field (between 5.04 and 5.09 km). **b.** The fault damage zone is visible by the ~ 50 – 60 m wide depression area (picture taken at ~ 100 m SW of the road, looking towards SW). Note that at the cable location no depression area is visible. The depression is only the surface expression at the position of the picture (Picture Martin Lipus, GFZ). **c.** Short record (6 s) of strain phases from a local earthquake trapped in the fault damage zone. Phases are reflected until ~ 4.98 km, which may indicate a hidden fault with surface expression. Waves inside and outside the fault zone have different apparent velocities.

Material characterization of volcano subsurface (Mt. Azuma, Japan and Etna volcano, Italy)

To comprehend the underlying volcanic source mechanisms, it is crucial to characterize the subsurface at volcanoes (Bean et al., 2008). DFOS can be particularly useful, especially when the optical cable is already installed. Nishimura et al. (2021) highlight that DFOS records can be used to determine site amplification factors and relative amplitudes of coda waves of regional earthquakes at Azuma volcano. The data show a strong correlation between the fiber optic cable and subsurface volcano structures, including lava flows and topography (Fig. 10). However, as the fiber optic cable is deployed in a protecting plastic tube by a telecom company, its coupling with the ground is not well understood.

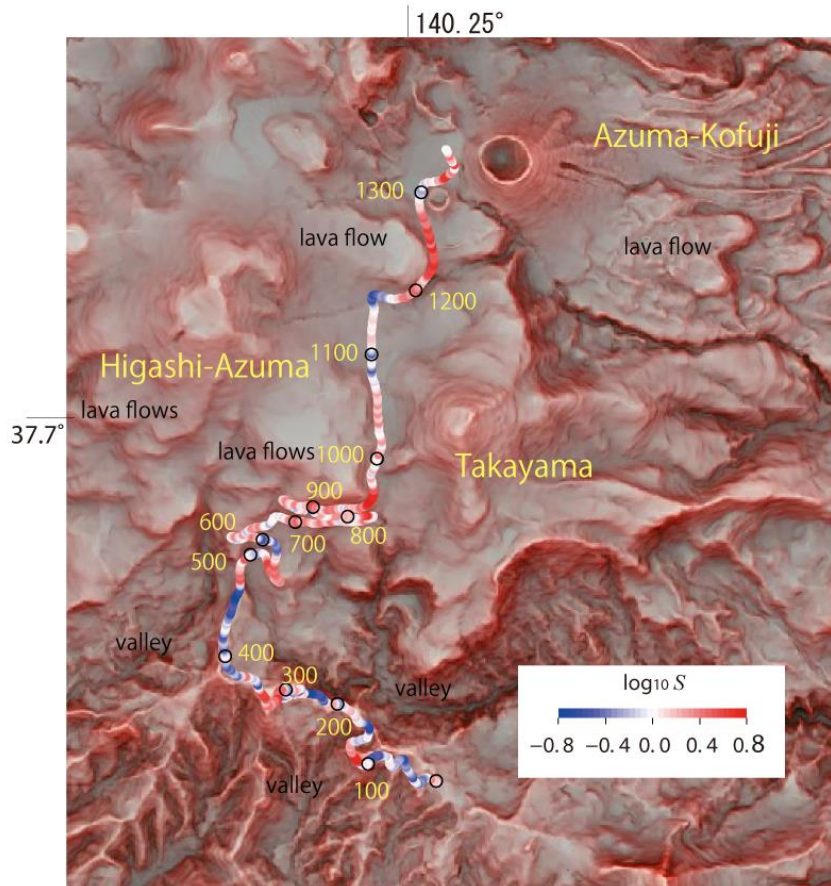


Figure 10. (Adapted from Nishimura et al., 2021). Site amplification factors along the fiber optic cable. Logarithmic amplitudes of the factors are indicated by color contours. Background is a red relief map emphasizing topography of the volcano provided by the Geospatial Information Authority of Japan. Numbers along the cable are trace numbers. Large site amplification factors, S , are recognized around the lobes of old lava flows extending from the active volcanoes (traces around 500-1050 and 1200-1300), while small site amplification factors are mainly found on the ridges around steep valleys in the southern part (traces around 350-450, 200 and 1-100).

If the fiber optic cable is not already in place, a dedicated cable can be deployed. For instance, Jousset et al. (2022) deployed a dedicated cable directly into a scoria layer at Etna volcano (Figs. 1 and 11), resulting in optimal and consistent coupling with the ground along the entire cable. Advanced and powerful methods of subsurface structural exploration could be performed, such as Multi-channel Analysis of Surface Waves (MASW; Park, 2011; Lancelle et al., 2021). MASW provides dispersion curves that can be inverted to obtain vertical 1D shear wave velocity profiles. Jousset et al. (2022) performed jumps also known as tap tests, at various locations along the cable to geo-locate the distributed sensing records. The jumps can also serve as sources of surface waves for MASW analysis. For each jump performed along the

cable, two sub-datasets were obtained: a forward sub-dataset (records towards increasing channel numbers) and a backward sub-dataset (records towards decreasing channel numbers). The dispersion curve was computed using the phase-shift method (Park, 2011). It is worth noting that the seismic wave field separation method (Schwarz, 2019) was used to improve the signal to-noise ratio of the dispersion curves. Finally, the observed modes in the dispersion curves were picked. Using a Markov chain Monte Carlo scheme (Killingbeck et al., 2018) the picks were inverted to derive a vertical profile of shear wave velocities for both the forward and the backward subsets. Figure 12 demonstrates two examples of this procedure, showing that subsurface structures can be determined using MASW on fiber optic dynamic strain data sets. The dispersion analyses show numerous modes, indicating a strongly dispersive medium due to multiple superposed volcanic strata with varying velocities. This is consistent with a sequence of lava flows and scoria deposits. Inversions of these dispersion curves yield vertical profiles of layers. The first layer with shear-wave velocity of 200 ms^{-1} and 3–5 m thickness. Deeper layers have velocities up to 600 ms^{-1} at about 20–25 m depth. The inverted models reflect structures associated to faults and lava flows at the volcano (Napoli et al., 2021).

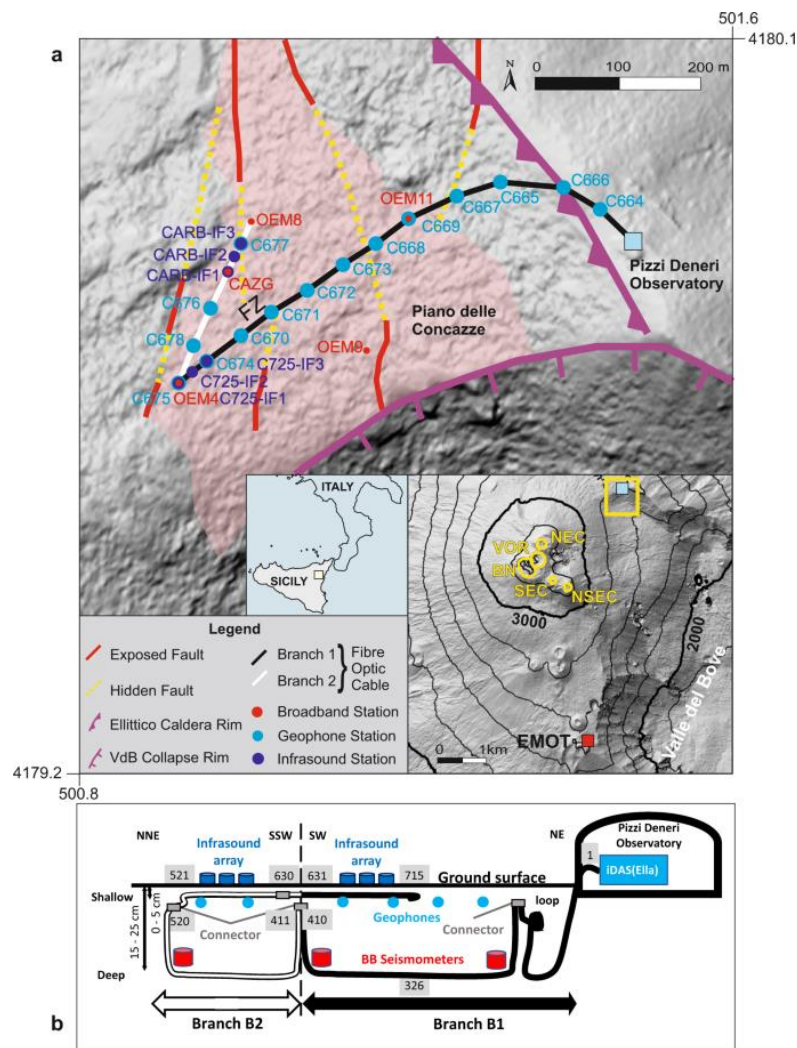


Figure 11. (Adapted from Jousset et al., 2022). Fiber optic cable, seismometer and infrasound sensor locations and deployment near Etna volcano summit (Piano delle Concazze) and Valle del Bove on the

digital elevation model **a.** The iDAS interrogator set up at Pizzi Deneri Observatory (light blue square), is connected to the fiber indicated by the black (“branch B1”) and the white (“branch B2”) lines, respectively.

b. Sketch of the cable deployment. From the interrogator (inside and around the observatory, channel 1–50), the cable is buried in compacted material (channels 50 until 200) and then in loose scoria deposits (transparent reddish area in a.), at about 15–25 cm depth (deep section) along B1 with channels 1 to 410, then the cable turns (still within the deep section) along B2 with channels 411 until 520, then the cable has a shallow section (under a few cm of scoria and lying directly above the deep cable), from channels 521 until 630 (with same geographic location as deep channels 520 until 411, respectively), and finally, the shallow cable turns along B1 (still above the deep cable) from channels 631 until 715 (with same geographic location as deep channels 410 until 326). Insets: Local and regional contexts. Summit craters’ locations: NSEC (New South-East Crater); SEC (South East Crater); BN (Bocca Nuova); VOR (Voragine); NEC (North-East Crater). Red square: Thermal camera location: EMOT. The yellow box indicates the location of the main map. This figure serves as map for figures 12 and 13 of the chapter.

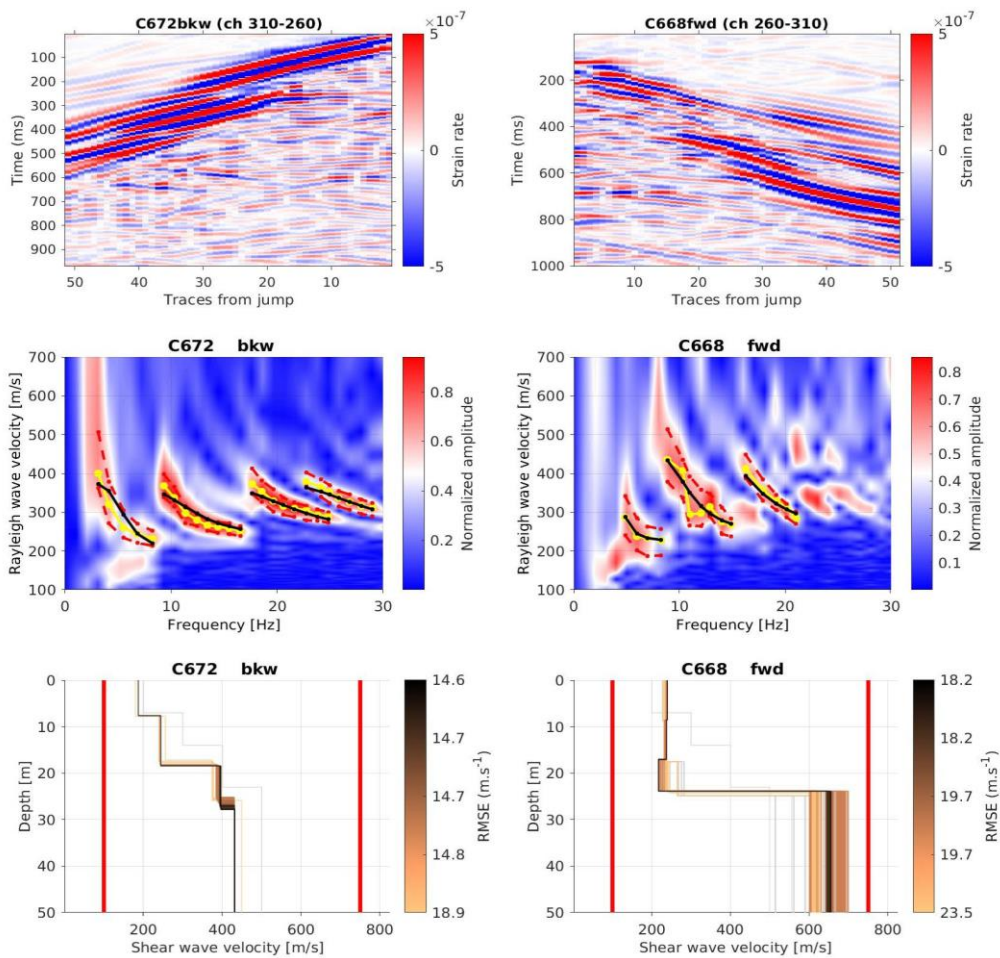


Figure 12. (adapted from Jousset et al., 2022). Multichannel Analysis of Surface Waves (MASW) and Markov chain Monte Carlo inversion of dispersion curves from DDSS records along a cable of 1.5 km at Etna volcano along the cable shown in Figure 11. Graphs represent analysis results for 2 jumps performed at locations given by the name of co-located geophones (C668, left column and C672, right column). Jousset et al. (2022) define a forward branch (fwd) signals for channel numbers larger than the channel of the jump, and a backward branch (bkw) signals for channel numbers smaller than the channel of the jump. The fwd and bkwd records are both used separately for the dispersion curve analysis. **(top subplots)** Enhanced strain signals (Method: Coherent wave field enhancement and separation). **(middle subplots)** Dispersion spectra in phase velocity/frequency domain. Green dotted lines are the picked dispersion values with their corresponding uncertainty (red dotted lines). Black dotted lines represent the multimode dispersion curves computed using the best inverted model causing the lowest root mean square error (RMSE). **(bottom subplots)** 1D wave velocity retrieved after Markov chain Monte Carlo inversion. Red lines indicate limits of tested models during the inversion. In contrast to the backward branch at C672, the forward branch at C668 crosses a major structure in the form of a fault zone causing a more complicated Rayleigh wave field (Fig. 11).

3.4 Dynamics of volcanoes: monitoring degassing with fiber optic cables

Gas is one of the fundamental drivers of volcanic activity, with two end-members: passive degassing occurs gently through structural features of the volcano (Segovia, 1991), while explosive degassing occurs when the strength of the structural feature is exceeded, e.g., due to high gas flux. Therefore, it is essential to monitor degassing and study the underlying driving processes. This section reports examples of two end-members using DFOS: a volcanic explosion at Etna volcano (Italy) and degassing through bubbles in a volcanic lake, the Laacher see (Germany).

Volcanic explosions (Etna volcano, Italy)

Volcanic explosions happen when the strength of the rock cannot withstand the overpressure caused by magmatic and/or hydrothermal fluids. This can occur when there is lower rock permeability within the volcanic conduit, which prevents higher fluid flux and causes overpressure. To study explosive events, infrasound and seismic signals can be used (Johnson and Ripepe, 2011). In the summer of 2018, Jousset et al. (2022) deployed a temporary array of multiparametric sensors at Etna volcano. The array consisted of a 1.3 km standard fiber optic cable buried in a trench of approximately 20 cm deep into a scoria layer. Additionally, a series of geophone and infrasound sensors were deployed along the cable (Fig. 11). The sensors recorded volcanic explosions (Fig. 13). These volcanic events produce seismic waves which travel in the ground faster than the acoustic waves in the atmosphere. The volcanic material exhibits a non-linear response when the infrasound wave encounters the scoria layer in which the cable is buried. This is indicated by the presence of a high-frequency signal (18-23 Hz), that is absent in the infrasound signal.

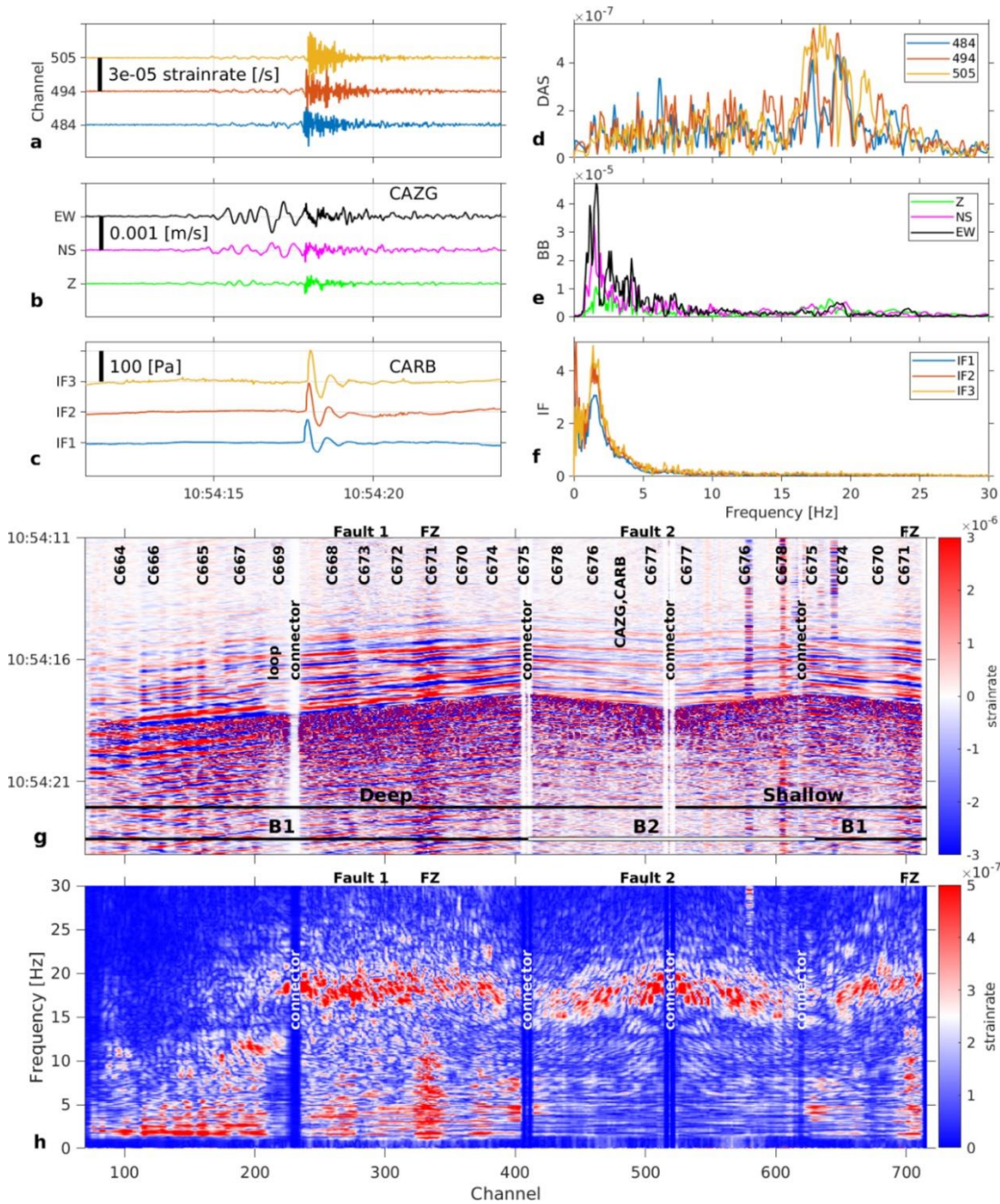


Figure 13. **a** Strain rate from distributed dynamic strain sensing (DDSS) records at channels 484 (blue), 494 (red) and 505 (yellow), corresponding to positions of infrasound sensors in (c). Fiber channel position accuracy ± 3 m. **b**. Velocity seismograms from broadband seismometer CAZG, near DDSS channel 494. **c** Pressure records from infrasound sensors CARB-IF1, 2, 3. **d** Strain rate (a) spectra. **e** Ground velocity (b) spectra. **f** Pressure (c) spectra. **g** Strain rate record at the 710 DDSS channels along the 1.3 km fiber around the explosion time. B1 and B2 are two geographically distinct branches, oriented in two different directions. FZ: fault zone (~ 50 m width), at channels 315–340 (deep cable) and channels >700 (shallow cable). **h** Strain rate-frequency distribution along the cable. Note higher strain rate amplitudes at low frequencies 1–10 Hz (seismic signal) for branch B1 and at high frequencies 18–21 Hz (infrasound induced signal) for both branches (see Fig. 11 for locations).

Bubbles and degassing (Laacher See, Germany)

Passive gas monitoring is typically carried out by directly sampling fumaroles in the crater (Chiodini et al., 2011) or through remote sensing (Taddeucci et al., 2021). The relationship between seismic activity and gas flux has also been identified and studied (Zuccarello et al., 2013). During a period of quiescence (no eruption) at Etna volcano, Jousset et al. (2022) used DFOS to identify STP (Small Tremor Pulse) and DG (degassing) signals as slightly larger amplitude phases within the volcanic tremor. These signals were interpreted as resulting from variations in the uprising gas flux within the volcanic conduit until the vent. Degassing processes at quiescent volcanoes can help detect potential signs of unrest, as shown by Caudron et al. (2024) at the volcanic lake Laacher See (Germany). The lake is situated in a caldera, indicating past violent volcanic activity within a large volcanic complex in the Rhine graben. In recent years, there has been signs of possible unrest, identified by the occurrence of deep LP earthquakes and possibly large-scale deformation (Hensch et al., 2019). During June-July 2021, an experiment was conducted to test DDSS by deploying a 500 m long fiber optic cable on south-western side of the lake at a depth of approximately 20 m (Fig. 14a). The coupling at the bottom of the lake was ensured by two divers. Strain rate measurements were collected at a spatial resolution of 1 m and different temporal sampling rates (5 and 8 kHz). Videos of the dynamic of underwater bubbles were simultaneously acquired with a smartphone, enabling observations of bubbles rising from the sediment towards the surface at different times. The experiment recorded occurrence rates and frequencies. Close to the bubbling spots, the waveforms are similar to the signals recorded by Vazquez et al. (2015) during laboratory experiments. The signal observed in the lake had a high-frequency onset of approximately 1 kHz, followed by a lower frequency signal at around 200 Hz (Fig. 14b). The signal waveform varied slightly along the cable with decreasing signal-to-noise ratio, as a function of distance from the main bubbling spot. However, it is also possible that changes may be related to different coupling conditions. These results suggest that DDSS technology is sensitive to degassing under water, and therefore could be used for monitoring submarine bubble flux.

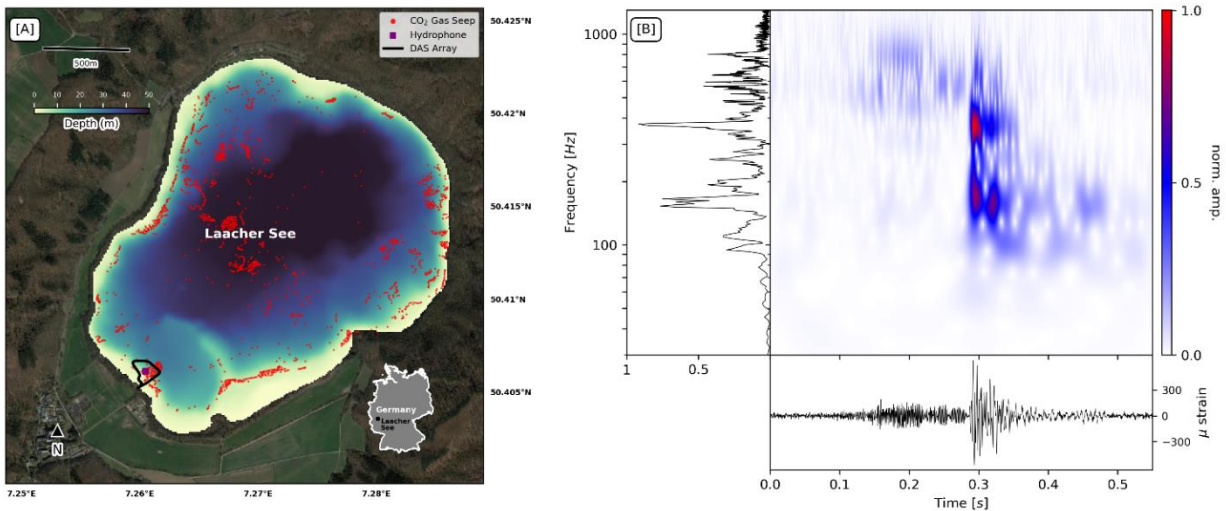


Figure 14. a. Laacher See aerial image and location of the fiber optic cable (triangle in red to the South) **b.** Spectrum (left), waveform (bottom) and spectrogram (center) associated with a bubbling event.

3.5 Monitoring long term deformation (Etna volcano, Italy)

BOTDR can be used to measure “quasi-static” deformation. A BOTDR interrogator (Fig. 1) was attached to a submarine cable in the port of Catania, Italy. The results show increasing strain along the cable for the first 5 km of the cable from May to September 2020 followed by a sustained drop in strain thereafter (Fig. 15). This variation occurred during a period of significant inflation and deflation before and after the paroxysmal episodes in December 2020 and January 2021. Terrestrial GNSS stations have observed the phenomenon on land (Bruno et al., 2022). This preliminary result demonstrates the potential of BOTDR in locating zones of deformation at high resolution and sensitivity in submarine environments surrounding volcanic islands, where obtaining measurements is challenging. As Brillouin scattering is influenced by temperature (see §2.3.b), temperature fluctuations must be accounted for when measuring strain near the surface. However, for submarine cables, temperature variation is lower than on the ground surface. Ongoing research aims to invert for both temperature and strain simultaneously (Bao et al., 2021).

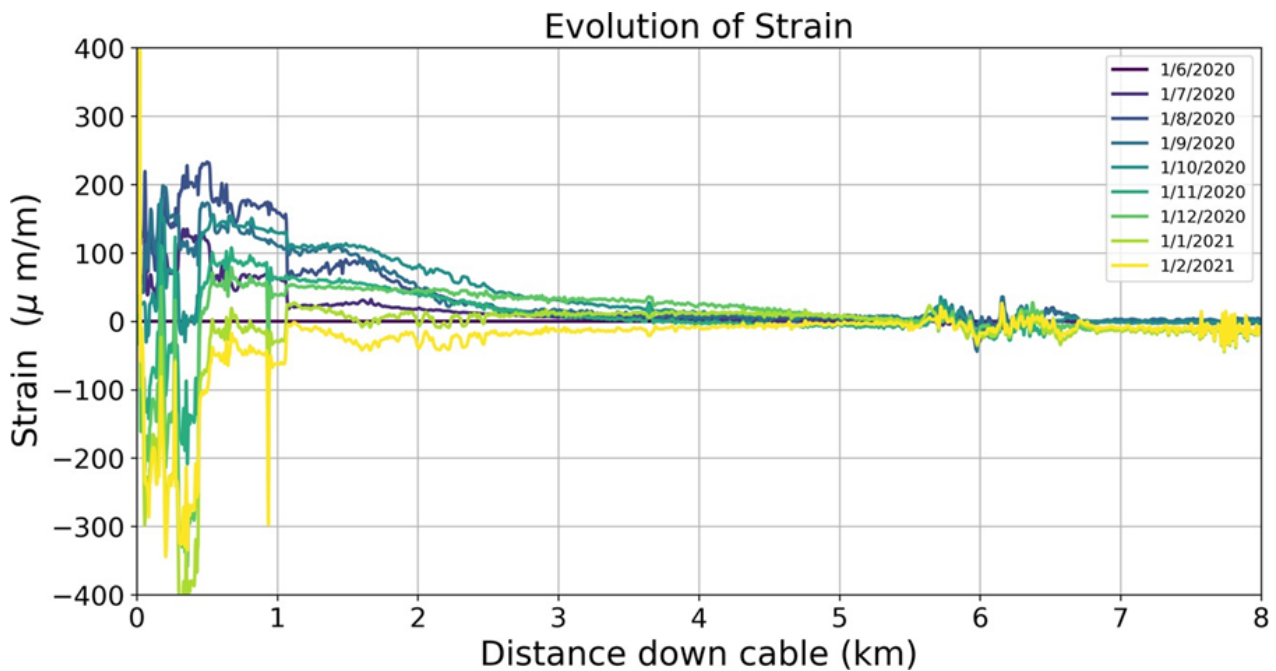


Figure 15. Strain variation along fiber optic cable deployed offshore Catania using a BOTDR interrogator. X-axis is the distance down the cable with measurements taken every 4 m and averaged over the whole day. The strain measurements have been taken over the course of a day at the start of each month and averaged. All strain measurements are set relative to 1 June 2020 (dark blue line). Line color denotes time that strain measurement was taken.

4. Towards integrating fiber optic technologies within volcano monitoring systems

Volcano monitoring involves continuously observing key parameters and their variations on an active volcano in order to estimate its activity status, anticipate its behavior before an eruption, forecast the probability of an eruption and define potential scenarios to improve risk management (e.g., Thierry et al., 2015). To achieve this goal, it is necessary to locate earthquakes, identify fluid movements within the volcano, and understand the sources of slow inflation/deformation, in real-time. Section 3 illustrated that the full wave field can be measured, providing examples of promising approaches that could improve the monitoring capabilities of volcano observatories. This section illustrates and discusses how fiber optic methodologies could contribute to operative volcano monitoring.

4.1 Integration of DFOS in existing monitoring systems

Monitoring seismicity: combination of seismometers and DDSS measurements (Reykjanes, Iceland)

The combination of fiber optic Distributed Dynamic Strain Sensing data via fiber optics and conventional seismometers can be an effective approach for accurately locating seismic events. For instance, Flovenz et al. (2022) showed that the combination of data from a fiber optic telecom cable with data from 26

broadband seismic stations enhanced the detection of earthquakes and improved their location accuracy during the swarm of volcano-tectonic earthquakes before the Geldingadalir eruption 2021 (the first eruption of the Fragaradalsfjall fires, Halldórsson et al., 2022). By using a waveform stacking and migration method, seismic and continuous DDSS data were combined to produce a complete earthquake catalogue covering the period from 1 February 2020 to 30 August 2020. A total of over 39,500 VT earthquakes occurring in swarms with magnitudes of $M > -1$, were automatically detected and located. The seismic sensors and the optical cable were located directly above the hypocenters, ensuring a good azimuthal distribution of all stations, resulting in high quality lateral and vertical hypocenters. Seismicity shallower than 4 km depth was concentrated within an elliptical area, where an uplift occurred. The uplift was interpreted as resulting from the vaporization of water from an aquifer, which is being harnessed by a geothermal company. The study of Flovenz et al. (2022) suggest that the earthquakes at the center of the uplift are triggered by elastic bending stresses in the roof above the aquifer. The absence of earthquakes deeper than 4 km depth at the uplift center supports the hypothesis of an up-doming brittle ductile transition (BDT) at about 6–7 km depth (Fig. 16 and Flovenz et al., 2022).

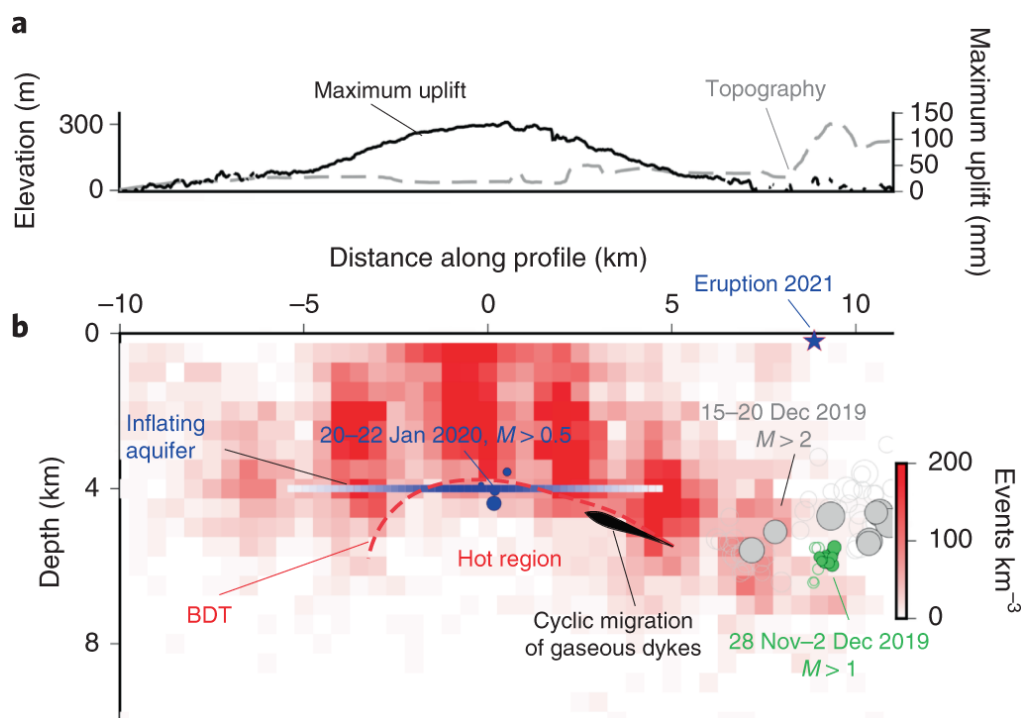


Figure 16. (Adapted from Flovenz et al., 2022). Sketch of fluid migration paths and aquifer location compared with observed seismicity and uplift. **a.** Maximum uplift (solid black line) and topography (dashed grey line, $x = 0$ at the center of the uplift). **b.** Density of micro-earthquakes between February and August 2020 (gridded file and color scale) estimated in a 1-km-wide band along profile SW-NE using a combination of broadband seismic stations and Distributed Dynamic Strain sensing. The inferred brittle ductile transition (BDT) is indicated by the red dashed line. The manually relocated, largest events from the earthquake swarms from November (green circles) and December 2019 (grey circles) and at the

beginning of unrest (blue circles) are shown. The position and source intensity of the aquifer model are indicated.

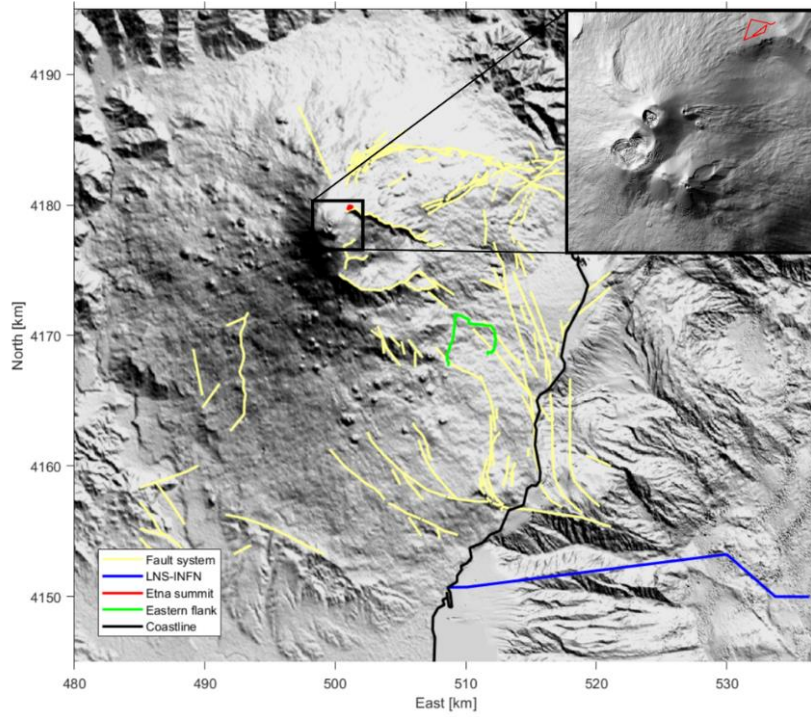
Multi interrogator approach (Etna volcano, Italy)

Cables are linear objects, and their aperture may not be sufficient to cover the ideal network for optimal hypocenter location (Toledo et al., 2020). To increase the aperture and the spatial coverage for larger targets, such as Etna volcano, multiple fibers and interrogators can be used simultaneously. The availability of several interrogators at once is a clear issue. At Etna volcano, three independent interrogators were connected with three different fiber optic cables for about ten days from 11 September 2019 to 23 September 2019 (Krawczyk et al., 2020). The INGV permanent monitoring network recorded a total amount of 134 local seismic volcano-tectonic earthquakes. Figure 17 shows the records of an M2.4 earthquake located in Valle del Bove at a depth of 4.3 km with three fiber optic cables at once.

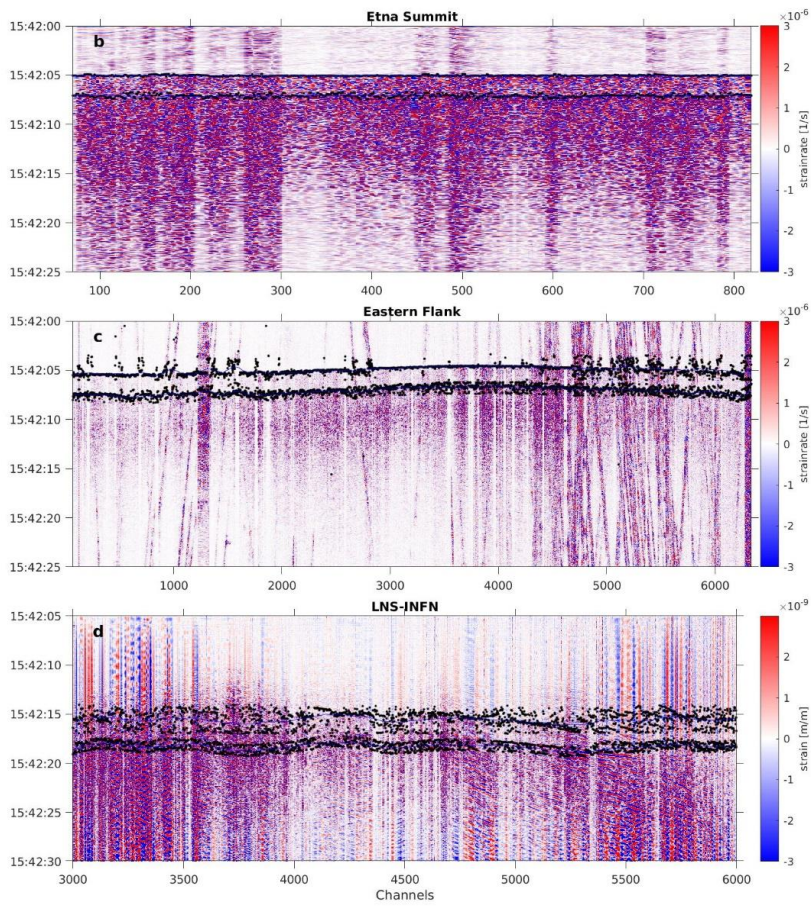
It is worth noting that the amplitudes of the strain rate signals do not follow the expected geometrical amplitude decay of seismic waves from the source to the fibers. This discrepancy may be due to the variety of coupling conditions between the ground and the different cables, as observed at Mt. Azuma (Fig. 10). The cable at the summit was perfectly coupled with scoria (Currenti et al., 2021; Jousset et al., 2022; Figs. 1 and 4). On the contrary, the telecom cable in the urban environment on the Eastern flank is likely to be deployed in pre-existing cased conduits and therefore transfer of ground strain to the fiber core is less efficient (Reinsch et al., 2017). Underwater, the recorded strain may be lower due to the cable's coupling conditions with the sea floor, and its increased strength to withstand water column pressure at a depth of 2000 m and submarine currents. This prevents ground strain from being transferred to the sensing fiber (Currenti et al., 2023; Diaz-Meza et al., 2023).

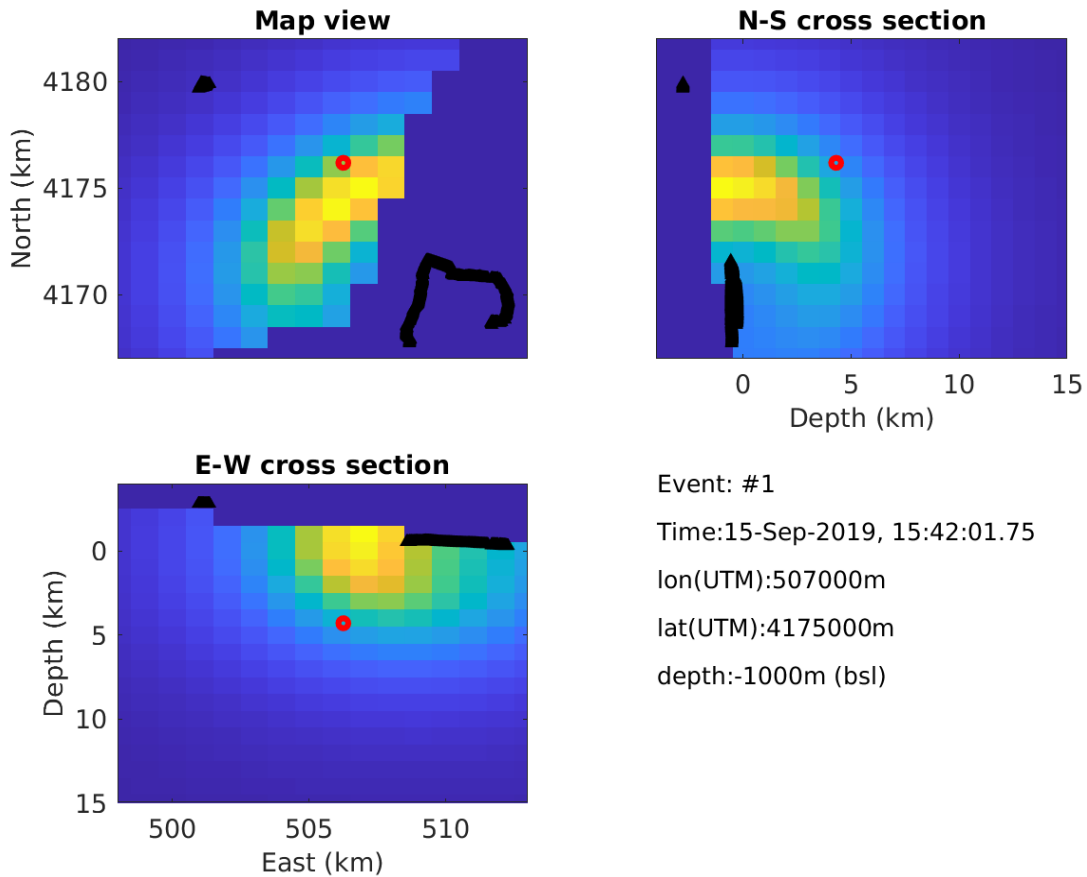
Nevertheless, the event's location can be determined using basic automatic picking (Jousset et al., 2011; 2018) based on arrival times detected on two of the three cables (Fig. 17). The black dots on each fiber represent the automatically picked times for both P- and S-waves arrivals, using a non-cable-specific and unoptimized STA/LTA algorithm. To perform the location inversion, a spatial interpolation is conducted between picks to eliminate the scattering caused by local conditions and to attempt to remove anthropogenic signals. The interpolated picked arrival times are then used to conduct an inversion for the location using a grid search, resulting in a probability density function of the earthquake's location. This hypocenter encompasses the INGV location obtained from conventional seismometers in the monitoring network. This example demonstrates that by designing a suitable series of interrogated

fibers, either by deploying dedicated cables or/and interrogating already existing ones, distributed dynamic strain methods can provide new and dense information to better locate earthquakes.



a.





e.

Figure 17. **a.** Map of Etna volcano indicating the locations of the three cables interrogated simultaneously. **b., c. d.** Records of a volcano-tectonic earthquake on the 15 September 2019 at 15:42:02 in Valle del Bove with several fiber optic cables. Back dots represent the automatic picking of P and S for each channel, using STA/LTA conventional detector and an Akaike Information Criteria picker (Jousset et al., 2011, 2018). **b.** PDN array, at the summit of Etna volcano (spatial sampling 2 m); **c.** Linera array /Telecom Italia cable on the slope of eastern flank (spatial sampling 2 m); **d.** submarine cable from Catania harbor down to the INFN submarine observatory (2300 m depth, 25 km from the coast). **e.** Three cross-sections showing the probability distribution function of the earthquake location (warm colors indicate higher probability) obtained by inverting interpolated arrival times for the Etna summit and Eastern flank cables only. The black signs represent the location of the cables. The red dot represents the earthquake location provided by the monitoring network of INGV (24 permanent well distributed stations); INGV location: latitude: 506256 m; longitude 4176194 m; depth 4300 m below sea level).

4.2 Challenges, open questions and solutions for using Distributed Fiber Optic Sensing technologies

Directionality

A challenge of fiber optic distributed sensing is high anisotropy of sensitivity. The system is mostly insensitive in the direction perpendicular to the fiber. For example, a purely theoretical P-wave (which has a theoretical particle motion in the direction of the wave propagation) will not be detected by a straight fiber deployed in the direction perpendicular to the wave propagation. Conversely a theoretically pure S-wave will be perfectly detected, if it travels perpendicular to the fiber direction. The sensitivity depends on the wave field's orientation with respect to the direction of the fiber (Li et al., 2022). To address this issue, the deployment of cables in various directions has been proposed and tested, such as the PoroTomo array (Feigl et al., 2021). However, processing data from such multi-directional cable with many short linear sections requires much more complex processing steps and array methods (Johnson & Dudgeon, 1993; Van der Ende & Ampuero, 2021; Muñoz & Soto, 2022) compared to using longer sections of aligned fiber (Currenti et al., 2021; Jousset et al., 2022; Diaz-Meza et al., 2023). Encircling expected epicenters with cables can improve hypocenter determination (e.g., Currenti et al., 2023; Klaasen et al. 2023). Additionally, using multiple cables interrogated independently can lead to even more accurate location determinations, as shown in Fig. 17. Depending on the frequency aimed at (0.1 to 100 Hz on volcanoes), an ideal network could be a triangle, a spiral or star-like deployment of ~1 km aperture.

Coupling

Several options exist to deploy the cable in boreholes. Cementing the fiber optic cable behind casing generally ensures better coupling than using wireline cables deployed temporarily in the borehole (Cox et al., 2012). At volcanoes, due to limited number of boreholes, cables at the surface is likely the sole option, which is also more cost-effective. The reliability of strain measurements depends heavily on the coupling of the cable with the surrounding media. When the cable is bonded to a structure, coupling is less an issue. However, when it is placed in sediment, coupling depends on the yield stress at the cable-soil interface. In laboratory experiments cables placed in sediment remained well-coupled at small displacements (< 15 mm, Wu et al., 2020). However, with increasing strain, the response becomes non-linear and the cable eventually decouples from the soil (Zhang et al., 2016; Viens et al., 2022). The transfer of strain from the ground to the sensing elements in the fiber has been theoretically analyzed (Reinsch et al., 2017). Diaz-Mesa et al. (2023) also demonstrated that the cable's structure also affects the records. Further research is necessary to better understand cable coupling and determine if and how anchors could be used to improve it. Modelling tools, such as the one developed by Celli et al. (2024) will help in this respect.

Data management and processing: storage and big data.

One of the major challenges of DFOS for real-time applications is the significant amount of data they generate. For instance, Jousset et al. (2022) recorded 12 terabytes of data per week by sampling a 1.5 km long fiber every 4 meters for 15 days, albeit not continuously. Similarly, Flovenz et al. (2022) recorded 9 terabytes of data per week (250 terabytes in total) of DDSS fiber optic records by sampling a 21 km long fiber every 4 meters for 7 months, continuously. Down-sampling the data either spatially or temporally may be suggested, but this would result in a loss of information, both spatially and temporally. This hinders the significant advantages of these new tools. Quinteros et al. (2021) proposed a solution for storing and sharing data with researchers that do not have access to interrogators. However, the continuous management of the data and the extraction of valuable information for optimal monitoring still need to be defined. The rise in data streams from fiber optic sensing necessitates intelligent data processing (Arrowsmith et al., 2021). Currently, conversion and pre-processing tools and software are currently being developed (Isken et al., 2021; Quinteros, 2021; Spica et al., 2023), but more advanced tools are needed. Machine learning and artificial intelligence approaches could be highly advantageous (Tejedor et al., 2017). Techniques such as neural network approaches (Linville et al., 2019; Wu et al., 2021) are also being targeted. Liehr et al. (2019) proposed the use of artificial neural networks for raw measurement data interpolation and signal shift computation for reducing data analysis time. They demonstrated the benefits of this approach in making the WS-COTDR method usable for real-time applications using telecom dark fiber. As DDSS signals can be presented as 2D or 3D images, it is appropriate to use image processing techniques (Szegedy et al., 2015; Soto et al., 2016; Martins et al., 2019). Machine learning has been successfully applied to detect Very Long Period volcanic events on DDSS records at Vulcano island (Currenti et al., 2023).

Improving the sensitivity and saturation mitigation

The signal to noise ratio of DFOS measurements can be enhanced by stacking records from several parallel fibers of the same cable. This can be achieved by connecting the end of one fiber with another fiber in the same cable resulting in a loop that covers the same geographical location twice. This allows the same locations to be measured twice by simply prolonging the fiber. This technique is feasible for short cables, as DDSS can provide reasonably accurate measurements up to more than 20-30 km in a single fiber. This approach enables stacking of the records (Zwartes & Mateeva, 2015) and enhance accuracy, positioning DDSS as a serious competitor to conventional seismometers. However, signal quality becomes less accurate as the interrogated cable lengthens, creating a trade-off (Diaz-Meza et al., 2023). Fiber technologies have been mainly focused on the ability to measure weak signals. However, in some cases, large strain or strain rate may occur, such as during earthquakes or explosions, and this can cause the recorded signal to saturate. Saturation occurs when the strain rate exceeds the interferometric

ability of the interrogator, resulting in a skip in the optical phase. In practice, it is possible to correct for the phase skip and recover strain rates exceeding the theoretical limit allowed by the interrogator, as long as the strain/strain rate is not too large, and the interrogator is properly set up (Diaz-Meza et al., 2023).

Fibers (helicoidal and engineered fibers)

Zhi et al. (2003) conducted a detailed investigation into the effects of fiber structure on Rayleigh scattering. Lumens et al. (2013) attempted to overcome the directionality limitation by designing dedicated cables, such as helicoidal fiber (Kushinov, 2016), which comprises fibers built in a helical shape along the cable. The aim is to probe the strain field in all directions, and potentially overcome the drawback of linear fibers. For instance, Horman et al. (2013) tested helicoidal cable with the aim of measuring its broad-side sensitivity. They compared the record obtained from the cable with that obtained from 3C geophones. The results indicate that the cable is indeed sensitive in all directions, although the extent of the sensitivity improvement still needs to be proven. However, some experiments have shown that the signal is less accurate when using the helicoidal cable, than when using linear fibers (Bellefleur et al., 2020; Hendi et al., 2023). Another method to enhance the sensitivity is to modify the fiber's structure by incorporating permanent structure modifications of periodic index variations along its length. This allows for optimal light transmission with a specific gauge length, resulting in purposeful enhancement of the backscattered light and in increased sensitivity (Diaz-Meza et al., 2023).

Interrogators

Many recording systems have been proposed and tested in particular for Distributed Fiber Optic Sensing including new generation of DDSS interrogators and smaller instruments with less power consumption. The current consumption of DDSS interrogators is around 200 W (Peng & Chao, 2016; Feng et al., 2018; Hartog et al., 2018; Richter et al., 2019). Discoveries at the quantum level (Cohen et al., 2015; Favero, 2015) suggest that even very small vibration levels can be detected. Measuring the micro-mechanical properties of biomaterials through nano-indentation is a common technique (Mattei et al., 2017). In the field of volcanology, an ideal interrogator should be capable of simultaneously measuring temperature and strain using the three scattering types: Rayleigh scattering for high-frequency strain sensing (0.1 Hz to 200 Hz), Brillouin scattering for the ultra-low static strain (DC to minute), and Raman scattering for temperature signals with <0.05-degree resolution. The latter can be used to correct the temperature effect of other scattering processes. The ideal system should be capable of detecting nanostrain signals over a wide frequency range, with high resolution and over a long distance. Currently, such an interrogator does not exist.

5. Conclusions and perspectives

This chapter presented an introduction to the applications of fiber optic technologies in measuring temperature and the ground motion for volcano research and monitoring across a wide frequency range. Fiber optic methodologies encompass a broad range of instrumentation and techniques. Recent advancements in electronics and optics have led to the development of new instruments that utilize fiber optic principles, such as Fabry-Perot interferometry, Sagnac effect, and light scattering processes in glass. These instruments have become commercially increasingly affordable in the recent years.

We have illustrated the significant benefits of fiber optic sensing for volcanologists, providing increased spatial resolution and accuracy in probing volcanoes. This leads to new insights on structural features and volcanic processes, allowing for a more complete characterization of the volcano's subsurface structure and a better quantification of processes and seismic wave field. Fiber optic technologies enable a novel approach to monitoring the seismic wave fields and volcanic activity in conjunction with other observation sensors, such as infrasound and geochemistry.

We have discussed advantages and limitations of the methods. The ease of deployment and options provided in remote, steep or space-limited areas are advantages of rotation sensors. Rotation is directly measured and complements the understanding of the wave field. In complex environments it is possible to assess the composition of the seismic wave field and its changes directly. New methodologies such as the ones proposed by Gautier et al. (2022) may be useful in the future for more accurate measurements of rotation. DFOS has considerable advantages over observations with a single point sensor due to the high number of measurements. However, DFOS measurements may present higher instrumental noise. Calibration of DFOS is challenging due to the high spatial variability of coupling to the ground all along the fiber. Although DFOS has only one component measurement, proper array design and dense spatial resolution and temporal sampling provide additional and redundant information. Conventional processing methods in seismology need to be adapted for fiber optic records. For instance, the application of ambient noise processing (Brennguier et al., 2008) is challenging for fiber records due to the high sensitivity of DFOS to local structures. Additionally, research is underway to access the full strain tensor, including all six strain components, using fiber optic methods.

It is worth noting that many volcanoes do not have pre-existing optical fibers, and a significant initial investment seems necessary. In this context, we provide a rough cost estimation for a typical campaign. Let's record a fiber of 2500 channels (15 km, 4 m spatial sampling) for 10 days. The rental cost for an interrogator was 100,000 € (100 €/channel) in 2015 and 10,000 € (10 €/channel) in 2018. Interrogator

costs are expected to be around 100,000 € (in 2023), and the cost of a standard cable is estimated to be ranging 1-10 €/meter (150,000 € for 15 kilometers for the higher end). Assuming a cost of 1000 € (lower end of cost) for a virtual broadband seismometer with only 1 component only. Deploying 2500 broadband stations along the fiber, this would cost 2,500,000 €, excluding deployment costs. Even with the investment required for purchasing and deploying the cable by digging a trench, the overall cost of the fiber optic approach is significantly lower. Distributed fiber optic sensing offers benefits such as little maintenance, energy and time savings, and the ability to collect dense, accurate and detailed data. For example, the cable deployed at the summit of Etna volcano in the summer 2019 (Currenti et al., 2021) remained unused and with no maintenance for 4 years due to Covid-19 pandemic. In the summer 2023, it became possible to reconnect an interrogator to the fiber. In less than one hour the acquisition system was set up transforming the cable in hundreds of sensors able to record small volcanic events similar to those observed in 2018 (Jousset et al., 2022). This was achieved using four fiber instances, each with 750 channels (Diaz-Mesa et al., 2023).

Farghal et al. (2022) discuss the potential of DDSS for early earthquake detection applications. Their conclusions can be transferred and adapted for volcano hazard assessment and improved monitoring, leading to more certain and timely alerts. One strategy is to combine multiple types of instruments to perform joint inversions for hypocenters, source mechanisms and structural features using data from seismometers, rotational sensors and fiber optic interrogators. A detailed plan for combining these sensor types has yet to be established, building on initial attempts (e.g., Flovenz et al., 2022; Obermann et al., 2022) and exploring new processing algorithms using machine learning and artificial intelligence (Wu et al., 2021; Trainor-Guitton et al., 2022).

Following the onset of the volcanic crisis at Vulcano Island in September 2021, Currenti et al. (2023) demonstrated that a rapid response to a volcanic crisis can be achieved using existing telecom infrastructures. Collaboration between institutions and private companies with available infrastructures, such as telecom companies, is essential and requires preparedness before the crisis begins. Discussions and agreements with the telecom providers at the Sicilian volcanoes over the last years were preparatory to rapidly access the fiber optic network and perform DDSS measurements at Vulcano Island during the crisis (Krawczyk et al., 2020; Napoli et al., 2020). Such preliminary steps are essential for any successful crisis management.

Therefore, we are optimistic and confident that the development of fiber optic technologies on volcanoes will provide additional understanding of volcanic processes. This will lead to a better

description of the internal structure and more accurate anticipation of the volcano behavior prior to and during eruptions resulting in improved volcano monitoring and crisis management.

Acknowledgments

We would like to acknowledge the following institutions and funding bodies. In Japan: Fukushima River and National Highway Office, Tohoku Regional Bureau, Ministry of Land, Infrastructure, Transport and Tourism (MLIT). Additionally, we used a red relief image map of Azuma volcano (Japan) provided by the Asia Air Survey, Myanmar Co., and MLIT was used. The Geospatial Information Authority of Japan provided the digital elevation model used in the numerical simulations. We thank the Ministry of Education, Culture, Sports, Science and Technology (MEXT) of Japan for their support under the Observation and Research Program for Prediction of Earthquakes and Volcanic Eruptions and ERI JURP 2020-S-04. We also thank HS Orka, ISOR (Iceland Geosurvey), IMO (Iceland Meteorological Office) for their contributions in Iceland. The fiber optic cables used are managed by INFN-LNS/EMSO (Italy), the FLY-LION3 consortium (Mayotte), Telecom Italia (Italy), Mila (Iceland) or deployed for specific purposes. FLY-LION3 is a submarine cable owned by a consortium consisting of "SRR, Société Réunionnais du Radiotéléphone", "Comores Câbles" and "Orange". We would like to express our gratitude to Parco dell'Etna and the municipalities (Linguaglossa and Castiglione di Sicilia) for granting us the necessary authorizations to deploy the cable and instruments at Piano delle Concazze. The geophones, broadband seismometers and data logger equipment in Italy and Iceland are from the Geophysical Instrumental Pool of Potsdam (GIPP). The fiber optic interrogators used in this study were funded by various institutions: for Mayotte, they were co-funding by Le Mans University, ESEO (Ecole Supérieure d'Electronique de l'Ouest) and IPGP (Institut de Physique du Globe de Paris) with the support from FEDER (50%), as part of the research regional project of Pays de la Loire (RFI WISE). For Iceland and Italy, they were funded by the GeoForschungZentrum Potsdam and the Helmholtz Association. For Mt Meager and Grímsvötn, they were funded by ETH Zürich; for Laacher See: Fieldwork and data collection at LS were made possible thanks to the Transatlantic Research Partnership, a program of the FACE Foundation, and the French Embassy. C.C. acknowledges support from the F.R.S.- FNRS through the MIS CalderaSounds funding. We acknowledge the Helmholtz Association for funding. The European Union Seventh Framework Programme under the Grant No. 608553 (project IMAGE); Horizon 2020 ERC Advances Grant 786304 (project FOCUS); European Union's Horizon 2020 Research and Innovation Program for IMPROVE ETN under the grant agreement 858092, for SPIN ITN under the Marie Skłodowska-Curie Grant Agreement Number 955515, for Geo-INQUIRE under the grant agreement 101058518; the GeoForschungZentrum Potsdam and the Helmholtz Association; the IS-FNRS funding (Belgium). The PNRR project "SAMOTHRACE" (Italy). We deeply thank Sascha Liehr (DiGOS GmbH) for sharing his expertise in photonics and reviewing an earlier version of this manuscript. Some figures were created using Generic

Mapping Tools (Wessel et al., 2019) and Matplotlib (Hunter, 2007). The final version of the manuscript was checked for English using Deep-L.

References

Agnew D.C. (1986). Strainmeters and tiltmeters. *Review of Geophysics* 24 (3), 579-624.

Ajo-Franklin J., Dou S., Lindsey N., Monga I., Tracy C., Robertson M., Tribaldos V.R., Ulrich C., Freifeld B., Daley T. & Li X. (2019). Distributed acoustic sensing using dark fiber for near-surface characterization and Broadband seismic event detection. *Scientific Reports* 9: 1328, doi: /10.1038/s41598-018-36675-8.

Aki K. & Richards P. G. (2002). *Quantitative Seismology*, 2nd Ed. University Science Book.

Archibald P. C. & Bennett H. E. (1978). Scattering from Infrared Missile Domes. *Optical Engineering* 17 (6), 176647. <https://doi.org/10.1117/12.7972298>

Atterholt J., Zhan Z. & Yang Y. (2022). Fault Zone Imaging with Distributed Acoustic Sensing: Body-To-Surface Wave Scattering. *Journal of Geophysical Research* 127, 11, e2022JB025052

Arrowsmith S.J., Trugman D.T., MacCarthy J., Bergenm K.J., Lumley D. & Magnani M. B. (2021). Big data seismology. *Reviews of Geophysics* 60, e2021RG000769. <https://doi.org/10.1029/2021RG000769>.

Biagioli F., Metaxian J.-P., Stutzmann E., Ripepe M., Bernard P., Trabattoni A., Longo R. & Bouin M.-P. (2024). Array Analysis of Seismo-Volcanic Activity with Distributed Acoustic Sensing. *Geophysical Journal International* 236, 1, 607–620 <https://doi.org/10.1093/gji/ggad427>

Bao X. & Chen L. (2012). Recent progress in distributed fiber optic sensors. *Sensors (Basel)*, 12, 8601-8639.

Bao X., Zhou Z. & Wang Y. (2021). Review: distributed time-domain sensors based on Brillouin scattering and FWM enhanced SBS for temperature, strain and acoustic wave detection. *Photonix*, 2, 14.

Barnoski M. K. & Jensen S. M. (1976). Fiber waveguides: A novel technique for investigating attenuation characteristics. *Applied Optics* 15, 9, 2112–2115.

Barnoski M. K., Rourke M. D., Jensen S. M. & Melville S. M. (1977). Optical time domain reflectometer, *Appl. Opt.* 16, 2375-2379.

Barrías A., Casas J.R. & Villalba S. (2017). Application study of embedded Rayleigh based distributed optical fiber sensors in concrete beams. *Procedia Engineering* 199, 2014-2019.

Bastianini F., R. Di Sante, F. Falcetelli, D. Marini & G. Bolognini (2019). Optical fiber sensing cables for Brillouin-based distributed measurements. *Sensors* 19, 5127. doi:10.3390/s19235172

Basu D., Whittaker A. S. & Costantinou, M. C. (2017). On the design of a dense array to extract rotational components of earthquake ground motion, *Bull Earthquake Eng*, 15, 827–860, <https://doi.org/10.1007/s10518-016-9992-6>, 2017.

Basu D., Whittaker A.S. & Costantinou M.C. (2013). Extracting rotational components of earthquake ground motion using data recorded at multiple station, *Earthquake Engng Struct Dyn*, 42, 451-468, <https://doi.org/10.1002/eqe.2233>.

Battaglia J. & Aki K. (2003). Location of seismic events and eruptive fissures on the Piton de la Fournaise volcano using seismic amplitudes. *Journal of Geophysical Research: Solid Earth* 108, B8, 2364, doi:10.1029/2002JB002193.

Bean C. J., Lokmer I. & O'Brien G. S. (2008). Influence of near-surface volcanic structure on long-period seismic signals and on moment tensor inversions: Simulated examples from Mount Etna. *Journal of Geophysical Research* 113, DOI:10.1029/2007JB005468

Bean C. J., de Barros L., Lokmer I., Métaxian J.-P., O'Brien G. & Murphy S. (2014). Long-period seismicity in the shallow volcanic edifice formed from slow-rupture earthquakes. *Nature Geoscience* 7, 1, 71–75. doi:10.1038/ngeo2027.

Becker M. W., Ciervo C., Cole M., Coleman T. & Mondanos M. (2017). Fracture hydromechanical response measured by fiber optic distributed acoustic sensing at milliHertz frequencies. *Geophysical Research Letters* 44, 7295–7302, doi: 10.1002/2017GL073931.

- Bellefleur G., Schetselaar E., Wade D., White D., Enkin R. & Schmitt D.R. (2020). Vertical seismic profiling using distributed acoustic sensing (DAS) with scatter-enhanced fiber-optic cable at the Cu-Au New Afton porphyry deposit, British Columbia, Canada. *Geophysical Prospecting* 68, 313-333. <https://doi.org/10.1111/1365-2478.12828>.
- Bernard P., Plantier G., Ménard P., Hello Y., Savaton G., Metaxian J.-P., Ripepe M., Bouin M.-P., Boudin F., Feron R., Deroussi S. & Moretti R. & the optic-OBS-strain-2022 team (2022). Innovative high resolution optical geophysical instruments at the termination of long fibers: first results from the Les Saintes optical ocean bottom seismometer, and from the Stromboli optical strainmeter, EGU General Assembly, Vienna, Austria, 23–27 May 2022, EGU22-10574, <https://doi.org/10.5194/egusphere-egu22-10574>.
- Bernauer F., Wassermann J., Guattari F., Bigueur A., Gaillot A., Toldi E., Ponceau D., Schreiber U. & Igel H. (2018). BlueSeis3A: Full Characterization of a 3C Broadband Rotational Seismometer. *Seismological Research Letters*, 89 (2A). doi: 10.1785/0220170143
- Bernauer F., Wassermann J. & Igel H. (2012). Rotational sensors—a comparison of different sensor types. *J. Seismol* 16, 595–602. <https://doi.org/10.1007/s10950-012-9286-7>
- Bernauer F., Behnen K., Wassermann J., Egdorf S., Igel H., Sammler K., Hoffmann M., Edme P., Sollberger D., Schmelzbach C., Robertsson J., Paitz P., Igel J., Smolinski K., Fichtner, F., Rossi, Y. Izgi G., Vollmer D., Eibl E. P. S. Buske S., Veress C., Guattari F., Laudat T. Mattio L., Sèbe O., Lallemand C., Brunner B., Kurzych A.T., Dudek M., Jaroszewicz L.R., Kowalski J.K., Bońkowski P.A., Bobra P., Zembaty Z., Vackář J., Málek J. & Brokesova J. (2021). Rotation, Strain, and Translation Sensors Performance Tests with Active Seismic Sources. *Sensors* 21(1), 264. doi: 10.3390/s21010264.
- Bernauer F., Wassermann J. & Igel H. (2020). Dynamic Tilt Correction Using Direct Rotational Motion Measurements. *Seismological Research Letters* 91 (5), 2872-2880. 10.1785/02200200132.
- Bernini R., Minardo A & Zeni L. (2012). Distributed Sensing at centimetre scale spatial resolution by BOFDA: measurements and signal processing. *IEEE Photonics J.*, 4, 48-56.
- Bhadra A., Ghose S. & Raychaudhuri B. (2022). A quest for the origin of the Sagnac effect. *Eur. Phys. J. C* 82, 649, <https://doi.org/10.1140/epjc/s10052-022-10620-6>
- Biondi E., Zhu W., Li J., Williams E. F. & Zhan Z. (2023). An upper-crust lid over the Long Valley magma chamber. *Science Advances* 9, 42. DOI: 10.1126/sciadv.adi9878
- Blanc W., Schenato L., Molardi C., Palmieri L., Galtarossa A. & Tosi D. (2022). Distributed fiber optics strain sensors: from long to short distance. Special Issue: Glass, a ubiquitous material. D. Neuville Ed. *Comptes Rendus AS Geosciences*. <https://doi.org/10.5802/crgeos.129>
- Blanck H., Jousset P., Hersir G.P., Ágústsson K. & Flóvenz Ó. G. (2020). Analysis of 2014–2015 on- and off-shore passive seismic data on the Reykjanes Peninsula, SW Iceland. - *Journal of Volcanology and Geothermal Research*, 391, 106548. <https://doi.org/10.1016/j.jvolgeores.2019.02.001>
- Bodin P., Gomberg J., Singh S. K. & Santoyo M. (1997). Dynamic deformations of shallow sediments in the Valley of Mexico, part I: Three-dimensional strains and rotations recorded on a seismic array, *Bull. Seismol. Soc. Am.* 87, 528–539.
- Bogris A., Nikas T., Simos C. Simos I., Lentas K., Melis N.S., Fichtner A., Bowden D., Smolinski, K. Mesaritakis C. & Chochliouros I. (2022). Sensitive seismic sensors based on microwave frequency fiber interferometry in commercially deployed cables. *Sci Rep* 12, 14000. <https://doi.org/10.1038/s41598-022-18130-x>
- Bona A., Dean T., Correa J., Pevzner R., Tertyshnikov K.V. & Van Zaanen L. (2017). Amplitude and Phase Response of DAS Receivers. Extended abstract, 79th EAGE Conference & Exhibition, Paris, France.
- Bonaccorso A., Linde A., Currenti G., Sacks S. & Sicali A. (2016). The borehole dilatometer network of Mount Etna: A powerful tool to detect and infer volcano dynamics, *J. Geophys. Res. Solid Earth*, 121, doi:10.1002/2016JB012914
- Briggs M.A., Lautz L.K. & McKenzie J. M. (2011). A comparison of fibre-optic distributed temperature sensing to traditional methods of evaluating groundwater inflow to streams. *Hydrological Processes* 26, 9, 1277-1290, <https://doi.org/10.1002/hyp.8200>.
- Brokešová J., Málek J., Vackář J., Bernauer F., Wassermann J. & Igel H. (2021). Rotaphone-CY: The Newest Rotaphone Model Design and Preliminary Results from Performance Tests with Active Seismic Sources. *Sensors* 21 (2), E562 doi: 10.3390/s21020562.
- Bouchon M. & Aki K. (1982) Strain, tilt and rotation associated with strong motion ground motion in the vicinity of earthquake faults. *Bulletin of the Seismological Society of America* 72, 1717-1738.
- Brenguier F., Shapiro N. M., Campillo V., Ferrazzini, Z. Duputel, O. Coutant & A. Nercessian (2008). Towards forecasting volcanic eruptions using seismic noise. *Nature Geoscience* 1 (2), 126–130.

- Brillouin Léon (1914). Diffusion de la lumière par un corps transparent homogène. *Comptes Rendus de l'Académie des Sciences* (in French). 158: 1331–4.
- Bruno V., Aloisi M., Gambino S., Mattia M., Ferlito C. & Rossi M. (2022). The most intense deflation of the last two decades at Mt. Etna: the 2019-2021 evolution of ground deformation and modelled pressure sources. *Geophysical Research Letters* 49, 6, e2021GL095195. <https://doi.org/10.1029/2021GL095195>
- Burdick S., van der Hilst R. D., Vernon F.L., Martynov V., Cox T., Eakins J., Mulder T., Astiz L. & Pavlis G.L. (2009). Model Update December 2008: Upper Mantle Heterogeneity beneath North America from P-wave Travel Time Tomography with Global and USArray Transportable Array Data. *Seismological Research Letters* 80, 4, 638–645. <https://doi.org/10.1785/gssrl.80.4.638>
- Butt M.A., Voronkov G.S., Grakhova E.P., Kutluryov R. V., Kazanskiy N.L. & Khonina S.N. (2022). Environmental Monitoring: a comprehensive review on optical waveguide and fiber-based sensors. *Biosensors* 12, 1038. <http://doi.org/10.3390/bios12111038>.
- Cai Q., Xiangly B. & Du A. (2015). Spatial heterodyne spectrometer based on the Mach-Zehnder interferometer. *Optics Communications* 355, 239-245.
- Canitano A., Mouyen M., Hsu Y-J., Linde A., Sacks S. & Lee H-M. (2021). Fifteen Years of Continuous High-Resolution Borehole Strainmeter Measurements in Eastern Taiwan: An Overview and Perspectives. *GeoHazards* 2(3):172-195. <https://doi.org/10.3390/geohazards2030010>
- Carlino S., Mirabile M., Troise C., Sacchi M., Zeni L., Minerdo A., Caccavale M., Darányi V. & De Natale G. (2016). Distributed-Temperature Sensing using optical methods: a first application in the offshore area of Campi Flegrei caldera (southern Italy) for volcano monitoring. *Remote Sensing* 8, 674, doi:10.3390/rs8080674.
- Castongia E., Wang H.F., Lord N., Fratta D., Mondanos M. & Chalari A. (2017). An experimental investigation of distributed acoustic sensing (das) on lake ice. *Journal of Environmental and Engineering Geophysics*, 22(2): 167–176.
- Caudron C., Miao Y., Spica Z.J., Wollin C., Haberland C., Jousset P., Yates, A., Vandemeulebrouck J., Schmidt B., Krawczyk C.M. & Dahm T. (2024). Monitoring underwater volcano degassing using fiber-optic sensing. *Scientific Report* 14, 3128. <https://doi.org/10.1038/s41598-024-53444-y>
- Celli N. L., Bean C. J. & O'Brien G. (2024). Full-waveform simulation of DAS records, response and cable-ground coupling. *Geophysical Journal International* 236, 659-674.
- Cesca S., Letort J., Razafindrakoto H. N., Heimann S., Rivalta E., Isken M. P., Nikkhoo M., Passarelli L., Petersen G.M., Cotton F. & Dahm T. (2020). Drainage of a deep magma reservoir near Mayotte inferred from seismicity and deformation. *Nature Geoscience*, 13(1), 87-93.
- Chang X., Wen X., Gao D., Luo M., Teng P., Zhu Z., Zhang J., Lim K., Copner N. & Yang X. (2022). Optoelectrode based on conductive fiber Fabry-Perot probe for simultaneous electrochemical and optical sensing. *Measurement* 205, 112198.
- Chawah P., Chéry J., Boudin F., Cattoen M., Seat H.C., Plantier G., Lizion F., Sourice A., Bernard P., Brunet C., Boyer D. & Gaffet S. (2015). A simple pendulum borehole tiltmeter based on a triaxial optical-fiber displacement sensor. *Geophysical Journal International* 203, 2, 1026–1038. <https://doi.org/10.1093/gji/ggv358>
- Chen M., Masoudi, A. & Brambilla G. (2019). Performance analysis of distributed optical fiber acoustic sensors based on ϕ -OTDR. *Optics Express* 27, 7, pp. 9684-9695. doi: 10.1364/OE.27.009684.
- Chen M., Masoudi A., Parmigiani F. & Brambilla G. (2018). Distributed acoustic sensor based on a two- mode fiber. *Optics Express* 26, 19, pp. 25399-25407. doi: 10.1364/OE.27.009684.
- Chiodini G., Avino R., Caliro S. & Minopoli C. (2011). Temperature and pressure gas ge indicators at the Solfatara fumaroles (Campi Flegrei). *Ann. Geophys.* 54(2). Available from: <https://www.annalsofgeophysics.eu/index.php/annals/article/view/5002>
- Chouet B. (1996). Long-period volcano seismicity: its source and use in eruption forecasting. *Nature* 380, 309–316. <https://doi.org/10.1038/380309a0>
- Chouet B. & Matoza R. S. (2013). A multi-decadal view of seismic methods for detecting precursors of magma movement and eruption. *Journal of Volcanology and Geothermal Research* 252, 108–175.
- Chow D. M., Yang Z., Soto M. A. & Thévenaz L. (2018). Distributed forward Brillouin sensor based on local light phase recovery. *Nature communications*, 9(1), 2990.

- Cohen J.D., Meenehan S.M., MacCabe G.S., Gröblacher S., Safavi-Naeini A.H., Marsili F., Shaw M.D & Painter O. (2015). Phonon counting and intensity interferometry of a nanomechanical resonator. *Letter to Nature* 520, 522-525. Doi: 10.1038/nature14349.
- Contrafatto D., Currenti G., Jousset P., Larocca G., Messina A., Pellegrino D., Pulvirenti M., Rapisarda S., Zuccarello L., Chalari A. & Krawczyk C.M. (2019). Monitoring volcanic activity with fibre-optic Distributed Acoustic Sensing – first experiments at the Etna volcano. *Geophysical Research Abstracts* 21, EGU2019-13088-1.
- Correa J., Egorov A., Tertyshnikov K., Bona A., Pevzner R., Dean T., Freifeld B. & Marshall S. (2017). Analysis of signal to noise and characteristics of DAS VSP at near and far offsets – a CO2CRC Otway Project data example. *The leading Edge, Special Section: fiber optic distributed sensing*. 994a1-994a7. Doi:10.1190/tle36120994a1.1.
- Coutant O., De Mangin M. & Le Coarer E. (2015). Fabry-Perrot Optical strainmeter with an embeddable, low- power interrogation system. *Optica* 2, 5, 400-404.
- Cox B., Wills P., Kiyashshenko D., Mestayer J., Lopez J., Bourne S., Lupton R., Solano G., Henderson N., Hill D. & Roy J. (2012). Distributed Acoustic Sensing for geophysical measurement, monitoring and verification. *CSEG recorder*, 7-13.
- Culshaw B. (2004). Optical fiber sensor technologies: opportunities and perhaps pitfalls. *J. Lighwave Technol.* 22.
- Currenti G., Allegra M., Cannavò F., Jousset P., Prestifilippo M., Napoli R., Sciotto M., Di Grazia G., Privitera E., Palazzo S. & Krawczyk C.M. (2023). Distributed dynamic strain sensing of very long period and long period events on telecom fiber-optic cables at Vulcano, Italy. *Scientific Reports* 13, 4641. <https://www.nature.com/articles/s41598-023-31779-2>
- Currenti G., Jousset P., Napoli R., Krawczyk C. M. & Weber M. (2021). On the comparison of strain measurements from fiber optics with a dense seismometer array at Etna volcano (Italy) *Solid Earth*, 12, 993–1003, <https://doi.org/10.5194/se-12-993-2021>.
- Currenti G., Zuccarello L., Bonaccorso A. & Sicali A. (2017). Borehole volumetric strainmeter calibration from a nearby seismic broadband array at Etna volcano, *J. Geophys. Res.*, <https://doi.org/10.1002/2017JB014663>.
- Currenti G. & Bonaccorso A. (2019). Cyclic magma recharge pulses detected by high-precision strainmeter data: the case of 2017 inter-eruptive activity at Etna volcano, *Scientific Reports*, doi: 10.1038/s41598-019-44066-w
- Curtis A. & Kyle P. (2011). Geothermal point sources identified in a fumarolic ice cave on Erebus volcano, Antarctica using fiber optic distributed temperature sensing. *Geophysical Research Letters* 38, L16802, 10.1029/2011GL048272.
- Daley T., Freifeld B. M., Ajo-Franklin J., Dou S., Pevzner R. Shulakova V., Kashikar S. Miller D.E., Goetz J., Hennings J. & Lueth S. (2013). Field testing of fiber optic distributed acoustic sensing (DAS) for subsurface seismic monitoring. *The leading Edge*, 936-942.
- Daley T., Miller D. E., Dodds K., Cook P. & Freifeld B.M. (2015). Field testing of modular borehole monitoring with simultaneous distributed acoustic sensing and geophone vertical seismic profiles at Citronelle, Alabama. *Geophysical prospecting*, doi: 10.1111/1365-2478.12324.
- Dean T., Cuny T. & Hartog A. H. (2016). The effect of gauge length on axially incident P-waves measured using fiber optic distributed vibration sensing. *Geophysical Prospecting* doi: 10.1111/1365-2478.12419.
- DeWolf S., Wyatt F. K., Zumberge M. A. & Hatfield W. (2015). Improved vertical optical fiber borehole strainmeter design for measuring Earth strain. *Review of Scientific Instruments* 86, 114502 (2015) <https://doi.org/10.1063/1.4935923>
- Di H., Xin Y. & Jian J. (2018). Review of optical fiber sensors for deformation measurement. *Optik* 168, 703-713.
- Diaz-Meza S., Jousset P., Currenti G., Wollin C., Krawczyk C.M., Clarke A. & Chalari A. (2023). On the comparison of records from Standard and Engineered fibre optic cables at Etna volcano (Italy). *Sensors* 23 (7), 3735. <https://doi.org/10.3390/s23073735>
- Di Lieto B., Romano P., Scarpa R. & Linde A. T. (2020). Strain signals before and during paroxysmal activity at Stromboli volcano, Italy. *Geophysical Research Letters*, 47, e2020GL088521. <https://doi.org/10.1029/2020GL088521>
- Donner S., Chin-Jen L., Hadziioannou C., Gebauer A., Vernon F., Agnew D. C., Igel H., Schreiber U. & Wassermann J. (2017) Comparing Direct Observation of Strain, Rotation, and Displacement with Array Estimates at Piñon Flat Observatory, California, *Seismological Research Letters*, 88, 4, <https://doi.org/10.1785/0220160216>.
- Dou S., Lindsey N., Wagner A.M., Daley T.M., Freifeld B., Robertson M., Peterson J., Ulrich C., Martin E.R. & Ajo-Franklin J.B. (2017). Distributed Acoustic Sensing for Seismic Monitoring of The Near Surface: A Traffic-Noise Interferometry. *Scientific Reports* 7, 11620, doi:10.1038/s41598-017-11986-4.

- Eibl E. P. S., Roskopf M., Sciotto M., Current, G., Di Grazia G., Jousset P., Krüger F. & Weber M. (2022). Performance of a Rotational Sensor to Decipher Volcano Seismic Signals on Etna, Italy. *Journal of Geophysical Research: Solid Earth* 127. E2021JB023617. <https://doi.org/10.1029/2021JB023617>.
- Farghal N.S., Saunders J.K. & Parker G.A. (2022). The potential of using fibre optic distributed acoustic sensing in earthquake early warning applications. *Bulletin of the Seismological Society of America* 112, 3, 1416-1435.
- Favero I. (2015). Listening to quantum grains of sound. *Nature* 520, pp 441-442.
- Feigl K., Taverna N. & Rossol M. (2021). PoroTomo Natural Laboratory Horizontal and Vertical Distributed Acoustic Sensing Data. DOI 10.15121/1778858
- Feng S., Xu, T., Huang J., Yang Y., Ma L. & Li F. (2018). Sub-Meter Spatial Resolution Phase-Sensitive Optical Time-Domain Reflectometry System Using Double Interferometers. *Applied Sciences*.
- Fenta M.C., Potter D.K. & Szanyi J. (2021). Fibre optic methods of prospecting: a comprehensive and modern branch of geophysics. *Survey in Geophysics* 42, 551-584.
- Feron R., Bernard P., Feuillooy M., Menard P., Necessian A., Deroussi S., Kitou G-T. & Plantier G. (2020). First optical seismometer at the top of La Soufrière volcano, Guadeloupe. *Seismological Research Letters*, 2020, 91 (5), 2448-2457. 10.1785/0220200126
- Ferraro P. & De Natale G. (2002). On the possible use of optical fiber Bragg gratings as strain sensors for geodynamical monitoring. *Optics Lasers Eng.* 37, 115–130.
- Feuillet N., Jorry S., Crawford W. C., Deplus C., Thinon I., Jacques E., Saurel J.M., Lemoine A., Paquet F., Satriano C., Aiken C., Foix O., Kowalski P., Laurent A., Rinnert E., Cathalot C., Donval J.P., Guyader V., Gaillot A., Scalabrin C., Moreira M., Peltier A., Beauducel F., Grandin R., Ballu V., Daniel R., Pelleau P., Gomez J., Besançon S., Geli L., Bernard P., Bachelery P., Fouquet Y., Bertil D., Lemarchand A. & Van der Woerd J. (2021). Birth of a large volcanic edifice offshore Mayotte via lithosphere-scale dyke intrusion. *627 Nature Geoscience*, 14(10), 787-795.
- Fichtner A., Klaasen S., Thrastarson S., Cubuk-Sabuncu Y., Paitz P. & Jonsdottir K. (2022). Fiber optic observation of volcanic tremor through floating ice sheet resonance. *The Seismic Record*, 2, 148-155, doi:10.1785/0320220010.
- Flovenz O., Wang R., Hersir G., Dahm T., Hainzl S., Vassileva M., Drouin V., Heimann S., Isken M., Gudnasson E., Agustsson K., Agustsdottir T., Horalek J., Motagh M., Walter T., Rivalta E., P. Jousset, Krawczyk C. & Milkereit C. (2022). Cyclical geothermal unrest as a precursor to Iceland's 2021 Fagradalsfjall eruption. *Nature Geoscience* 15, 397–404. <https://doi.org/10.1038/s41561-022-00930-5>
- Frignet B.G. & Hartog H. (2014). Optical vertical seismic profile on wireline cable. SPWLA 55th Annual Logging Symposium, May 18-22, 2014.
- Galindez-Jamioy C.A. & López-Higuera J.M. (2012). Brillouin Distributed Fiber Sensors: An Overview and Applications. *Journal of Sensors*, 2012, 1-17.
- Gambino S. & Cammarata L. (2017). Tilt measurements on volcanoes: more than a hundred years of recordings. *Italian Journal of Geosciences* 136, 2.
- Gautier R., Guessoum M., Sidorenkov L. A., Bouton Q., Landragin A. & R. Geiger (2022). Accurate measurement of the Sagnac effect for matter waves. *Science Advances* 8, 23, DOI: 10.1126/sciadv.abn80.
- Gladwin M. T. & Hart R. (1985). Design parameters for borehole strain instrumentation, *Pure Appl. Geophys.*, 123, 59–80, doi:10.1007/BF00877049
- Gomberg J. & Agnew D. (1996) The accuracy of seismic estimates of dynamic strains: An evaluation using strainmeter and seismometer data from Piñon Flat Observatory, California. *Bulletin of the Seismological Society of America*, 86(1A), 212–220.
- Gorschkov B.G., Yüksel K., Fotiadi A.A., Wuilpart M., Korobko D.A., Zhirnov A.A., Stepanov K.V., Turov A.T., Konstantinov Y. A. & Lobach I.A. (2022). Scientific applications of distributed acoustic sensing: State of the art, review and perspective. *Sensors* 22, 1033. Doi: 10.3390/s22031033.
- Grattan K.T.V. & Sun T. (2000). Fiber optic sensors technology: introduction and overview. In: Grattan K.T.V., Meggitt B.T. (eds) *Optical Fiber Sensor Technology*. Springer, Boston, MA.

- Gutscher M.-A., Royer J.-Y., Graindorge D., Murphy S., Klingerhoeffler F., Aiken C., Cattaneo A., Barreca D., Quétel L., Riccobene G., Petersen F., Urlaub M., Krastel S., Gross F., Kopp H., Magheriti L. & Beranzoli L. (2019). Fiber optic monitoring of active faults at the seafloor: I the FOCUS project. *Photoniques*, 32-37.
- Gutscher M.A., Quétel L., Murphy S., Riccobene G., Royer J.-Y., Barreca G., Aurnia S., Klingelhoef F., Cappelli G., Urlaub M., Krastel S., Gross F. & Kopp H. (2023). Detecting strain with a fiber optic cable on the seafloor offshore Mount Etna, Southern Italy. *Earth and Planetary Science Letters* 616, 118230.
- Hadziioannou C., Gaebler P., Schreiber U., Wassermann J. & Igel H. (2012). Examining ambient noise using co-located measurements of rotational and translational motion. *Journal of Seismology*, 16 (4), 787-796. doi: 10.1007/s10950-012-9288-5
- Halldórsson S.A., Marshall E.W., Caracciolo A. Matthews S., Bali E., Rasmussen M.B., Ranta F., Robin J. G., Sigmarsson O., MacLennan J., Jackson M.G., Whitehouse M.J. Jeon H., van der Meer Q. H.A., Mibei G.K., Kalliokoski M.H., Repczynska M.M., Runarsdóttir R. H., Sigurðsson G., Pfeffer M.A., Scott S.W., Kjartansdóttir R., Kleine B.I., Openheimer C., Aiuppa A., Ilyinskaya E., Bitetto M., Giudice G. & Stefánsson A. (2022). Rapid shifting of a deep magmatic source at Fagradalsfjall volcano, Iceland. *Nature* 609, 529–534. <https://doi.org/10.1038/s41586-022-04981-x>
- Hansen S., Schmandt B., Levander A., Kiser E., Vidale J.E., Abers G.A. & Creager K.C. (2016). Seismic evidence for a cold serpentinized mantle wedge beneath Mount St Helens. *Nature Communications* 7, 13242. <https://doi.org/10.1038/ncomms13242>.
- Hartog A.H. (1983). A distributed temperature sensor based on liquid-core optical fibers. *J Lightwave Technol.* 1(3):498-509.
- Hartog A.H. (2002). Progress in Distributed Fiber Optic Temperature Sensing. *Environmental and Industrial Sensing. Proc. SPIE*, 4578.
- Hartog A.H. (2017). *An introduction to Distributed Optical Fiber Sensors*. CRC Press.
- Hartog A.H., Belal M. & Clare M.A. (2018). Advances in distributed fiber optic sensing for monitoring marine infrastructure, measuring the deep ocean, and quantifying the risks posed by sea floor hazards. *Marine Technology Society Journal* 52, 5, 58-73.
- Hartog A.H., Frignet B., Mackie D., Clark M. (2014). Vertical seismic optical profiling on wireline logging cable. *Geophysical Prospecting* 62, 4, 1365-2478 doi: 10.1111/1365-2478.12141.
- Hartog A.H., Liokumovich L.B., Ushakov N.A., Kotov O.I., Dean T., Cuny T., Constantinou A. & English F.V. (2018). The use of multi-frequency acquisition to significantly improve the quality of fiber optic distributed sensing. *Geophysical Prospecting* 66, 192-202.
- Hatfield W., Elliott D., Wyatt F. K., Xie S. & Zumberge M. A. (2022). Results From a Decade of Optical Fiber Strainmeters at Piñon Flat Observatory. <https://doi.org/10.1029/2022EA002381>
- Hasegawa T. & Hotate K. (1999). Measurement of Brillouin gain spectrum distribution along an optical fiber by direct frequency modulation of a laser diode. *SPIE 3860, Fiber Optic Sensor Technology and Applications*. doi: 10.1117/12.372976.
- He X., Zhang M., Xie S., Gu L., Liu F., Chen Z & Tao Q. (2018). Identification and observation of the phase fading effect in phase-sensitive OTDR. *OSA Continuum* 1, 3, doi: 10.1364/OSAC.1.000963.
- He Z., Liu Q. & Tokunaga T. (2013). Ultrahigh resolution fiber optic quasi-static strain sensors for geophysical research. *Photonic Sens.* 3, 295–303.
- Hellweg M. (2000). Physical models for the source of Lascar's harmonic tremor. *J. Volcanol. Geotherm. Res.* 101, 183-198.
- Hendi S., Gorjian M., Bellefleur G., Hawkes C. D. & White D. (2023). Investigation of the Effects of Surrounding Media on the Distributed Acoustic Sensing of Helically-Wound Fiber-Optic Cable with Application to the New Afton Deposit, British Columbia. *Solid Earth, EGU*, 14, 1, 89–99. <https://doi.org/10.5194/se-14-89-2023>
- Hensch M., Dahm T., Ritter J., Heimann S., Schmidt B., Stange S., Lehmann K. (2019). Deep low-frequency earthquakes reveal ongoing magmatic recharge beneath Laacher See Volcano (Eifel, Germany). *Geophysical Journal International* 216, 3, 2025–2036. <https://doi.org/10.1093/gji/ggy532>
- Horiguchi T., Kurashima T. & Tateda M. (1989) Tensile strain dependence of Brillouin frequency shift in silica optical fibers. *IEEE Photonics Technology Letters*, 1, 107-108.
- Horiguchi T., Shimizu K., Kurashima T., Tateda M. & Koyamada Y. (1995). Development of a distributed sensing technique using Brillouin scattering. *J. Lightwave Technol.* 13, 1296–1302.

- Hornman K., Kushnikov B., Zwartjes P. & Franzen A. (2013). Field trial of a broadside-sensitive distributed acoustic sensing cable for surface seismic. 75th EAGE Conference and Exhibition, London Tu0408.
- Hunter J. D. (2007). Matplotlib: A 2D Graphics Environment. *Computing in Science & Engineering* 9, 3, pp. 90-95.
- Huntley D., Bobrowsky P., Qing Z., Sladen W., Bunce C., Edwards T., Hendry M., Derek M. & Choi E. (2014). Fiber optic strain monitoring and evaluation of a slow-moving landslide near Ashcroft, British Columbia, Canada. In K. Sassa, P. Canuti, & Y. Yin (Eds.), *Landslide Science for a Safer Geoenvironment, The International Programme on Landslides (IPL) 1*, pp. 415–421. doi.org/10.1007/978-3-319-04999-1_58
- Igel H., Schreiber K. U., Flaws A., Schuberth B., Velikoseltsev A. & Cochard A. (2005). Rotational motions induced by the M 8:1 Tokachi-oki earthquake, September 25, 2003, *Geophys. Res. Lett.* 32, L08309, doi 10.1029/2004GL022336
- Isken M. P., Wollin C., Sebastian H., Quinteros J., Jäckel K.-H. & Jousset P. (2021). DAS Convert - Convert distributed acoustic sensing data. V. 1.0. GFZ Data Services. <https://doi.org/10.5880/GFZ.2.1.2021.005>
- Izgi G., Eibl E., Donner S. & Bernauer F. (2021). Performance test of the rotational sensor blue-seis-3A in a Huddle test in Fürstfeldbruck. *Sensors* 2021, 21 (9), 3170. <https://doi.org/10.3390/s21093170>.
- Janneh M., Bruno F.A., Guardano S., Donnamura G.P., Iannaccone G., Gruca G., Werzinger S., Gunda A., Rijnveld N., Cutolo A., Pisco M. & Cusano A. (2023). Field demonstration of an optical fiber hydrophone for seismic monitoring at Campi-Flegrei cadera. *Optics and Laser technology* 158: 108920.
- Johnson D. H. & Dudgeon D. E. (1993). *Array Signal Processing: Concepts and Techniques* (Pearson Ed.).
- Johnson J. & Ripepe M. (2011). Volcano infrasound: a review. *J. Volcanol. Geotherm. Res.* 206, 3–4 .
- Jolly A., Thompson G. & Norton G. (2002). Locating pyroclastic flows on Soufriere Hills Volcano, Montserrat, West Indies, using amplitude signals from high dynamic range instruments. *Journal of Volcanology and Geothermal Research* 118, 299-317.
- Jousset P. (2019). Illuminating Earth's faults. *Science* 366 (6469):1076-1077. doi: 10.1126/science.aaz7750.
- Jousset P., Currenti G., Schwarz B., Chalari A., Tilmann F., Reinsch T., Zuccarello L, Primavera E. & Krawczyk C. M. (2022). Fiber optic distributed acoustic sensing of volcanic events. *Nature Communications* 13, 1753 (2022). <https://doi.org/10.1038/s41467-022-29184-w>
- Jousset P., Currenti G., Tilmann F., Zuccarello L., Chalari A., Reinsch T. & Krawczyk C.M. (2019). Towards seismic and volcanic hazard assessment with distributed acoustic sensing in fibre optic cable. *Geophysical Research Abstracts* 21, EGU2019-17281.
- Jousset P., Haberland C., Bauer K. & Arnason K. (2011). Hengill geothermal volcanic complex (Iceland) characterized by integrated geophysical observations, *Geothermics* 40, 1–24.
- Jousset P., Neuberg J. & Surton S. (2003). Modelling the time-dependent frequency content of low-frequency volcanic earthquakes. *Journal of Volcanology and Geothermal Research* 128, 201-223.
- Jousset P., Neuberg J. & Jolly A. (2004). Modelling low-frequency volcanic earthquakes in a viscoelastic medium with topography. *Geophysical Journal International* 159, 776-802.
- Jousset P., Reinsch T., Henniges J., Blanck H. & Ryberg, T. (2016). Strain and ground-motion monitoring at magmatic areas: ultra-long and ultra-dense networks using fiber optic sensing systems. *Geophys. Res. Abstr.* 18, EGU2016–EGU15707.
- Jousset P., Reinsch T., Ryberg T., Blanck H., Clarke A., Aghayev R., Hersir G. P., Henniges J., Weber M. & Krawczyk C. (2018). Dynamic strain determination using fiber optic cables allows imaging of seismological and structural features. *Nature Communications* 9, 2508, doi: s41467-018-04860-y.
- Jousset P. & Rohmer J. (2012). Evidence for remotely triggered microearthquakes during salt cavern collapse. *Geophysical Journal International* 191, 1, pp. 207–223. DOI: <http://doi.org/10.1111/j.1365-246X.2012.05598.x>
- Jousset P., Wuestefeld A., Krawczyk C., Baird A., Currenti G., Landrø M., Nowacki A., Spica Z., Barajas S. R., Lindner F., Konca Ö. A., Edme P., Lai V. H., Treshchikov V., Urmantseva L., Morten J. P., Lienhart W., Lipovsky B. P., Schoenball M., Ma K.-F. & the "DAS-month" team (sample only!): Global Distributed Fibre Optic Sensing recordings of the February 2023 Turkey earthquake sequence., EGU General Assembly 2023, Vienna, Austria, 24–28 Apr 2023, EGU23-17618, <https://doi.org/10.5194/egusphere-egu23-17618>, 2023.
- Julian B. R. (1994). Volcanic tremor: nonlinear excitation by fluid flow. *J. Geophys. Res.* 99, 11859-11877.

- Keil S., Wassermann J. & Igel H. (2021). Single-station seismic micro zonation using 6C measurements. *Journal of seismology* 25, 103–114.
- Keil S., Wilczek A., Wassermann J. & Kremers S. (2022). Comparing single-station 6C measurements and array measurements for seismic microzonation in Munich, Germany. *Geophysical Journal International* 231, 3, 1634-1652. <https://doi.org/10.1093/gji/ggac273>.
- Kersey A.D. (1996). A review of recent developments in fiber optic sensor technology. *Opt. Fiber Technol.* 2, 291-317.
- Killingbeck S. F., Livermore P. W., Booth A. D. & West L. J. (2018). Multimodal layered trans-dimensional inversion of seismic dispersion curves with depth constraints. *Geochem., Geophysics, Geosystems* 19, 4957–4971.
- Kislov K.V. & Gravurov V.V. (2021). Rotational Seismology: review of achievements and outlooks. *Seismic Instrumentation* 57, 2, 187-202.
- Klaasen S., Paitz P., Lindner N., Dettmer J. & Fichtner A. (2021). Distributed acoustic sensing in volcano-glacial environments—Mount Meager, British Columbia. *Journal of Geophysical Research: Solid Earth* 126, e2021JB022358. <https://doi.org/10.1029/2021JB022358>
- Klaasen S., Thrastarson S., Fichtner A., Cubuk-Sabuncu Y. & Jonsdottir K., 2022. Sensing Iceland's most active volcano with a «buried hair». *EOS*, 103, doi:10.1029/2022EO220007.
- Klaasen S., Thrastarson S., Çubuk-Sabuncu Y., Jónsdóttir K., Gebraad L., Paitz P. & Fichtner, A. (2023): Subglacial volcano monitoring with fibre-optic sensing: Grímsvötn, Iceland. *Volcanica* 6 (2), 301–311. doi: 10.30909/vol.06.02.301311.
- Kogure T. & Okuda, Y. (2018). Monitoring the vertical distribution of rainfall-induced strain changes in a landslide measured by distributed fiber optic sensing with Rayleigh backscattering. *Geophysical Research Letters* 45, 4033–4040. doi: 10.1029/2018GL077607.
- Koulakov I. & Shapiro N. (2021). Seismic Tomography of Volcanoes. *Encyclopedia of Earthquake Engineering*. DOI 10.1007/978-3-642-36197-5_51-1
- Krawczyk C.M., Jousset P., Currenti G., Weber M., Napoli R., Reinsch T., Riccobene G., Zuccarello L., Chalari A. & Clarke A. (2020). Monitoring volcanic and seismic activity with multiple fibre-optic Distributed Acoustic Sensing units at Etna volcano. *EGU General Assembly 2020*. EGU2020-15252 <https://doi.org/10.5194/egusphere-egu2020-15252>.
- Krawczyk C.M., Jousset P. & Reinsch T. (2019). Fibre-Optic Strain Sensing: Game Changer for (Urban) Seismic Surveying? In: *Proceedings, 1st Conference on Geophysics for Infrastructure Planning Monitoring and BIM*, v. 2019, pp. 1-5; <https://doi.org/10.3997/2214-4609.201902547>. European Association of Geoscientists & Engineers, ISSN 2214-4609.
- Krawczyk C.M. (2021). Wie Glasfaserkabel als Geosensoren zur Erkundung und Überwachung des Untergrunds genutzt werden können – Anwendungen und Potenzial von ortsverteilten faseroptischen Messungen (How fibre optic cables can be used as geosensors to explore and monitor the subsurface – Applications and Potential of distributed acoustic sensing). *Brandenburgische Geowissenschaftliche Beiträge*, 28 (1/2), 15-28; https://lbr.brandenburg.de/sixcms/media.php/9/BGB%201_2_2021_Krawczyk_dl.pdf
- Kreger S. T., Rahim N.A.A., Garg N., Klute S.M., Metrey D.R., Beaty N., Jeans J.W. & Gamber R. (2016). Optical frequency domain reflectometry: principles and applications in fiber optic sensing. *Conference SPIE Commercial + Scientific Sensing and Imaging*. DOI: 10.1117/12.2229057
- Kurashima T., Horiguchi T. & Tateda M. (1990). Distributed-temperature sensing using stimulated Brillouin scattering in optical silica fibers. *Optics letters*, 15, 1038-1040.
- Kurashima T., Horiguchi T., Izumita H., Furukawa S.I. & Koyamada Y. (1993). Brillouin optical-fiber time domain reflectometry. *IEICE Trans. Commun.* E76-B, 382-390.
- Kuvshinov B.N. (2016). Interaction of helically wound fiber optic cables with plane seismic waves. *Geophysical prospecting* 64, 3, 671-688, <http://dx.doi.org/10.1111/1365-2478.12303>.
- Lancelle C.E., Baldwin J. A., Lord N., Fratta D., Chalari A. & Wang H. F. (2021). Chapter 16: Using Distributed Acoustic Sensing (DAS) for Multichannel Analysis of Surface Waves (MASW). in: *Distributed Acoustic Sensing: Methods and Applications*. Yingping Li, Martin Karrenbach, Jonathan B. Ajo-Franklin Editors. <https://doi.org/10.1002/9781119521808.ch16>

- Landrø M., Bouffaut L., Kriesell H.I., Potter J.R., Rørstadbotnen R.A., Taweessintanon K., Johansen S.E, Brenne J.K., Haukanes A., Schjelderup O. & Storvik F. (2022). Sensing whales, storms, ships and earthquakes using an Arctic fibre optic cable. *Scientific Reports* 12, 19226, doi: 10.1038/s41598-022-23606-x.
- Langston C. A. (2018). Calibrating dense spatial arrays for amplitude statics and orientation errors. *Journal of Geophysical Research: Solid Earth*, 123, 3849–3870. <https://doi.org/10.1002/2017JB015098>.
- Langston C. A. & Liang, C. (2008). Gradiometry for polarized seismic waves, *J. Geophys. Res.*, 113, B08305, <https://doi.org/10.1029/2007JB005486>.
- Lefèvre H.C. (2014). *The fiber optic gyroscope*, Artech House, London, United Kingdom.
- Lemoine A., Briole, P., Bertil D., Roullé A., Fomelis M., Thion I., Raucoules D., de Michele M., Valtý P. & Colomer R.H. (2020). The 2018–2019 seismo-volcanic crisis east of Mayotte, Comoros islands: seismicity and ground deformation markers of an exceptional submarine eruption. *Geophysical Journal International* 223, 1, 22–44. <https://doi.org/10.1093/gji/ggaa273>
- Li A., Wang Y., Fang J., Li M.-J., Kim B.Y. & Shieh W. (2015). Few-mode fiber multi-parameter sensor with distributed temperature and strain discrimination. *Opt. Lett.* 40, 1488-1491.
- Li W., Chen Y., Liang Y., Lu Y., Meng Z. (2022). Directivity Dependence of a Distributed Fiber Optic Hydrophone on Array Structure. *Sensors* 22, 6297. <https://doi.org/10.3390/s22166297>
- Liehr S., Münzenberger S. & Krebber K. (2018). Wavelength-scanning coherent OTDR for dynamic high strain resolution sensing. *Optical Express* 26, 10573-10588.
- Liehr S., Jäger L.A., Karapanagiotis C., Münzenberger S. & Komarik S. (2019). Real-time dynamic strain sensing in optical fibers using artificial neural networks. *Optics Express* 27, 5, 7405-7425.
- Lienhart W. (2015). Case studies of high- sensitivity monitoring of natural and engineered slopes. *Journal of Rock Mechanics and Geotechnical Engineering* 7, (4), 379–384. Doi: 10.1016/j.jrmge.2015.04.002.
- Linde A.T. & Sacks S. (1995). Continuous monitoring of volcanoes with borehole strainmeters. *Geophysical Monograph Series*. <https://doi.org/10.1029/GM092p0171>
- Lindner F. Wassermann J., Schmidt-Aursch M., Schreiber K.U. & Igel H. (2016). Seafloor Ground Rotation Observations: Potential for Improving Signal-to-Noise Ratio on Horizontal OBS Components. *Seismological Research Letters* 88 (1). doi: 10.1785/0220160051.
- Lindsey N. J. & Martin E. R. (2021). Fibre-optic seismology. *Annual reviews of Earth and Planetary Sciences*. 49, 309-336 doi: 10.1146/annurev-earth-072420-065213.
- Lindsey N. J., Martin E. R., Dreger D. S., Freifeld B., Cole S., James S. R., Biondi B. L. & Ajo-Franklin J. B. (2017). Fiber optic network observations of earthquake wave fields. *Geophysical Research Letters* 44, 23, 1944-8007, DOI:10.1002/2017GL075722.
- Lindsey N. J., Rademacher H. & Ajo-Franklin J. B. (2020). On the broadband instrument response of fiber optic DAS arrays, *J. Geophys. Res. Solid Earth*, 125, <https://doi.org/10.1029/2019JB018145>.
- Lindsey N. J., Dawe T.C. & Ajo-Franklin J.B. (2019). Illuminating seafloor faults and ocean dynamics with dark fiber distributed acoustic sensing. *Science* 366, 6469, 1103-1107 DOI: 10.1126/science.aay58
- Linker R. & Klar A. (2017). Detection of sinkhole formation by strain profile measurements using BOTDR: Simulation study. *Journal of Engineering Mechanics*, 143, B4015002.
- Linville L., Pankow K. & Draeos T. (2019). Deep learning models augment analyst decisions for event discrimination. *Geophysical Research Letters*, 46. <https://doi.org/10.1029/2018GL081119>
- Lipus M., Reinsch T., Schjmidt-Hattenberger C., Henniges J. & Reich M. (2018). Gravel pack monitoring with a strain sensing fiber optic cable. *Oil Gas European Magazin* 04/2018, 179-185. Doi: 10.19225/181202.
- Liu S., Yu F., Hang R., Xu W., Shao L. & Wang F. (2022). Advances in phase-sensitive optical time-domain reflectometry. *Opto-Electronic Advances, Review*, 5, 3, 200078, 1-28. Doi: 10.29026/oea.2022.200078.
- Liu Y., Ma L., Yang C., Tong W. & He Z. (2018). Long-range Raman distributed temperature sensor with high spatial and temperature resolution using graded-index few-mode fiber. *Optics Express* 26(16), 20562-20571. DOI: 10.1364/oe.26.020562

- Lu P., Lalam N., Badar M., Liu B., Chorpene B.T., Buric M. P. & Ohodnicki P. R. (2019). Distributed optical fiber sensing: review and perspective. *Appl. Ohys. Review* 6, 041302. Doi: 10.1063/1.5113955.
- Lumens P., Franzen A., Hornman K., Karam S.G., Hemink G., Kuvshinov B., La Follet J., Wyker B. & Zwartjes, P. (2013). Cable development for distributed geophysical sensing, with a field trial in surface seismic. *Proceedings Volume 8794, Fifth European Workshop on Optical Fibre Sensors*; 879435. <https://doi.org/10.1117/12.2025693>
- Maccioni E., Giacomelli U., Carbone D., Gambino S., Orazi M., Peluso R. & Sorrentino F. (2019). Shallow bore-hole three-axial fiber Bragg grating strain sensor for Etna volcano monitoring. *Review of Scientific Instruments* 90, 094501. <https://doi.org/10.1063/1.5086516>
- Madsen K. N., Thompson M., Parker T. & Finfer D. (2013). A VSP field trial using distributed acoustic sensing in a producing well in the North Sea. *First break* 31, 51-56.
- Madsen K.N., Tondel R. & Kvam O. (2016). Data-driven depth calibration for distributed acoustic sensing. *The leading Edge*, 610-614, doi:10.1190/tle35070610.1.
- Marra G., Clivati C., Lockett R., Tampellini A., Kronjäger J., Wright L., Mura A., Levi F., Robinson S., Xuereb A., Baptie B. & Calónico D. (2018). Ultrastable laser interferometry for earthquake detection with terrestrial and submarine cables. *Science* 361, 6401, 486-490. DOI: 10.1126/science.aat44
- Marra G., Fairweather D. M., Kamalov V., Gaynor P., Cantono M., Mulholland S., Baptie B., Castellanos J. C., Vagenas G., Gaudron J.-O., Kronjäger J., Hill I. R., Schioppo M., Barbeito-Edreira I., Burrows K. A., Clivati C., Calónico D. & Curtis A. (2022). Optical interferometry-based array of seafloor environmental sensors using a transoceanic submarine cable. *Science*, 376 (6595). DOI: 10.1126/science.abo1939
- Martins H. F., Fernandez-Ruiz M.R., Costa L., Williams E., Zhan Z., Martin-Lopez S. & Gonzalez-Herraez M. (2019). Monitoring of remote seismic events in metropolitan area fibers using distributed acoustic sensing (DAS) and spatio-temporal signal processing. *Optical Fiber Communication Conference (OFC)*. DOI:10.1364/ofc.2019.m2j.1.
- Martuganova E., Stiller M., Norden B., Henniges J. & Krawczyk C. M. (2022). 3D deep geothermal reservoir imaging with wireline distributed acoustic sensing in two boreholes. - *Solid Earth*, 13, 8, 1291-1307. <https://doi.org/10.5194/se-13-1291-2022>
- Masoudi A., Bela, M. & Newson T.P. (2013). A distributed optical fiber dynamical strain sensor based on phase-OTDR. *Measurement Science and Technology* 24, 085204 (7 pp). doi: 10.1088/0957-0233/24/8/085204.
- Masoudi A. & Brambilla G. (2022). Distributed acoustic sensing with optical fibres : fundamental and applications. *The Journal of the Acoustical Society of America* 152, 4, A260-A260
- Masoudi A. & Newson T.P. (2016). Contributed Review: Distributed optical fiber dynamic strain sensing. *Review of Scientific Instruments* 87, 011501, doi: 10.1063/1.4939482.
- Masoudi A. & Newson T.P. (2017). High spatial resolution distributed optical fiber dynamic strain sensor with enhanced frequency and strain resolution. *Optic letters* 42, (2), doi:10.1364/OL.42.000290.
- Matias I., Ikezawa S. & Corres J. (2017). *Fiber Optic Sensors – Current Status and Future Possibilities*. Springer ISBN 978-3-319-42624-2, 381 pp.
- Matoza R. S. & Roman D.C. (2022). One hundred years of advances in volcanology and acoustics. *Bulletin of Volcanology*, 84:86. Doi:10.1007/s00445-022-01586-0.
- Mattei G., Looze N. & Brel E.J. (2017). Measuring micro-mechanical properties of (bio)materials by nano-indentation. *Optics11 B.V.*
- McGarr A., Sacks I.S., Linde A.T., Spottiswoode S.M. & Green R.W.E. (1982). Coseismic and other short-term strain changes recorded with Sacks-Evertson strainmeters in a deep mine, South Africa. *Geophys. J. R. astr. Soc.* 70, 717-740.
- Miah K. & Potter D. K. (2017). A review of hybrid Fiber optic distributed simultaneous vibration and temperature sensing technology and its geophysical applications. *Sensors* 17, 2511. Doi: 10.3390/s17112511.
- Michlmayr G., Chalari A., Clarke A. & Or D. (2017). Fiber optic high-resolution acoustic emission (AE) monitoring of slope failure. *Landslides* 14, 3, 1139–1146. doi: 10.1007/s10346-016-0776-5.
- Mikumo T. & Aki K. (1964). Determination of local phase velocity by intercomparison of seismograms from strain and pendulum instruments. *JGR* 69, 4, 721-731. <https://doi.org/10.1029/JZ069i004p00721>

- Molenaar M.M. & Cox B. (2013). Field cases of hydraulic fracture stimulation diagnostics using fiber optic distributed sensing (DAS) measurements and analyses. Society of Petroleum Engineers (SPE) Middle east unconventional Gas conference and exhibition (Muscat, Oman). SPE 164030.
- Moreno Y., Zhijun Y., Correa N., Diaz G., Santamaria M., Castillo E. & Him A.G. (2022). Optical fiber-based sensors and their recent applications in science and engineering. *Scientia*, 32, 2.
- Muanenda Y., Oton C.J. & Di Pasquale F. (2019). Application of Raman and Brillouin scattering phenomena in distributed optical fiber sensing. *Frontiers in Physics*, 7, p.155.
- Müller G. (2007). Theory of elastic waves, (Scientific Technical Report STR; 07/03), Potsdam: Deutsches GeoForschungsZentrum GFZ, 228 p. <https://doi.org/10.2312/GFZ.b103-07037>
- Muñoz F. & Soto M.A. (2022). Enhancing fibre-optic distributed acoustic sensing capabilities with blind near-field array signal processing. *Nat Commun* 13, 4019. <https://doi.org/10.1038/s41467-022-31681-x>
- Murphy S., Garreau P., Palano M., Ker S., Quetel L., Jousset P., Riccobene G., Aurnia S., Currenti G. & Gutscher M.-A. (2022). Strain evolution on a submarine cable during the 2020-2021 Etna eruption. EGU general assembly EGU22-7742.
- Mussot A., Naveau C., Conforti M., Kudlinski A., Copie F., Szriftgiser P. & Trillo S. (2018). Fibre multi-wave mixing combs reveal the broken symmetry of Fermi-Pasta-Ulam recurrence. *Nature Photonics* 12(5):303–8. doi:10.1038/s41566-018-0136-1.
- Napoli R., Currenti G., Chalari A., Jestin C., Contrafatto D., Jousset P., Larocca G., Pellegrino D., Pulvirenti M. & Sicali A. (2020). Challenges of DAS measurements in seismic urban areas: case study at Etna volcano eastern flank, EGU General Assembly 2020, Online, 4–8 May 2020, EGU2020-11000, <https://doi.org/10.5194/egusphere-egu2020-11000>.
- Napoli R., Currenti G. & Sicali A. (2021). Magnetic signatures of subsurface faults on the northern upper flank of Mt Etna (Italy). *Ann. Geophysics* 64, PE108
- Naveau C., Vanderhaegen G., Szriftgiser P., Martinelli G., Droques M., Kudlinski A., Conforti M., Trillo S., Akhmediev N. & Mussot A. (2021). Heterodyne Optical Time Domain Reflectometer Combined with Active Loss Compensation: A Practical Tool for Investigating Fermi Pasta Ulam Recurrence Process and Breathers Dynamics in Optical Fibers. *Frontiers in Physics* 9, 10.3389/fphy.2021.637812
- Neuberg J. (2000). Characteristics and causes of shallow seismicity in andesitic volcanoes. *Philos. Trans. R. Soc. Lond.*, 358, 1533-1546.
- Nickès M. & Ravet F. (2010). Distributed fiber sensors: depth and sensitivity. *Nature Photonics* 4, 431-432.
- Nigbor R.L. (1994). Six-degree-of-freedom ground-motion measurement. *Bulletin Seismological Society of America* 84 (5), 1994, 1665–1669. <https://doi.org/10.1785/BSSA0840051665>
- Nishimura T., Emoto K., Nakahara H., Miora S., Yamamoto M., Sugimura S., Ishikawa A. & Kimura T. (2021). Source location of volcanic earthquakes and subsurface characterization using fiber optic cable and distributed acoustic sensing system. *Scientific Reports* 11, 6319, <https://doi.org/10.1038/s41598-021-85621-8>
- Noe S., Husmann D., Müller N., Morel J. & Fichtner A. (2023). Long-range fiber-optic earthquake sensing by active phase noise cancellation. *Scientific Reports* 13, 13983 (2023). <https://doi.org/10.1038/s41598-023-41161-x>
- Nöther N., Wosniok A., Krebber K. & Thiele E. (2008). A distributed fiber optic sensor system for dike monitoring using Brillouin optical frequency domain analysis. SPIE library, *Smart Structures and Materials*. Proceedings 6933, <https://doi.org/10.1117/12.775133>.
- Nur I., Kores C.C., Geskus D. & Pollnau M. (2016). Fabry-Pérot resonator: spectral line shapes, generic and related Airy distributions, linewidths, finesses, and performance of low or frequency-dependent reflectivity. *Optics Express* 24, 15,16366-16389.
- Obermann A., Sánchez-Pastor P., Wu S.-M., Wollin C., Baird A. F., Isken M. P., Clinton J., Goertz-Allmann B. P., Dahm T., Wuestefeld A., Shi P., Lanza F., Gyger L., Wetter S., Hjörleifsdóttir V., Langet N., Brynjarsson B., Jousset P. & Wiemer S. (2022). Combined Large-N Seismic Arrays and DAS Fiber Optic Cables across the Hengill Geothermal Field, Iceland. *Seismological Research Letters* (2022) 93 (5): 2498–2514. <https://doi.org/10.1785/0220220073>.
- Ogasawara H., Takeuchi J., Shimoda N., Ishii H., Nakao S., van Aswegen G., Mendecki A.J., Cichowicz A., Ebrahim-Trollope R., Kawakata H., Iio Y., Ohkura T. & Ando M. (2005). High-Resolution Strain Monitoring During M>2 Events in a South African Deep Gold Mine in Close Proximity to Hypocentres, in Y Potvin & M Hudyma (eds), *RaSiM6: Proceedings of the Sixth International*

- Symposium on Rockburst and Seismicity in Mines Proceedings, Australian Centre for Geomechanics, Perth, 385-391, https://doi.org/10.36487/ACG_repo/574_39
- Ohno H., Naruse H., Kihara M. & Shimada A. (2001). Industrial applications of the BOTDR optical fiber strain sensor. *Optical fiber technology*, 7, 45-64.
- Oliveira C. S. & Bolt B. A. (1989). Rotational components of surface strong ground motion, *Earthquake Engineering Structural Dynamics* 18, 517–526.
- Palano M., Calcaterra S., Gambino P., Porfidia B. & Sparacino F. (2023). GNSS-based long-term deformation at Mount Etna volcano (Italy). *Results in Geophysical Sciences* 14 (2023) 100056, 2666-8289.
- Palmieri L. & Schenato L. (2013). Distributed Optical Fiber Sensing Based on Rayleigh Scattering. *The Open Optics Journal* 7, (Suppl-1, M7) 104-127.
- Paolucci R. & Smerzini C. (2008). Earthquake-induced Transient Ground Strains from Dense Seismic Networks, *Networks. Earthquake Spectra* 24 (2), 453–470, <https://doi.org/10.1193/1.2923923>.
- Park C. B. (2011). Imaging dispersion of MASW data – full versus selective offset scheme. *J. Environ. Eng. Geophysics* 16, 13–23.
- Parker T., Shatalin S. & Farhadiroushan M. (2014). Distributed Acoustic Sensing – a new tool for seismic applications. *First break* 32, 61-69.
- Pastor-Graells J., Martins H. F., Garcia-Ruiz A., Martin-Lopez S. & Gonzalez-Herraez M. (2016). Single-shot distributed temperature and strain tracking using direct detection phase-sensitive OTDR with chirped pulses. *Opt. Express* 24(12), 13121–13133.
- Pätzelt J. (2023). Seismic site characterization using broadband and DAS ambient vibration measurements on Mt Etna, Italy. Master thesis, University of Potsdam, 95 pp. <https://doi.org/10.25932/publishup-61379>
- Pechstedt R.D. & Jackson D.A. (1995). Design of a compliant-cylinder-type fiber optic accelerometer: theory and experiment. *Applied Optics* 34, 16, 3009-3017.
- Peng F. & Cao X. (2016). A hybrid Peng, ϕ /B-OTDR for simultaneous vibration and strain measurement. *Photonic Sensors* 6, 2, 121-126.
- Peng F., Duan N., Rao Y. J. & Li J. (2014). Real-time position and speed monitoring of trains using ϕ -OTDR. *IEEE Photonic Technology Letters* 26, 20, 2055-2057.
- Perot A. & Fabry C. (1899). On the Application of Interference Phenomena to the Solution of Various Problems of Spectroscopy and Metrology. *Astrophysical Journal* 9: 87.
- Personick S.D. (1983) Review of fundamentals of optical fiber systems. *IEEE Journal of selected areas in communications* vol. sac-1, 3, 373-380.
- Pevac S. & Donlagic D. (2019). Multiparameter fiber optic sensors: a review. *Optical Engineering* 58 (7), 072009.
- Philen D. L., White I.A., Kuhl J. F. & Mettler S. (1982). Single-Mode fiber ODTR: experiment and theory. *IEEE Journal of Quantum Electronics* QE18, 10, 1499-1508, doi:10.1109/TMTT.1982.1131282.
- Picarelli L., Damiano E., Greco R., Minardo A., Olivares L., & Zeni L. (2015). Performance of slope behavior indicators in unsaturated pyroclastic soils. *Journal of Mountain Science* 12, 6, 1434–1447. doi: 10.1007/s11629-014-3104-3.
- Pisco M., Bruno F.A., Galluzzo D., Nardone L., Gruca G., Rijnveld N., Bianco F., Cutolo A. & Cusano A. (2018). Opto-mechanical lab-on-fibre seismic sensors detected the Norcia earthquake. *Scientific Reports* 8, 6680. <https://doi.org/10.1038/s41598-018-25082-8>.
- Posey R., Johnson G.A. & Vohra S.T. (2000). Strain sensing based on coherent Rayleigh scattering in an optical fiber. *Electronic Letters* 36, 20, 1688-1689.
- Quinteros J., Carter J. A., Schaeffer J., Trabant C. & Pedersen A. (2021). Exploring approaches for large data in seismology: user and data repository perspectives. *Seismological Res. Lett.* 92, 1531–1540.
- Quinteros J. (2021). dastools - Tools to work with data generated by DAS systems. GFZ Data Services. doi:10.5880/GFZ.2.4.2021.001
- Ramakrishnan M., Rajan G., Semenova Y. & Farrell G. (2016). Overview of Fiber Optic Sensor Technologies for Strain/Temperature Sensing Applications in Composite materials. *Sensors* 16, 99 doi:10.3390/s16010099 982.

- Raman C. V. (1928). A new radiation. *Indian Journal of Physics*. 2: 387–398. hdl:10821/377
- Ravet F. (2011). Distributed Brillouin Sensor Application to Structural failure Detection. In *New Developments in 985 Sensing technology for structural Health Monitoring*; Springer Berlin Heidelberg: Berlin, Germany, p93-136 986.
- Rayleigh Lord (1881). On the electromagnetic theory of light. *The London, Edinburgh, and Dublin Philosophical Magazine and Journal of Science* 12 (73): 81–101. doi:10.1080/14786448108627074
- Reinsch T., Henniges J. & Asmundsson R. (2013). Thermal, mechanical and chemical influences on the performance of optical fibers for distributed temperature sensing in a hot geothermal well. *Environmental Earth Sciences* 70, 3465-3480.
- Reinsch T., Jousset P., Henniges J. & Blanck H. (2016). Distributed Acoustic Sensing Technology in Magmatic Geothermal Areas – First Results from a Survey in Iceland - Proceedings, European Geothermal Congress, 990 Strasbourg, France.
- Reinsch T., Thurley T. & Jousset P. (2017). On the mechanical coupling of a fiber optic cable used for distributed acoustic/vibration sensing applications — a theoretical consideration. - *Measurement Science and Technology* 28, 12. <http://doi.org/10.1088/1361-6501/aa8ba4>
- Reinsch T., Jousset P., Krawczyk C.M. (2021). Fiber Optic Distributed Strain Sensing for Seismic Applications. In H.K. Gupta (Ed.), *Encyclopedia of Solid Earth Geophysics*, 2nd Edition *Encyclopedia of Earth Sciences Series*, Springer Nature Switzerland, pp. 379-383; https://doi.org/10.1007/978-3-030-58631-7_284. Series Online ISBN 978-3-030-58631-7.
- Retailleau L., Saurel J.M., Laporte M., Lavayssière A., Ferrazzini V., Zhu W., Beroza G.C., Satriano C., Komorowski J.C. & OVPF Team. (2022). Automatic detection for a comprehensive view of Mayotte seismicity. *Comptes Rendus. Géoscience*, 354(S2), pp.1-18.
- REVOSIMA-IPGP (2021). Bulletin de l'activité sismo- volcanique à Mayotte. www.ipgp.fr/fr/revosima.
- Richter P., Parker T., Woerpel C., Wu Y., Rufino R. & Farhadiroushan M. (2019). Hydraulic fracture monitoring and optimization in unconventional completions using a high-resolution engineered fiber Distributed Acoustic Sensor. *First Break* 37, Special topic: passive seismic and unconventional. 64-68. 999
- Rodgers P. W. (1968). The response of the horizontal pendulum seismometer to Rayleigh and Love waves, tilt, and free oscillations of the earth. *Bulletin of the Seismological Society of America*, 58 (5), 1385{1406. Retrieved from <https://doi.org/10.1785/BSSA0580051385> doi: 10.1785/BSSA0580051385
- Rust A. C., Balmforth N. J. & Mandre S. (2008). The feasibility of generating low-frequency volcano seismicity by flow through a deformable channel. *Geol. Soc. Lond.* 307, 45-56.
- Sacks S., Suyehiro S. & Evertson D.W. (1971). Sacks-Evertson strainmeter, its installation in japan and some preliminary results concerning strain steps. *Proc. Japan Acad* 47, 9, 707-712.
- Sagnac G. (1913a). L'éther lumineux démontré par l'effet du vent relatif d'éther dans un interféromètre en rotation uniforme (The demonstration of the luminiferous aether by an interferometer in uniform rotation). *Comptes Rendus*, 157, 708–710.
- Sagnac G. (1913b). Sur la preuve de la réalité de l'éther lumineux par l'expérience de l'interférographe tournant (On the proof of the reality of the luminiferous aether by the experiment with a rotating interferometer) *Comptes Rendus* 157, 1410–1413
- Sandwell D. T. (1987). Biharmonic spline interpolation of GEOS-3 and SEASAT altimeter data. *Geophysical Research Letters* 14, 139–142, <https://doi.org/10.1029/GL014i002p00139>.
- Sandwell D. T. & Wessel, P. (2016). Interpolation of 2-D vector data using constraints from elasticity. *Geophysical Research Letters* 43, 10,703–10,709, <https://doi.org/10.1002/2016GL070340>
- Schenato L. (2017). A review of distributed fiber optic sensors for geo-hydrological applications. *Applied Sciences* 7 (9), 896. doi: 10.3390/app7090896.
- Schmelzbach C., Donner S., Igel H., Sollberger D., Taufiqurrahman T., Bernuer F., Häusler M., Van Renterghem C, Wassermann, J. & Robertsson J. (2018), *Advances in 6-C seismology: Applications of combined translational and rotational measurements in global and exploration seismology*. *Geophysics* 83, 3, doi: 10.1190/GEO2017-0492.1.
- Schölderle F., Lipus M., Pfrang D., Reinsch T., Krawczyk C.M. & Zosseder K. (2022). Faseroptische Bohrlochüberwachung – DTS- und DAS-Messungen am Geothermie-Standort Schäftlarnstraße, München. *Geothermische Energie*, 102, 18-20; https://www.geothermie.de/fileadmin/user_upload/Bibliothek/GTE/Geothermische.Energie.Nr.102.pdf.

- Schwarz B. (2019). Coherent wave field subtraction for diffraction separation. *Geophysics* 84, V157–V168.
- Seat H. C., Chawah P., Cattoen M., Sourice A., Plantier G., Boudin F., Chéry J., Brunet C., Bernard P. & Suleiman M. (2012). Dual-modulation fiber Fabry-Perot interferometer with double reflection for slowly-varying displacements. *Optics Letters*, 37(14):2886
- SEAFOM (2018). Measuring Sensor Performance Document – 02 (SEAFOM MSP 02). DAS parameter definition and tests. <https://seafom.com/published-documents>
- Segovia N. (1991). Radon and volcanic activity: Recent advances. *International Journal of Radiation Applications and Instrumentation. Part D. Nuclear Tracks and Radiation Measurements* 19, 409-414. [https://doi.org/10.1016/1359-0189\(91\)90227-9](https://doi.org/10.1016/1359-0189(91)90227-9)
- Shatalin S., Parker T. & Farhadiroushan M. (2021). High definition seismic and microseismic data acquisition using distributed and engineered fiber optic acoustic sensors. *Distributed Acoustic Sensing in Geophysics: Methods and Applications*, 1–32.
- Shen Z.K., Wang M., Zeng Y. & Wang, F. (2015). Optimal Interpolation of Spatially Discretized Geodetic Data, *Bulletin of the Seismological Society of America*, 105, 4, 2117–2127, <https://doi.org/10.1785/0120140247>.
- Simonelli A., Igel H., Wassermann J., Belfi J., Di Virgilio A., Beverini N. & De Luca G. (2018). Rotational motions from the 2016, Central Italy seismic sequence, as observed by an underground ring laser gyroscope. *Geophysical Journal International* 214 (1), 705–715. doi: 10.1093/gji/ggy186.
- Sladen A., Rivet D., Ampuero J.P., De Barros L., Hello Y., Calbris G. & Lamare P. (2019). Distributed sensing of earthquakes and ocean-solid Earth interactions on seafloor telecom cables. *Nat Commun* 10, 5777. <https://doi.org/10.1038/s41467-019-13793-z>.
- Sollberger D., Greenhalgh S. A., Schmelzbach C., Van Renterghem, C. & Robertsson J. O. A. (2018). 6-C polarization analysis using point measurements of translational and rotational ground-motion: theory and applications. *Geophysical Journal International*, 213, 77-97. doi: 10.1093/gji/ggx542
- Somma R., Troise C., Zeni L., Minardo A., Fedele A., Mirabile M. & De Natale G. (2019). Long-term monitoring with fiber optic distributed temperature sensing at Campi Flegrei: The Campi Flegrei Deep drilling project. *Sensors* 19, 1009. Doi: 10.3390/s19051009.
- Song K.Y & Hotate K. (2007). Distributed Fiber strain sensor with 1-kHz sampling rate based on Brillouin optical correlation domain analysis. *IEEE Photon. Technol. Letters* 19, 23, 1928-1930. Doi: 10.1109/LPT.2007.908772.
- Soto M.A., Ramirez J.A. & Thévenaz L. (2016). Intensifying the response of distributed optical fiber sensors using 2D and 3D image restoration. *Nature Communications* 7, 10870. Doi:10.1038/ncomms10870.
- Soto M.A. & Thévenaz L. (2013). Modeling and evaluating the performance of Brillouin distributed optical fiber sensors. *Optics Express* 21, 25, 31347-31366. <https://doi.org/10.1364/OE.21.031347>.
- Spica Z. J., Ajo-Franklin J., Beroza G. C., Biondi B., Cheng F., Gaité B., Luo B., Martin E., Shen J., Thurber C., Viens L., Wang H., Wuestefeld A., Xiao H. & Zhu T. (2023). PubDAS: A PUBLIC Distributed Acoustic Sensing Datasets Repository for Geosciences, *Seismological Research Letters*. <https://doi.org/10.1785/0220220279>
- Spudich P., Steck L. K., Hellweg M., Fletcher J. & Baker L. M. (1995). Transient stresses at Parkfield, California, produced by the M 7.4 Landers earthquake of June 28, 1992: observations from the UPSAR dense seismograph array, *J. Geophys. Res.* 100, 675–690, <https://doi.org/10.1029/94JB02477>.
- Spudich P. & Fletcher J.B. (2008). Observation and Prediction of Dynamic Ground Strains, Tilts, and Torsions Caused by the Mw 6.0 2004 Parkfield, California, Earthquake and Aftershocks, Derived from UPSAR Array Observations. *Bulletin of the Seismological Society of America* 98, 4, 1898–1914, <https://doi.org/10.1785/0120070157>
- Sun Y. Shi B., Zhang D., Tong H., Wei G. & Xu, H. (2016). Internal Deformation Monitoring of Slope Based on BOTDR. *Journal of Sensors*, ID 9496285, 1-8. <https://doi.org/10.1155/2016/9496285>
- Sun Y., Li H., Fan C., Yan B., Chen J., Yan Z. & Sun Q. (2022). Review of a specialty fiber for distributed acoustic sensing technology. *Photonics*, 9, 277. <https://doi.org/10.3390/photonics9050227>.
- Surono, Jousset P., Pallister J., Boichu M., Buongiorno M.F., Budisantoso A., Costa F., Andrastuti S., Prata F., Schneider D., Clarisse L., Humaida H., Sumarti S., Bignami C., Griswold J., Carn S., Oppenheimer C. & Lavigne F. (2012). The 2010 explosive eruption of Java's Merapi volcano – a “100-year” event. *J. Volcanol. Geothermal. Res.*, 241-242, 121-145.

- Suryanto W., Igel H., Wassermann J., Cochard A., Schuberth B., Vollmer D., Scherbaum F., Schreiber U. & Velikoseltsev A. (2006). First comparison of array-derived rotational ground motions with direct ring laser measurements, *Bull. Seismol. Soc. Am.* 96, 2059–2071, <https://doi.org/10.1785/0120060004>.
- Szegedy C., Vanhoucke V., Ioffe S., Shlens J. & Wojna Z. (2015). Rethinking the Inception Architecture for Computer Vision. arXiv. <http://arxiv.org/abs/1512.00567>
- Szstakowski M. & Zyczkowski M. (2005). Fiber optic sensor or perimeter security with intruder localization. *Proceedings of SPIE - The international Society for optical Engineering*. Doi: 10.1117/12.622776.
- Taddeucci J., Scarlato P., Del Bello E., Spina L., Ricci T., Gaudin D. & Tournigand P.Y. (2021). The dynamics of explosive mafic eruptions: new insights from multiparametric observations. In *Forecasting and Planning for Volcanic Hazards, Risks, and Disasters, Volume 2 in Hazards and Disasters, Chapter 9*, 379–411.
- Tanimoto T., Hadziioannou C., Igel H., Wassermann J., Schreiber U. & Gebauer A. (2015). Estimate of Rayleigh-to-Love wave ratio in the secondary microseism by co-located ring laser and seismograph. doi: 10.1002/2015GL063637.
- Taylor H.F. & Lee C.E (1993). Apparatus and method for fiber optic intrusion sensing. US patent 5, 194, 847.
- Tejedor J., Macias-Guarasa J., Martins H. F., Pastor-Graells J., Corredera P. & Martin-Lopez S. (2017). Machine Learning Methods for Pipeline Surveillance Systems Based on Distributed Acoustic Sensing: A Review. *Applied Sciences*, 7(8), 841.
- Thelen W.A., Matoza R.S. & Hotovec-Ellis A.J. (2022). Trends in volcano seismology: 2010 to 2020 and beyond. *Bulletin of Volcanology*, 64: 26.
- Thévenaz L. (2010). Brillouin distributed time-domain sensing in optical fibers: state of the art and perspectives. *Frontiers of Optoelectronics in China*, 3, 13-21.
- Thierry P., Neri M., Le Cozannet G., Jousset P. & Costa A. (2015). Preface: Approaches and methods to improve risk management in volcanic area. *Nat. Hazards Earth Syst. Sci.*, 15, 197–201. doi:10.5194/nhess-15-197-2015.
- Thrustarson S., Torfason R., Klaasen S., Paitz P., Cubuk-Sabuncu Y., Jonsdottir K. & Fichtner A. (2021). Detecting seismic events with computer vision: Applications for fiber optic sensing. *Earth and Space Science Open Archive*, doi:10.1002/essoar.10509693.1.
- Toledo Z. T. A., Jousset P., Maurer H. & Krawczyk C. (2020). Optimized Experimental Network Design for Earthquake Location Problems: applications to geothermal and volcanic field seismic networks. *Journal of Volcanology and Geothermal Research*, 391, 106433.
- Trainor-Guitton W., Martin E.R., Rodriguez-Tribaldos V., Traverna N. & Dumont. V. (2022). Distributed sensing and machine learning hone seismic listening. *EOS* 103, <https://doi.org/10.1029/2022EO220121>.
- Trebugov A.V., Svetukhin V.V., Novikov S.G., Berintsev A.V. & Prikhodko V.V. (2016). A novel fiber optic distributed temperature and strain sensor for building applications. *Results in Physics* 6, 131-132.
- Tu G., Zhang X., Wang S., Zhu F., Xia L. & Nakarmi B. (2015). The development of Phi-OTDR system for quantitative vibration measurement. *IEEE Photonics Techn. Letters* 27, 12, 1349-1352.
- Tyler S. W., Selker J. S., Hausner M. B., Hatch C. E., Torgersen T., Thodal C. E. & Schladow S. G. (2009), Environmental temperature sensing using Raman spectra DTS fiber-optic methods, *Water Resour. Res.*, 45, W00D23, doi:10.1029/2008WR007052.
- Ukil A., Braendle H. & Krippner P. (2011). Distributed temperature sensing: Review of technology and applications. *IEEE Sensors Journal*, 12(5), 885-892.
- Van den Ende M. P. A. & Ampuero J.-P. (2021). Evaluating seismic beamforming capabilities of distributed acoustic sensing arrays, *Solid Earth*, 12, 915–934, <https://doi.org/10.5194/se-12-915-2021>.
- Van Renterghem C., Schmelzbach C., Sollberger D., Robertsson J.O.A. (2018). Spatial wave field gradient-based seismic wave field separation, *Geophysical Journal International* 212, 3, 1588–1599, <https://doi.org/10.1093/gji/ggx499>
- Vasquez A., Manasseh R. & Chicharro R. (2015). Can acoustic emissions be used to sizes bubbles seeping from a sediment bad? *Chemical Engineering Science* 131, 187-196.
- Verdon J., Horne S.A., Clarke A., Stork A.L., Baird A. & Kendall M. (2020). Microseismic monitoring using a fibre-optic DAS array. *Geophysics* doi: 10.1190/geo2019-0752.1.

- Viens L., Bonilla L. F., Spica Z. J., Nishida K., Yamada T. & Shinohara M. (2022). Nonlinear earthquake response of marine sediments with Distributed Acoustic Sensing. *Geophysical Research Letters* 49, 21. <https://doi.org/10.1029/2022GL100122>
- Walter F., Gräff D., Lindner F., Paitz P., Köpfl M., Chmiel M. & Fichtner A. (2020). Distributed acoustic sensing of microseismic sources and wave propagation in glaciated terrain. *Nature Communications*. DOI: 10.1038/s41467-020-15824-6.
- Wang H. F., Zeng X., Miller D. E., Fratta D., Feigl K. L., Thurber C. H. & Mellors R. J. (2018). Ground motion response to an ML 4.3 earthquake using co-located distributed acoustic sensing and seismometer arrays, *Geophysical Journal International*, 213, 2020–2036, <https://doi.org/10.1093/gji/ggy102>.
- Wassermann J., Bernauer F., Shiro B., Johansson I., Guattari F. & Igel H. (2020). Six-Axis Ground Motion Measurements of Caldera Collapse at Kilauea Volcano, Hawai'i | More Data, More Puzzles? *Geophysical Research Letters*, 47 (5), 1{7. doi: 10.1029/2019GL085999
- Wassermann J., Braun T., Ripepe M., Bernauer F., Guattari F. & Igel H. (2022). The use of 6DOF measurement in volcano seismology - A first application to Stromboli volcano. *Journal of Volcanology and Geothermal Research*. 424, 107499.
- Wassermann J., Wietek A., Hadziioannou C. & Igel H. (2016). Toward a single station approach for microzonation: Using vertical rotation rate to estimate love-wave dispersion curves and direction finding. *Bulletin of the Seismological Society of America*, 106 (3), 1316-1330. doi: 10.1785/0120150250
- Watson G., Daniels W. & Wang C. (1981). Measurements of Raman intensities and pressure dependence of phonon frequencies in sapphire. *Journal of Applied Physics*, 52 (2). 956-958 doi:10.1063/1.328785
- Wessel P., Luis J. F., Uieda L., Scharroo R., Wobbe F., Smith W. H. F. & Tian D. (2019). The Generic Mapping Tools version 6. *Geochemistry, Geophysics, Geosystems*, 20, 5556–5564. <https://doi.org/10.1029/2019GC008515>
- Williams E.F., Fernández-Ruiz M.R., Magalhaes R., Vanthillo R., Zhan Z., González-Herráez & Martins H.F. (2019). Distributed sensing of microseisms and teleseisms with submarine dark fibers. *Nature Communications* 10, 5778. <https://doi.org/10.1038/s41467-019-13262-7>
- Willis M.E., Barfoot D., Ellmuthaler A., Wu X., Barrios O., Erdemir C. Shaw S. & Quinn D. (2016). Quantitative quality of distributed acoustic sensing vertical seismic profile data. *The leading Edge*, 605-609, doi:10.1190/tle35070605.1.
- Witze A. (2015). Volcano risk quantified. *Nature* 519, 16–17.
- Wosniok A., Nöther N. & Krebber K. (2009). Distributed fiber optic system for temperature and strain monitoring based of Brillouin optical fibre frequency domain analysis. *Proceedings of the Eurosensors XXIII Conference*. <https://doi.org/10.1016/j.proche.2009.07.099>.
- Wu J., Jiang H., Su J., Shi B., Jiang Y. & Gu K. (2015). Application of distributed fibre optic sensing technique in land subsidence monitoring. *J. Civil Struct. Health Monitoring* 5, 587-597.
- Wu H., Zhu H.-H., Zhang C.-C., Zhou G.-Y., Zhu B., Zhnag W. & Azarafza M. (2020). Strain integration-based soil shear displacement measurement using high-resolution strain sensing technology. *Measurement*, 166, 108210.
- Wu H., Zhou B., Zhu K., Shang C., Tam H.-Y. & Lu C. (2021). Pattern recognition in distributed fiber-optic acoustic sensor using an intensity and phase stacked convolutional neural network with data augmentation. *Optics Express*, 29(3), 3269-3283.
- Wuestefeld A., Spica Z. J., Aderhold K., Huang H-H., Ma K-F., Lai V. H., Miller M., Urmantseva L., Zapf D., Bowden D. C., Edme P., Kiers T., Rinaldi A. P., Tuinstra K., Justin C., Diaz-Meza S., Jousset P., Wollin C., Ugalde A., Ruiz Barajas S., Gaité B., Currenti G., Prestifilippo M., Araki E., Tonegawa T., de Ridder S., Nowacki A., Lindner F., Schoenball M., Wetter C., Zhu H-H., Baird A. F., Rørstadbotnen R. A., Ajo-Franklin J., Ma Y., Abbott R. E., Hodgkinson K. M., Porritt R. W., Stanciu C., Podrasky A., Hill D., Biondi B., Yuan S., Luo B., Nikitin S., Morten J. P., Dumitru V-A., Lienhart W., Cunningham E. & Wang H. (2023). The Global DAS Month of February 2023. *Seismological Research Letters*, doi: <https://doi.org/10.1785/0220230180>.
- Xiong J., Wang Z., Wu Y., Yongxiang & Rao Y. (2018). 100km dynamic strain sensing via CP-ΦOTDR. *Asia Communications and Photonics Conference (ACP), OSA Technical Digest (Optica Publishing Group, 2018), paper Su1B.8*.
- Yang J., Chung Y., Sprinzak D., Heiblum M., Mahalu D. & Shtrikman H. (2003). An electronic Mach-Zehner interferometer. *Nature* 422, 415-418.
- Yang Y., Zhan Z., Shen Z. & Atterholt J. (2022). Fault Zone Imaging with Distributed Acoustic Sensing: Surface-To-Surface Wave Scattering. *Journal of Geophysical Research*. <https://doi.org/10.1029/2022JB024329>

- Yeh Y.L., Wang W.H. & Wen S. (2021). Dense seismic arrays deny a massive magma chamber beneath the Taipei metropolis, Taiwan. *Sci Rep* 11, 1083. <https://doi.org/10.1038/s41598-020-80051-4>
- Yu C., Zhan Z., Lindsey N. J., Ajo-Franklin J. B. & Robertson M. (2019). The potential of DAS in teleseismic studies: Insights from the Goldstone experiment. *Geophysical Research Letters* 46, 1320–1328, <https://doi.org/10.1029/2018GL081195>.
- Yuan S., Simonelli, A., Lin C. J., Bernauer F., Donner S., Braun T., Wassermann J. & Igel, H. (2020). Six degree-of-freedom broadband ground-motion observations with portable sensors: Validation, local earthquakes, and signal processing. *Bulletin of the Seismological Society of America* 110 (3), 953–969. doi: 10.1785/0120190277
- Yuan S., Gessele K., Gabriel A.-A., May D., Wassermann J. & Igel H. (2021). Seismic source tracking with six degree-of-freedom ground motion observations. *Journal of Geophysical Research, solid Earth* 126, e2020JB021112, doi: 10.1029/2020JB021112.
- Zetie K.P., Adams S.F. & Tocknell R.M. (2000). How does a Mach-Zehnder interferometer work? *Physics Education* 35, 1, 46-48.
- Zhan Z. (2019). Distributed Acoustic Sensing Turns Fiber Optic Cables into Sensitive Seismic Antennas, *Seismol. Res. Lett.* 91, 1–15, doi: 10.1785/0220190112.
- Zhan Z., Cantono M., Kamalov V., Mecozzi A., Müller R., Yin S. & Castellanos J. C. (2021). Optical polarization-based seismic and water wave sensing on transoceanic cables. *Science* 371, 6532, 931-936 DOI: 10.1126/science.abe6648.
- Zhang C.C., Zhu H.H., Liu S.P. & Zhang D. (2018). A kinematic method for calculating shear displacements of landslides using distributed fiber optic strain measurements. *Engineering Geology*, 234, 83-96.
- Zhang C.C., Zhu H.H. & Shi B. (2016). Role of the interface between distributed fiber optic strain sensor and soil in ground deformation measurement. *Scientific Reports* 6, 36469
- Zhang L., Costa L. D., Yang Z., Soto M. A., Gonzalez-Herráez M. & Thévenaz L. (2019). Analysis and Reduction of Large Errors in Rayleigh-Based Distributed Sensor. *Journal of Lightwave Technology* 37, 18, 4710-4719.
- Zhi W., Guobin R., Shuqin L. & Shuisheng J. (2003). Loss of properties due to Rayleigh scattering in different types of fiber. *Optic Express* 11, 1, 39-47.
- Zhu H.H., Liu W., Wang T., Su J.W. & Shi B. (2022). Distributed Acoustic sensing for monitoring Linear Infrastructures: current status and trends. *Sensors* 22, 7550. Doi: 10.3390/s22197550.
- Zuccarello L., Burton M. R., Saccorott, G., Bean C. J. & Patanè D. (2013). The coupling between very long period seismic events, volcanic tremor, and degassing rates at Mount Etna volcano. *Journal of Geophysical Research* 118, 1–12.
- Zumberge M. A., Wyatt F. K., Dong X. Y. & Hanada H. (1988). Optical fibers for measurement of earth strain. *Applied Optics* 27 (19) 4131-4138. <https://doi.org/10.1354/AO.27.004131>.
- Zwartjes P. & Mateeva A. (2015). Multi-Fiber DAS walk-away VSP at Kapuni. 3rd EAGE Workshop on Borehole Geophysics, Athens, Greece, Expanded Abstracts, BG05.